NASA
Technical
Paper
2042

August 1982

Experimental Investigation of Active Loads Control for Aircraft Landing Gear

John R. McGehee
and Robert C. Dreher

NASA

NASA Technical Paper 2042

1982

Experimental Investigation of Active Loads Control for Aircraft Landing Gear

John R. McGehee
and Robert C. Dreher
Langley Research Center
Hampton, Virginia

NASA
National Aeronautics
and Space Administration

Scientific and Technical Information Branch

CONTENTS

SUMMARY

Aircraft dynamic loads and vibrations resulting from landing impact and from runway and taxiway unevenness are recognized as significant factors in causing fatigue damage, dynamic stress on the airframe, crew and passenger discomfort, and reduction of the pilot's ability to control the aircraft during ground operations. One potential method for improving operational characteristics of aircraft on the ground is the application of active-control technology to the landing gears to reduce ground loads applied to the airframe.

An experimental investigation was conducted which simulated the landing dynamics of a light airplane to determine the feasibility and potential of a series-hydraulic active-control main landing gear. The experiments involved a passive gear and an active-control gear. Results of this investigation show that a series-hydraulically controlled gear is feasible and that such a gear is very effective in reducing the loads transmitted by the gear to the airframe during ground operations.

INTRODUCTION

Aircraft dynamic loads and vibrations resulting from landing impact and from runway and taxiway unevenness are recognized as significant factors in causing fatigue damage, dynamic stress on the airframe, crew and passenger discomfort, and reduction of the pilot's ability to control the aircraft during ground operations. These ground-induced dynamic loads and vibrations have been encountered with some conventional subsonic transport aircraft (refs. 1 and 2). They are magnified for supersonic-cruise aircraft because of the increased structural flexibility inherent in these slender-body, thin-wing designs. These operational problems with supersonic-cruise aircraft have occurred at high take-off and landing speeds on some runways which provide only marginal performance for some conventional aircraft. A potential method for improving operational characteristics of such aircraft on the ground is the application of active-control technology to the landing gears to reduce the ground loads applied to the airframe.

In reference 3, a model of a series-hydraulic active landing gear for controlling the loads during impact and roll-out was developed and programmed for digital-computer operation. The control operates to limit the airplane mass-center force to a minimum (command limit force) compatible with the available shock-strut stroke and the airplane kinetic energy. As long as the mass-center force is greater than the limit force, the control system removes fluid from the strut at a rate which varies with the magnitude of the force difference. As the mass-center force decreases toward the limit force, the control system reduces the rate at which fluid is removed from the strut. When the mass-center force becomes less than the limit force, the control system adds fluid to the strut. In reference 3, analytical results, using the developed control laws, indicated that the active gear substantially reduced forces transmitted to the airframe. Consequently, an electronic control was designed, fabricated, and tested and the results are presented in reference 4. The drop-test (zero ground speed) results of reference 4, which used a modified landing gear from a general aviation airplane, indicated active-gear force reductions, relative to the forces obtained with the passive gear, from 9 to 31 percent depending on the aircraft sink rate and the gear charging pressure.

The purpose of this paper is to present the results of an experimental investigation of a series-hydraulic active-control gear to demonstrate the feasibility and the potential of this type of active-control concept. For this investigation, a strut from a single main gear of a 3000-kg-class (200-slug) airplane was modified to accommodate a series-hydraulic active-control system. Landing-simulation tests were conducted at ground speeds to 80 knots and vertical-drop tests at zero ground speed. The forward-speed tests involved landing impacts and roll-outs over discrete bumps as well as roll-outs over natural surface unevenness.

APPARATUS

LANDING-GEAR MODIFICATION

The series-hydraulic control concept requires the hydraulic fluid in the landing-gear piston to be removed or added to control the shock-strut hydraulic force. To accomplish this fluid exchange, the gear was modified (see fig. 1) to provide a conduit between the fluid in the piston and a control servovalve. Components of the light-aircraft main landing gear used in this investigation are shown in figure 1(a). The modification to the gear consisted of adding a smaller diameter tube inside the existing single-wall orifice support tube to provide an annular passage through the cylinder into the piston. The existing orifice plate, but not the orifice, was reduced in diameter and installed in the smaller diameter tube as shown in figure 1(b). To provide for flow between the annular passage and the servovalve, a cylinder head adapter was mounted on top of the cylinder, was mated with the annular passage in the orifice support tube, and was connected to the servovalve by a flexible hose. Details of the modified strut assembly are shown in figure 1(c).

The piston was modified by mounting a pressure transducer in the base of the piston (fig. 1(a)) to provide a signal to the electronic controller for biasing the servovalve power spool to maintain the fully extended charging pressure in the strut prior to touchdown on the runway surface. A slide wire mounted on the cylinder with the wiper shaft attached to the half fork at the base of the piston provided a strut stroke signal for use by the electronic controller in applying the control laws.

HYDRAULIC POWER UNIT

The hydraulic power unit used in this investigation is shown in figure 2 attached to the test carriage at the Langley Landing Loads Track. This unit supplies high-pressure (20.7 MPa (3000 psig)) fluid to the control servovalve, provides a low-pressure (101 kPa (14.7 psig)) reservoir for storing and recycling fluid removed from the gear by the control servovalve, provides pressure relief to avoid damage to the gear in the event of a servovalve failure in the high-pressure mode of operation, and permits operation of the modified gear in either the passive or active modes. To keep the unit compact for mounting to the carriage, several 90° elbows were required in the piping between the servovalve and the gear; therefore, this installation did not provide for minimum flow losses. The various components of the hydraulic power unit are shown in figure 2 and component specifications are listed in table I. Some of the more pertinent components are discussed in the following sections.

The three-stage servovalve used in this investigation had a maximum fluid-flow capability of 0.757 m^3/min (200 gpm) for a pressure drop across the valve of 6.9 MPa (1000 psig). For low-pressure operation (that is, flow from the gear into the low-pressure reservoir) and a static gear pressure in the range of 3.4 MPa (500 psig),

the maximum flow rate through the servovalve would be approximately 0.534 m^3/min (141 gpm). For high-pressure operations (that is, flow from the high-pressure accumulator into the gear) and a static gear pressure of 3.4 MPa (500 psig), a maximum flow rate through the servovalve of approximately 1.20 m^3/min (316 gpm) could be expected. The servovalve was mounted on the hydraulic power unit with the power-spool axis oriented normal to the direction of carriage acceleration to reduce inertial effects during carriage launch.

Two pressure-relief valves used to protect the system were set, based upon results of vertical-drop tests, to operate for pressures greater than 5.2 MPa (750 psig). The intake ports of the valves were installed between the servovalve and the isolation valve, and the exhaust ports were connected to the low-pressure reservoir.

The isolation valve (a manually operated gate valve) was mounted between the control servovalve and a flexible hose which was attached to the landing-gear cylinder head adapter. The valve permitted tests of the modified gear in the active (valve open) or passive (valve closed) modes. When fully open, the valve provided a flow area equivalent to a 3.8-cm-diameter (1.5-in.) tube. Since the flexible hose had a flow area equivalent to a 3.18-cm (1.25-in.) diameter, the isolation valve accommodated a fluid flow rate greater than that of the flexible hose. The 3.05-m (10-ft) length of flexible hose provided a conduit for fluid flow between the hydraulic power unit and the landing gear.

The bias-pressure pickup supplied a feedback signal to the electronic controller for regulating the charging pressure of the fully extended gear prior to touchdown during the active-gear tests. The surge suppressor helped to alleviate pressure spikes applied to the bias-pressure gage during servovalve operation in the high-pressure mode. The control panel contained a switch and fuses for operation of the electric motor.

ELECTRONIC EQUIPMENT

The control, signal-conditioning, and diagnostic electronic equipment are shown in a bench setup in figure 3. The function of the control equipment, namely the electronic controller and the servocontroller, is to apply the control laws, operate the servovalve, and thus, control the gear force applied to the airframe. The signal-conditioning equipment consists of a regulated power supply, a control box, amplifiers, and analog filters for preparing the signals from the various data transducers for recording on frequency-modulated (FM) tape recorders. The diagnostic equipment shown (oscilloscope, oscillograph, and teletypewriter) was employed during the investigation to isolate problems encountered with the electronic controller and to validate hardware and software modifications to the control system.

TEST FIXTURE

The test fixture and equipment are shown in figure 4 mounted on the test carriage of the Langley Landing Loads Track. The test fixture consists basically of a standoff structure, a vertical-drop frame, and a pitching beam. The standoff structure (which is attached to the framework of the carriage) supported a set of rails to restrict the drop frame to vertical motion. The drop frame, which is attached to the standoff structure by an electrically operated quick-release mechanism, moved on rollers along these rails. In a test, the drop frame was released

allowing the landing-gear tire to contact the runway surface. At touchdown, the tire produced a pitching moment which caused the pitching beam to rotate to a horizontal position. Also at touchdown, the drop frame activated a microswitch to enable the controller.

Lift, elevator, and nose gear force simulators were incorporated into the drop frame. The lift force simulator consisted of a double-acting air cylinder and piston mounted vertically on the drop frame and charged to a pressure of 207 kPa (30 psig). A steel plate was attached to the end of the piston rod, which passed through a hole in a fixed plate attached to the standoff structure. The piston was positioned so that the plate on the end of the piston rod was at a distance above the fixed plate equal to the vertical-drop height. These two plates made contact at touchdown, thereby developing a force equal to but opposing the gravitational force applied to the drop mass. The lift force was dumped shortly after touchdown by an electronically operated solenoid valve mounted in the air cylinder line. The elevator force simulator, a constant-force, bending-wire, energy-dissipating mechanism mounted between the drop frame and the pitching beam, opposed the pitching moment developed by the landing gear, thereby simulating a nose-up elevator force. The nose gear force simulator consisted of a shaped-aluminum honeycomb block mounted on a member of the drop frame so that contact with the pitching beam at an angle of 2° simulated nose gear touchdown. As the beam continued to rotate, the honeycomb was crushed providing a constant force of 8.9 kN (2000 lbf) to remove the rotational energy during simulated nose gear impact. The bending wire and honeycomb were replaced after each test.

The pitching beam was a welded, open, rectangular structure of steel I-beams 457 cm (180 in.) long and 61 cm (24 in.) wide. A cross beam aft of the forward end of the beam served as the crushing plate for the nose gear force simulator and attachment point for the elevator force simulator. The pitching beam was attached to the drop frame with a 5.08-cm-diameter (2-in.) steel pin, thus establishing the center of rotation of the beam. The modified main gear was attached to the pitching beam 68 cm (26.8 in.) aft of the beam center of rotation, which is the same as the fore-and-aft distance between the gear attachment to the wing and the center of gravity of the light airplane.

Since only one landing gear was tested, the total mass of the drop fixture was limited to 1518 kg (104 slugs), which is approximately one-half the mass of the light aircraft. Within this mass restriction, lead weights were attached at the rear of the pitching beam to balance the beam about the center of rotation. The pitching mass moment of inertia of the balanced beam was determined to be 997.9 kg-m^2 (736 slug-ft^2) which is only 40 percent of that required to simulate one-half the pitching mass moment of inertia of the light aircraft.

TEST FACILITY

The investigation was performed on the 29 500-kg (65 000-lbm) test carriage (shown in fig. 4) at the Langley Aircraft Landing Dynamics Facility[1] described in reference 5. All tests were conducted on a dry runway surface.

---

[1]Called the Langley aircraft landing loads and traction facility in reference 5.

TEST BUMPS

To determine the performance and evaluate the effectiveness of the active-control gear during traverse of abrupt elevation changes in the runway surface, two step bumps were installed (first bump at station 400) on the test surface so that the gear would encounter the bumps during the roll-out phase of the simulated landings. Photographs and the geometry of the step bumps are shown in figure 5. The dimensions of the bumps are given in figure 5(a). The profile of the bumps consisted of a 1.9-cm (0.75-in.) step at the leading edge which increased to 3.2 cm (1.25 in.) at 0.3 m (1.0 ft), remained constant at that height for 1.5 m (5.0 ft), and then decreased to a 1.9-cm (0.75-in.) step to the runway surface in 0.3 m (1.0 ft).

To determine the effect on the gear of the frequency of bump encounters, the bumps were spaced at distances determined by the forward speed of the carriage to produce frequencies of 2 and 4 Hz. The spacing d required to produce these frequencies at various forward speeds is shown in the table in figure 5(b).

In a recently repaired section of the runway surface, long wavelength changes in surface elevation of approximately the same magnitude as that of the step bumps were measured. These changes, which are designated as natural bumps in this paper, are illustrated and defined in figure 6. The photograph of figure 6 was taken with the surface flooded to a depth of approximately 1.3 cm (0.5 in.) to indicate the high points on the surface. The stations identified in the photograph correlate the peaks and troughs of the surface with the measured surface profile shown at the top of the figure. The most significant difference between the step bumps and the natural bumps is the wavelength, 2.1 m (7 ft) for the step bumps and approximately 18.0 m (59 ft) for the natural bumps.

INSTRUMENTATION

Twenty-seven variables measured and recorded during this investigation are listed and defined in table II. The types of measuring instruments used included: servo-type accelerometers to determine drop-frame forces; strain-gage-type transducers for measuring pneumatic and hydraulic pressures; slide-wire potentiometers for measuring displacements of the drop-frame and the landing-gear shock strut; a time-code generator for synchronizing timing of events; and an electronic timer for obtaining forward speed of the carriage. All outputs from the instruments were transmitted through signal-conditioning equipment, with the exception of those instruments supplying signals to the electronic controller. (See table II.) The outputs from the signal-conditioning equipment and the electronic controller were recorded on frequency-modulated tape recorders.

TEST PROCEDURE

The steps in the testing technique for the active gear were: (1) set the pitching beam to the desired pitch angle; (2) raise the drop frame to the appropriate height above the runway surface to provide the desired sink rate; (3) charge the lift force simulator to produce the required lift force; (4) open the isolation valve and charge the fully extended landing-gear strut to the desired hydraulic pressure; (5) propell the carriage to the desired speed; (6) actuate the quick-release mechanism at a preselected position along the runway to allow the drop frame and the landing gear to fall to the surface; (7) apply the lift force at touchdown, and shortly thereafter, activate a microswitch to enable the controller and also allow

the lift force to be removed in approximately 1 sec. The only difference in technique for the passive-gear tests was to leave the isolation valve closed to place the modified gear in a normal configuration. During each test, the drop frame, pitching beam, and landing gear were subjected to touchdown impact, rebound, pitch-over, and roll-out. At touchdown, the pitching beam rotated downward opposed by the elevator force simulator, contacted and crushed the nose gear simulator, and remained in a horizontal position during the roll-out.

For active- and passive-gear modes, tests were made with initial pitching-beam attitudes over a range of 0° to 13° and a range of sink rates from 0.9 to 1.7 m/sec (3 to 5.5 ft/sec). For the carriage, nominal forward speeds ranged from 8 to 80 knots. The 8-knot tests were made by towing the test carriage with a ground vehicle. In addition to forward-speed tests, stationary vertical-drop tests were made over a similar range of sink rates with the pitching beam locked in a horizontal position.

DATA REDUCTION

All data were filtered to 1000 Hz and recorded on analog magnetic tape. Following each test, the data channels were filtered to 100 Hz and reproduced on an oscillograph to permit evaluation of the quality of the test. After completion of the test program, the analog-tape data were processed through a low-pass filter (cut-off frequency of 400 Hz), digitized at 400 samples per second, and used to generate time-history plots for data analysis. The digitized data from the control accelerometer, the wing/gear (mass center) accelerometer, and the lift-cylinder pressure transducer were converted to forces (since the mass of the drop fixture and the piston area of the lift cylinder were constant) prior to generating the computer plots.

RESULTS AND DISCUSSION

Data and test conditions from the simulated landing tests of the active and passive modified landing gear are presented in table III. The control nomenclature and philosophy employed in this investigation are presented in the appendix. Representative data from tests over the range of touchdown parameters investigated are presented in figures 7 to 13. The data illustrate the control operation and show the effectiveness of the active gear in reducing forces applied to the mass center within the availabe shock-strut stroke.

ILLUSTRATION OF CONTROL OPERATION

To illustrate the operation of the electronic controller and the resulting effects on the pertinent landing-gear variables, oscillograph traces of controller outputs and landing-gear variables for a typical landing test are shown in figure 7. Figure 7(a) shows data obtained during landing impact and figure 7(b) shows data obtained during traverse of the step bumps. The data traces in figure 7(a) originate at an arbitrarily selected time (0 sec) before release of the drop fixture, continue through drop-fixture acceleration to touchdown, touchdown impact, and roll-out to static conditions at approximately 2.5 sec. The traces in figure 7(b) are for traverse of the step bumps for the time period of 15.5 to 17.5 sec. A detailed explanation of the controller functions and effects are presented in the following discussion.

Free-Fall

The data of figure 7(a) show that, at approximately 0.2 sec, the drop fixture was released and accelerated under the influence of gravity, as indicated by the control and mass-center acceleration traces, to touchdown at approximately 0.4 sec. The mass center also displaced toward the runway surface during this time period. The only other controller-output quantity that varied during this period was the force error. This quantity is simply a scaled value of the control acceleration, since the computation of the force error is not performed prior to controller enable.

Touchdown

The controller is enabled at touchdown (0.4 sec), and simultaneously, the lift force is applied as indicated by the increase in the lift-cylinder pressure. The control and mass-center accelerations make the transition from acceleration through zero to deceleration. The force error indicates the summation of the control force (scaled value of the control acceleration) and the limit force command, which is zero at the time of controller enable. The hydraulic and pneumatic pressures in the strut have not changed since the strut has not stroked (strut position equal zero). The strut position error, which is the summation of the input value of the desired static stroke (12.7 cm (5.0 in.) for this investigation) and the instantaneous value of the strut position, is set equal to the input value of the static stroke, since the strut position is zero. The controller initiates energy calculations, and when the tire/ground interface force exceeds the charging force of the strut, the strut begins to stroke, then the strut hydraulic pressure, pneumatic pressure, and deceleration force increase. The strut position error decreases as the strut position approaches the input value of the static stroke. When the potential energy of the strut equaled or exceeded the kinetic energy of the mass center at approximately 0.43 sec, the controller stored the instantaneous scaled value of the control acceleration as the limit force command and initiated control by enabling the servo loop.

Impact

The gear is now under active control. The control deceleration increases, the limit force command is constant, and hence, the force error increases. However, there is a slight delay before the servo spool displaces to initiate removal of fluid from the strut, and hence, the strut hydraulic pressure increases. At a time of approximately 0.45 sec, the servo spool is against the mechanical stop and is removing fluid from the strut, as shown in figure 7(a) by the decrease in the hydraulic pressure, even while the shock strut is compressing at near the maximum rate. The hydraulic pressure decreases to a value below the charging pressure of the fully extended strut, and the control deceleration reaches a maximum value and starts to decrease. As the control deceleration decreases and the limit force command remains constant at the impact value, the force error changes sign as it passes through zero, requiring that fluid be added to the strut to maintain the control deceleration force at the value of the limit force command until the wing/gear interface velocity (mass-center velocity for this investigation) has decreased to the transition velocity. Note that again there is a slight delay between the force error signal, which changes sign at approximately 0.57 sec, and the response of the servo-spool displacement, which starts transition from removal of fluid to the addition of fluid at approximately 0.60 sec.

Transition

The mass-center velocity (touchdown sink rate minus decrement in wing/gear interface velocity) decreases during the 0.57- to 0.60-sec time period to the value of the transition velocity, and the controller starts transition of the impact limit force command to the roll-out limit force command of zero. The control continues to add fluid to the strut in an attempt to maintain the control deceleration force equal to the instantaneous transition value of the limit force command. The mass-center displacement, and hence the strut position, reach a maximum value and start to decrease as the mass rebounds. The control continues to add fluid to the strut and initiates the transition of the limit force command. When the shock strut becomes fully extended (strut position equal to zero) at approximately 0.88 sec, the controller terminates the transition phase, sets the limit force command to zero, and deactivates control, as indicated by the force error returning to zero at approximately 0.88 sec. Again, a delay in the servo-spool response to the force-error signal results in fluid being added to the fully extended strut with a dramatic increase in strut hydraulic and pneumatic pressures. However, since the tire has rebounded above the runway surface, as indicated by the strut position, the increased strut pressures do not affect the control or mass-center forces. After the delay, the servo spool displaces through the bias position and removes fluid from the strut, thus reducing the strut pressures.

Roll-Out

Since the transition phase of the control logic was terminated by the controller during mass-center rebound, subsequent control of the gear is accomplished using the logic of the roll-out phase. The tire returns to the surface and the strut starts to stroke at approximately 1.06 sec. Fluid is being removed from the strut as indicated by the servo-spool displacement and the decreasing strut pressures. As the strut continues to compress and the servo spool approaches the bias position, the pressures stabilize, and the control and mass-center accelerations decrease. At approximately 1.49 sec, the control deceleration force exceeds the 2.2-kN (500-lbf) deadband limit. The controller sets the limit force command to 2.2 kN (500 lbf), the force error commands the removal of fluid from the strut, and after a slight delay, the servo-spool displacement indicates that fluid is being removed. The strut pressures, which have been increasing, decrease and control and mass-center decelerations diminish. At approximately 1.59 sec, the control deceleration force decreases below the 2.2-kN (500-lbf) deadband limit and the controller sets the limit force command to zero. The strut position and mass-center displacement reach their maximum value at approximately 1.7 sec, and since the strut position is greater than the desired static stroke, the controller adds fluid to the strut as indicated by the servo-spool displacement trace. At approximately 2.05 sec, the strut position is at the desired static stroke, as indicated by the zero value of the strut position error, and the servo spool returns to the bias position.

Step Bumps

The roll-out continues with no control required until the first step bump is encountered at approximately 15.54 sec (fig. 7(b)). The gear compresses, the strut pressures increase, and the control deceleration force exceeds the 2.2-kN (500-lbf) deadband limit at approximately 15.59 sec. The controller sets the limit force command to 2.2 kN (500 lbf), and the force error commands the removal of fluid from the strut. Fluid is removed as indicated by the servo-spool displacement, and the strut

pressures and the control deceleration decrease. At approximately 15.64 sec, the control deceleration force becomes less than the 2.2-kN (500-lbf) deadband limit and the controller sets the limit force command to zero and the servo-spool displacement returns to the roll-out bias position. At approximately 15.68 sec: the control acceleration force exceeds the 2.2-kN (500-lbf) deadband limit; the controller sets the limit force command to 2.2 kN (500 lbf), reverses the sign of the analog limit force command signal, and solves for the force error signal which indicates that fluid should be added to the strut. Fluid is added as indicated by the servo-spool displacement, and the strut pressures increase and the control acceleration decreases. The controller continues to function in the manner described through the second bump encounter, which occurs at approximately 16.16 sec.

The preceding discussion illustrates the response of the landing gear to the active-control system which is directed by the electronic controller through the application of the control logic and signals from the feedback transducers.

EFFECTIVENESS OF ACTIVE GEAR

The effectiveness of the active-control gear relative to the passive gear in reducing ground loads applied to the simulated airplane during touchdown impact and landing roll-out over an uneven surface is illustrated by comparisons of mass-center forces and shock-strut strokes for similar touchdown parameters. The variables of mass-center force and shock-strut stroke were selected, since the purpose of the active gear is to reduce the forces applied to the aircraft during ground operations within the stroking capability of the landing-gear shock strut. Data are presented and discussed for two categories of tests, vertical-drop tests and landing-simulation tests. Results of the vertical-drop tests (zero ground speed) illustrate the effectiveness of the active gear as a function of touchdown sink rate when the effects of strut binding friction due to pitch attitude and horizontal velocity (ground speed), are minimal. The data obtained from the landing-simulation tests, however, are more representative of the effectiveness that may be obtained during aircraft landings with the active gears.

The force plots, used for analyzing the effectiveness of the active-control gear, were faired through the mean values of the high-frequency oscillations to obtain the basic forcing function. Typical time histories of the mass-center force data and the fairing technique applied to these data are presented in figure 8 for an active-gear test. The force data in figure 8(a) were obtained during the impact phase of an active-gear test. The accelerometer was mounted at the mass center beside the control accelerometer which supplied the signal used by the electronic controller to apply the control laws. The force data shown in figure 8(b) were obtained from the mass-center control accelerometer during traverse of the step bumps.

Vertical-Drop Tests

The mass-center force and strut stroke data from vertical-drop tests of active and passive gears are presented in figure 9 for a pitch attitude of 0° at zero ground speed. The strut charging pressure varied from 1248 to 1834 kPa (181 to 266 psig) for these tests. The data are plotted from the time of release of the drop fixture (0 sec), through impact, rebound of the fixture, and touchdown for secondary impact. In figure 9, positive mass-center forces represent gravitational acceleration during free-fall to obtain the desired touchdown sink rate; whereas, the negative mass-

center forces represent the deceleration of the fixture from ground forces applied through the landing-gear shock strut.

Touchdown Impact

For the data in figure 9(a), the touchdown sink rate was 0.9 m/sec (3.0 ft/sec) and the charging pressure for the fully extended strut was 1248 kPa (181 psig). During initial impact, the active gear reduced the deceleration force by 8 percent relative to the passive gear. However, the shock-strut stroke required by the active gear to achieve this force reduction was 18 percent greater during the initial impact than the stroke of the passive gear. The strokes required by the active and passive gears during initial impact represent only a small percentage of the available stroke, as shown in figure 9. The major stroking of the gear occurs during secondary impact, as illustrated in figure 9(d).

The data in figure 9(b) are for a touchdown sink rate of 1.2 m/sec (4.0 ft/sec) and a charging pressure of 1351 kPa (196 psig) for the fully extended strut. For these conditions, the active gear reduced the decelerating force experienced by the passive gear by 19 percent and required a stroke 38 percent greater than that of the passive gear.

The data for a touchdown sink rate of 1.5 m/sec (5.0 ft/sec) and a charging pressure of 1351 kPa (196 psig) are presented in figure 9(c). The active gear reduced the decelerating force relative to that of the passive gear by 20 percent and required a 34-percent greater stroke.

Data are presented in figure 9(d) for a touchdown sink rate of 1.7 m/sec (5.5 ft/sec) and a strut charging pressure of 1834 kPa (266 psig). The data are plotted from the time of touchdown (0 sec) through initial impact, drop-fixture rebound, and secondary impact to an essentially static position (gear supporting drop-fixture mass). For these touchdown parameters, the active gear reduced the initial impact decelerating force relative to that of the passive gear by 32 percent with a corresponding 43-percent increase in shock-strut stroke.

Secondary Impact

During secondary impact, the active gear reduced the decelerating force by 57 percent, but at the expense of an apparently large increase in strut stroke when compared with the recorded passive-gear stroke. (See fig. 9(d).) However, upon observing the small stroke of the gear after the passive-gear drop test, the drop fixture was manually vibrated and the fixture settled onto the gear until the gear stroked to approximately 12.1 cm (4.75 in.). Therefore, the small value of the recorded stroke for the passive gear was attributed to frictional effects between the drop fixture and the standoff structure. Consequently, the active-gear stroke required was only 52 percent greater than that of the passive gear when the friction force was relieved. Such effects would be alleviated during the active-gear test because the control would be adding or removing fluid from the gear, thus applying oscillating forces to the test fixture.

Response to Control

The limit force command (an output signal generated by the electronic controller) is superposed on the mass-center force plot in figure 9(d) to illustrate the variation of mass-center force in response to the control system. During initial impact, the controller set the impact-limit force command to 9.2 kN (2080 lbf) and the mass-center force for the active gear peaked at 20.5 kN (4600 lbf), which is considerably lower than the 30 kN (6740 lbf) obtained during the passive-gear test. As long as the mass-center force is greater than the limit force command, the control system removes fluid from the strut at a rate which varies as the magnitude of the force difference. As the mass-center force decreases toward the limit force command, the control system reduces the rate at which fluid is removed from the strut, and when the mass-center force becomes less than the limit force command, adds fluid to the strut. This operation is illustrated between 0.2 and 0.4 sec, by the essentially constant mass-center force.

When the strut becomes fully extended at about 0.41 sec, the control becomes inactive, as indicated by the zero output of the limit force command. Control is initiated again when the gear starts to stroke during the secondary impact at approximately 0.61 sec. At this time the mass-center force indicates that the drop fixture is accelerating toward the surface with a force applied to the drop fixture of approximately 4.9 kN (1100 lbf). The controller sets the limit force command to 2.7 kN (600 lbf) and pumps fluid into the gear to decrease the accelerating force to a value within the ±2.7-kN (±600-lbf) deadband; and, when this is accomplished, sets the limit force command to zero. When the mass-center decelerating force exceeds 2.7 kN (600 lbf), the controller sets the limit force command to 2.7 kN (600 lbf) and removes fluid from the strut to limit the decelerating force. In the control philosophy section (the appendix), the force deadband was defined as ±2.2 kN (±500 lbf), based on results from analytical simulations. However, the force deadband during control operation was output as ±2.7 kN (±600 lbf), which is attributed to alteration of the signal in the electronic circuitry. This phenomenon occurred consistently throughout the test program. The control system was more effective during the secondary impact than during the initial impact, since the mass-center force exceeded the limit force command by only 23 percent during secondary impact; whereas, the mass-center force during initial impact peaked at a value 120 percent greater than the limit force. This increased effectiveness is attributed to the lower strut compression velocity during secondary impact which permits the control system, even with the delayed response previously noted, to be more effective.

In summary, the vertical-drop test results indicated that the effectiveness of the active gear increased with touchdown sink rate. During initial impact, decelerating force reductions of 8 percent at 0.9 m/sec (3 ft/sec) to 32 percent at 1.7 m/sec (5.5 ft/sec) were obtained. As shown in figure 9(d), decelerating force reductions as great as 57 percent may be obtained during secondary impact. Although it is not shown on all of the time-history plots, the maximum stroke occurs during secondary impact and the maximum stroke required for any of these tests, when the control system was operating properly, was less than 85 percent of the available stroke.

Landing-Simulation Tests

Landing-simulation tests provide a more realistic representation of the loads and motions imposed on the landing gear during an actual aircraft landing than those obtained during vertical-drop tests, which are normally employed to verify landing-

gear designs. The principal difference between these types of tests is the strut binding-friction force. Strut binding friction results from moments developed on the gear by the fore-and-aft forces applied at the axle during wheel spin-up at impact or by encounters with elevation unevenness of the landing surface during roll-out. The nominal touchdown ground speed for the aircraft simulated in this investigation was 80 knots at a pitch attitude of approximately 13°. However, tests were made at lower ground speeds to obtain data during traverse of the step and natural bumps at varying roll-out speeds. Consequently, touchdown impact data were obtained at all ground speeds investigated and are employed in the discussion of the effectiveness of the active gear.

Data from the landing-simulation tests of the active and passive gears are presented in figures 10 to 13 for the following touchdown and roll-out parameters: horizontal velocities (ground speeds) from 8 to 80 knots; pitch attitudes from 2° to 13°; sink rates from 0.9 to 1.7 m/sec (3.0 to 5.5 ft/sec); gear charging pressures at touchdown from 662 to 2317 kPa (96 to 336 psig), and step bump encounters at frequencies of 2 and 4 Hz. These data represent the three significant phases of the simulated landing tests; touchdown impact, traverse of the step bumps, and traverse of the natural bumps.

Touchdown Impact Phase

Data for the mass-center force, limit force command, and shock-strut stroke obtained during the touchdown impact phase of the landing-simulation tests are presented in figures 10(a) to 10(g) for the various touchdown parameters. The data are plotted from touchdown (zero time) through initial impact, mass (drop fixture) rebound, and secondary impact to an essentially static condition.

Strut charging pressure.- Prior to each test, the initial strut charging pressure was set to the same value for both the active and passive gears. However, the strut pressures of the active gear at touchdown for 40 and 80 knots are lower than those of the passive gear, as noted in figure 10. An examination of the test data during catapult and prior to touchdown showed that, for the active gear, the initial charging pressure decreased. This decrease is attributed to a launch acceleration force of approximately 3g for the test carriage, which apparently affects the operation of the servovalve that controls the strut pressure. As previously noted, the servovalve was mounted on the hydraulic power unit with the axis of motion of the power spool oriented 90° to the direction of carriage launch acceleration in an attempt to minimize inertial motion of the power spool during launch. This launch impulse is unique to the test facility and, hence, is not encountered in actual airplane landings.

Further indication that launch acceleration affects the strut charging pressure of the active gear is shown by the vertical-drop tests (fig. 9) and the 8-knot towed test (fig. 10(a)). With no launch acceleration, the values of strut charging pressures for both the active- and passive-gear tests were approximately the same. An attempt was also made to obtain the same strut charging pressure for the active and passive gears at impact by charging the active gear to a higher pressure than the passive gear prior to launch. This technique was partially successful as shown by comparing the active- and passive-gear pressures in figures 10(b) and 10(c). However, the technique was not as effective for the higher gear pressures (figs. 10(f) and 10(g)), possibly because of the higher servovalve flow rates which result when the pressure drop across the servovalve is greater.

Effect of ground speed.- The effectiveness of the active gear for reducing the forces applied to the airframe during the touchdown impact phase are illustrated by comparisons of active- and passive-gear forces during initial impact, rebound from initial impact, secondary impact, and initiation of roll-out. The effect of ground speed on the performance of the active gear is shown in figures 10(a) to 10(c) for a nominal sink rate of 1.7 m/sec (5.5 ft/sec) and ground speeds of 8, 40, and 80 knots, respectively. Data for a ground speed of 8 knots, figure 10(a), show that during initial impact the active gear reduced the decelerating force relative to that of the passive gear by 31 percent with a 57-percent increase in strut stroke. During rebound of the mass, the force was reduced by 55 percent. This reduction is a residual effect of control during the initial impact, since the control is not active during the rebound period once the shock strut becomes fully extended. Deactivation of the control is indicated by the zero value of the limit force command. During secondary impact, the limit force command shows that the control was reactivated when the decelerating force exceeded the -2.7-kN (-600-lbf) deadband limit force. The decelerating force was reduced by 30 percent with an 87-percent increase in strut stroke.

Data for a ground speed of 40 knots (fig. 10(b)) show that, during initial impact, the active gear reduced the decelerating force by 9 percent with a 40-percent increase in strut stroke. During rebound, the active-gear accelerating force was 37 percent greater than that which occurred with the passive gear. The mass-center decelerating force during secondary impact exceeded the -2.7-kN (-600-lbf) deadband (roll-out) limit force at a time of approximately 1 sec but was limited by the control to this value. The oscillatory motion of the limit force command, occurring at about 1 sec, results from the controller responding to the mass-center force oscillations above and below -2.7 kN (-600 lbf) as shown at a time of approximately 1.2 sec in figure 8(a). The strut stroke required by the active gear during secondary impact was 41 percent greater than that required by the passive gear.

The data for a ground speed of 80 knots (fig. 10(c)) show that, during initial impact, the active gear reduced the decelerating force by 11 percent with an increase in strut stroke of 168 percent. During rebound, the active gear was effective in reducing the accelerating force by 36 percent. The active-gear decelerating force during secondary impact was limited to the decelerating deadband limit force of -2.7 kN (-600 lbf) as shown at a time of 1.1 sec and required an increase in strut stroke of 258 percent relative to that occurring with the passive gear.

Binding-friction effects.- As previously stated, the series-hydraulic control concept reduces the ground loads applied to the airframe by controlling the shock-strut hydraulic force. Consequently, the effectiveness of the control is greatly reduced when significant friction force is present in the shock strut. The presence of significant binding-friction forces in the shock strut during the touchdown impact phase for the tests conducted at 40- and 80-knot ground speeds is discussed in the following section. Under dynamic conditions the presence of large binding-friction forces in a landing-gear shock strut cause a "stick-slip" phenomenon to occur as the strut strokes. (See ref. 6.) Vertical-drop tests of landing gears have minimal binding-friction effects where the shock-strut longitudinal axis is oriented normal to the surface and the ground speed is zero. For example, smooth stroking to the maximum touchdown impact value occurred for the active gear during the touchdown impact phase at ground speeds of 0 and 8 knots (figs. 9(d) and 10(a), respectively). In contrast, the active-gear strut-stroke data presented in figures 10(b) and 10(c) for the 40- and 80-knot ground speeds show that the strut stops stroking during the period of maximum stroking velocity and resumes stroking toward the maximum touchdown impact stroke, after which the "stick-slip" phenomenon is also observed as the strut

stroke decreases. Binding friction would also be more likely to occur during the touchdown impact phase, since the spacing between the shock-strut bearing surfaces is a minimum when the strut is fully extended. These factors support the observation that considerable binding friction was present during the touchdown impact phase of the tests conducted at 40- and 80-knot ground speeds and is attributed to the greatly increased "spin-up" drag loads developed at these higher speeds.

On the basis of the data presented in figures 10(a) to 10(c), the active gear was effective in reducing the ground loads applied to the mass center during touchdown impact at the ground speeds investigated. However, the presence of binding friction in the shock strut was most pronounced at the higher ground speeds and drastically reduced the effectiveness of the active gear. The effectiveness of the active gear during rebound is a function of the operation of the control during initial impact, and in two of the three tests presented, was very effective. During secondary impact, the mass-center decelerating force was limited by the control to the designed roll-out limit-force deadband of ±2.7 kN (±600 lbf).

Effect of strut charging pressure.- The active-gear data in figures 10(d) and 10(e) are for landing-simulation tests in which the strut pressure at touchdown was the only difference in the touchdown parameters. The pressure in the active gear was 662 kPa (96 psig) for the data shown in figure 10(d) and 993 kPa (144 psig) for the data shown in figure 10(e). During touchdown impact, the effectiveness of the active gear is a function of the responsiveness of the controller and the rate of flow of the hydraulic fluid through the servovalve. For these tests, the response of the controller is the same; hence, the effectiveness of the active gear would be a function of the servovalve flow which is dependent upon the pressure drop across the servovalve. The data in figure 10(d) for the lower strut pressure show a decelerating-force reduction of 13 percent during initial impact. The decelerating-force reduction during impact for the higher strut pressure (fig. 10(e)) was 20 percent. The stroking characteristics of the strut during initial impact are similar for both tests, indicating that the binding-friction forces are similar. Therefore, since the principal difference between these two active-gear tests was the strut pressure, the increase in the effectiveness of the active gear may be attributed to the increased flow capability of the servovalve to remove fluid from the strut because of the higher pressure drop across the valve.

Repeatability of active-gear data.- The data shown in figures 10(f) and 10(g) illustrate the degree of repeatability of active-gear data during initial impact for tests conducted at approximately the same touchdown parameters. The decelerating forces for the active gears were about the same during initial impact and resulted in a nominal 8-percent reduction relative to that generated with the passive gear. The strut strokes during initial impact for the two tests have different signatures. This difference is probably caused by strut binding. Consequently, the controller performed differently during the rebound phase. In both tests, the controller set the impact-limit force command to 3.6 kN (800 lbf), but transition was initiated at about 0.1 sec for the data presented in figure 10(f) and at about 0.2 sec for the data presented in figure 10(g). As a consequence, the accelerating forces for the two active-gear tests were different during rebound, and hence, the detailed operation of the controller differed during secondary impact. In spite of these differences, the control was effective in limiting the accelerating and decelerating forces to the roll-out limit command forces of ±2.7 kN (±600 lbf) during secondary impact and initiation of roll-out.

Data for the touchdown impact phase of the landing-simulation tests show that the active gear was effective in reducing the mass-center forces relative to those generated by the passive gear. During initial impact, mass-center force reductions of 31 percent at a ground speed of 8 knots to 8 percent at a speed of 80 knots were obtained. The reduction in the effectiveness of the active gear at the higher ground speeds may be attributed to the larger binding-friction forces generated in the strut which the hydraulic control system cannot control. As a result of control during initial impact, the active gear was generally very effective in controlling the mass-center accelerating forces during rebound of the drop-fixture mass. During secondary impact, the mass-center forces were limited by the control to the designed roll-out limit forces of ±2.7 kN (±600 lbf). The maximum shock-strut stroke required by the active gear, which occurs during the secondary impact of the touchdown impact phase, did not exceed 85 percent of the available stroke.

Traverse of Step Bumps

Mass-center force and strut stroke data from the landing-simulation tests of the active and passive gears during traverse of the step bumps are presented in figure 11 for the range of ground speeds and bump-encounter frequencies. The data are plotted from an arbitrary time before encounter with the first bump (zero time in the figure) through traverse of the second bump.

Encounter frequency of 2 Hz.- Data for the active and passive gears during traverse of the step bumps at ground speeds of 8, 40, and 80 knots and bump spacings for an encounter frequency of 2 Hz are presented in figures 11(a) to 11(c) to permit evaluation of the effectiveness of the active gear as a function of ground speed. The time histories of the mass-center force for the active and passive gears differ since the controller regulates the gear force in response to the dynamic loading resulting from previous control action. Therefore, the effectiveness of the active gear must generally be defined in terms of the peak forces generated by each of the gears during traverse of the step bumps. When compared on this basis, the data in figure 11(a) indicate that the active gear was very effective in reducing the mass-center decelerating forces during traverse of the step bumps at a ground speed of 8 knots; 28 percent reduction during initial contact with first bump, and 60 percent reduction during initial contact with the second bump. The active gear was also effective in reducing the mass-center decelerating forces during traverse of the bumps at 40 and 80 knots, as shown in figures 11(b) and 11(c), respectively. At a ground speed of 40 knots, the mass-center decelerating force reductions were 31 percent during initial contact with the first bump and 55 percent during initial contact with the second bump. For the 80-knot ground speed, the reductions were 28 and 15 percent, respectively.

As shown, the effectiveness of the active gear generally decreased during initial encounter with the second bump with increasing ground speed. This decrease in effectiveness may be attributed to two factors; large binding-friction forces developed in the strut during encounter with the step bumps and/or inadequate response of the control system. Previously, it has been shown that, during touchdown impact, large binding-friction forces reduce the effectiveness of the active gear. The magnitude of these forces during encounter with the step bumps is unknown. However, the strut has been stroked to near the static position prior to encounter with the bumps; hence, the distance between the strut bearings is greater and the binding-friction forces should be smaller than those occurring at touchdown. With regard to the control system response as the ground speed increases, the stroking rate of the shock-strut increases as the gear traverses the bumps; hence, the rate of

change of the strut hydraulic pressure and the shock-strut force increase. Thus, an increase in the response of the control system would be required at the higher ground speeds for the active gear to maintain the effectiveness demonstrated at the 8-knot ground speed.

Effect of ground speed.- The following discussion illustrates the deterioration of the response of the control system with increase in ground speed during traverse of the 2-Hz bumps. The control limited the mass-center decelerating forces to values within the range of the roll-out limit forces programmed into the computer (±2.7 kN (±600 lbf)) during encounter with the bumps at the 8-knot ground speed (fig. 11(a)). During encounter with the bumps at the 40-knot ground speed (fig. 11(b)), the mass-center decelerating forces for the active gear during initial contact with each of the bumps were 33 percent greater than the roll-out limit forces. The data for a ground speed of 80 knots (fig. 11(c)) show that the mass-center decelerating force for contact with the first bump was 83 percent greater than the roll-out limit force and was even greater during initial contact with the second bump. The fact that the control system could not limit the mass-center decelerating forces to the value of the programmed roll-out limit forces indicates that the response of the control system was marginal during encounter with the step bumps at speeds of 40 and 80 knots. The marginal performance of the control system during traverse of the step bumps is further illustrated by data in table III which show that, during traverse of the step bumps, only one test of the eight conducted at a ground speed of 40 knots and two of the seven conducted at a speed of 80 knots indicated effective operation of the active gear. This marginal performance of the control system at these speeds may be attributed to the following: the electronic controller was designed and tuned primarily for the touchdown impact phase and not the roll-out phase (see ref. 4), and the design of the hydraulic power unit was not optimized for providing minimum flow losses.

In spite of these factors, the active gear was surprisingly effective in reducing the mass-center forces relative to those obtained with the passive gear. This was true for those tests during which the control system was able to respond to the ground forcing function during traverse of the step bumps spaced for an encounter frequency of 2 Hz.

Encounter frequency of 4 Hz.- Data for the active and passive gears during traverse of step bumps spaced for encounter frequencies of 2 and 4 Hz at a ground speed of 40 knots are presented in figures 11(b) and 11(d), respectively. During initial contact with the first bump in the test conducted at the 4-Hz spacing, the active gear reduced the mass-center decelerating force by only 6 percent, compared with the 31-percent reduction achieved during the test conducted for an encounter frequency of 2 Hz. This difference may be attributed to the low-frequency response of the control system, as previously discussed, during bump encounters at the 40-knot ground speed. As a result of the control system operation following traverse of the first bump and the shorter time interval between bump encounters, the control system did not respond during traverse of the second bump, as indicated by the 54-percent increase in mass-center decelerating force for the 4-Hz test compared with the 55-percent reduction obtained during the 2-Hz test.

Servovalve/relief-valve interaction.- Another factor which influenced the effectiveness of the active gear during traverse of the step bumps was an unexpected interactive effect between the pressure-relief valves and the servovalve. The effect of inadvertent operation of these valves on the effectiveness of the active gear is illustrated in figure 12 for traverse of the step bumps at a ground speed of 80 knots and a bump encounter frequency of 2 Hz. At initial encounter with the first step

bump, the strut hydraulic pressure (fig. 12(b)) very quickly exceeds the opening pressure for the relief valves, thus initiating flow from the gear to the low-pressure reservoir. Maximum strut pressure occurring when the servo-spool displacement is zero indicates that flow was through the pressure-relief valves and not the control servovalve. The subsequent phase differences between the operation of the servovalve and the pressure-relief valves resulted in an undesirable interactive effect characterized by large mass-center force oscillations at a frequency of about 8 Hz. As shown in figure 12(a), the interactive phenomena continue until the gear has completely traversed the step bumps. As a result of this interaction the active gear was not effective in reducing the mass-center forces relative to those obtained with the passive gear. The interactive operation is the result of an overly conservative setting of the opening pressure for the relief valves and not a design fault in the electronic controller.

Summarizing the results obtained during traverse of the step bumps, the active gear was surprisingly effective in reducing the mass-center forces at all ground speeds investigated when the effects of prior control action, strut binding friction, control response, and/or servovalve/relief-valve interaction were not dominant factors.

Traverse of Natural Bumps

Presented in figure 13 are typical data for mass-center forces and shock-strut strokes from active- and passive-gear landing-simulation tests during traverse of the natural bumps at ground speeds of 40 and 80 knots. Data were not obtained for a ground speed of 8 knots. The data are presented to evaluate the effectiveness of the active gear during traverse of surface unevenness having approximately the same amplitude as that of the step bumps, but with a more gradual onset. The data are plotted from a time (zero time) corresponding to a track station of approximately 980 (see fig. 6) through track station 1180.

Effect of ground speed.- Data are presented in figure 13(a) for the active and passive gears during traverse of the natural bumps at a ground speed of 40 knots. The control deadband of ±2.7 kN (±600 lbf) is shown in the figure to illustrate that neither the active nor the passive gears produced mass-center forces greater than the roll-out (deadband) limit forces during traverse of the natural bumps at 40 knots. Within the roll-out limit command forces, the active and passive gears were able to accommodate the strut stroking rates and the maximum strokes imposed on the gear by the forcing function applied during traverse of the bumps at a speed of 40 knots. Consequently, the control system for the active gear was inactive and the forces produced by the active gear were about the same as those of the passive gear.

Data obtained from tests of the active and passive gears during traverse of the natural bumps at a ground speed of 80 knots are presented in figure 13(b). The numbers assigned to the mass-center decelerating-force peaks correspond to those shown on the track surface profile (fig. 6) and are used to correlate mass-center forces with the changes in surface profiles. To illustrate the effects of bump amplitudes and the rate of change of these amplitudes on gear forces, hence mass-center forces, the data obtained during traverse of bumps 1 and 2 are discussed. The track surface profile (fig. 6) shows that bump 1 has an amplitude almost twice that of bump 2, but had a shallower slope than bump 2. The mass-center forces for the passive gear (fig. 13(b)) during traverse of bump 2 are approximately twice those developed during traverse of bump 1. Thus, the rate of change of surface elevations had a greater

influence on the force developed by the gear than the amplitude of the elevation change. This agrees with oleo-pneumatic shock-strut theory that defines the hydraulic force (which accounts for about 90 percent of the dynamic force developed by the strut) as a function of the shock-strut velocity. Therefore, the series-hydraulic control system, assuming adequate control system response and similar binding-friction effects, should be more effective during traverse of the bumps having steeper slopes. As shown in figure 13(b), the active gear was effective in reducing the mass-center decelerating force, relative to that of the passive gear, by 62 percent during traverse of bump 2. During traverse of bump 1, the reduction in mass-center decelerating force was only 13 percent. The active gear was also effective in reducing the mass-center decelerating force during traverse of bump 3 by 24 percent. The control system response was adequate for controlling the gear during traverse of the natural bumps at the 80-knot ground speed, since all active-gear mass-center forces, decelerating and accelerating, were limited to the roll-out limit force command of ±2.7 kN (±600 lbf).

Data for strut hydraulic pressure and servo-spool displacement during traverse of the natural bumps at a ground speed of 80 knots are shown in figure 13(c). These data show that, when the strut hydraulic pressure does not exceed the opening pressure of the relief valves, the interactive effects between the control system and the relief valves are avoided and the control system performs effectively. (See fig. 13(b).)

Servovalve/relief-valve interaction.- Additional data in figures 13(d) and 13(e) for traverse of the natural bumps at a ground speed of 80 knots illustrate the detrimental effect of interaction between the control system and the pressure-relief valves. The active gear was effective in reducing the mass-center forces during traverse of the first and second bumps (see fig. 13(d)) when the strut hydraulic pressure was less than the opening pressure for the relief valves. (See fig. 13(e).) The mass-center decelerating and accelerating forces were reduced by 51 and 72 percent, respectively. However, the strut hydraulic pressure exceeded the opening pressure of the relief valves during encounter with the third bump, and the interactive effect resulted in overcontrol of the servovalve, as shown by the large transients in servo-spool displacement and the characteristic 8-Hz oscillations of the mass-center force. Consequently, the active gear was not effective during traverse of the third bump.

In summary, the results for the active and passive gears during traverse of the natural bumps show that the active gear is very effective in reducing the force applied by the gear to the mass center. The deterioration in the effectiveness of the active gear resulting from interaction between the control system and the pressure-relief valves is due to improper setting of the relief pressure and not to faulty control system design.

CONCLUDING REMARKS

An experimental investigation was conducted on a series-hydraulically controlled main landing gear for a light airplane to determine the feasibility and the potential of such a gear in reducing ground loads applied through the gear to the airframe. The investigation included vertical-drop (zero ground speed) and landing-simulation tests. The potential of the active gear was evaluated for performance during touchdown impact and during traverse of two types of surface unevenness: abrupt discontinuities (step bumps), representative of uneven settlement of runway sections; and longer wavelength variations in runway elevation (natural bumps).

Results show that, during the impact phase of a landing, the active gear was effective in reducing ground loads applied to the simulated airplane relative to those generated by the passive gear. Data from the vertical-drop tests show that the effectiveness of the active gear increases with increases in touchdown sink rate. For example, results showed an 8-percent reduction for a sink rate of 0.9 m/sec (3 ft/sec) and a 32-percent reduction for a sink rate of 1.7 m/sec (5.5 ft/sec). However, data for the touchdown impact phase of the landing-simulation tests show that, for a constant touchdown sink rate, the effectiveness of the active gear is reduced as the touchdown ground speed is increased; 31 percent reduction at 8 knots, 9 percent reduction at 40 knots, and 11 percent reduction at 80 knots. These reductions in effectiveness may be attributed to increases in shock-strut binding-friction forces resulting from increased wheel "spin-up" drag at the higher ground speeds.

Data obtained during traverse of the step bumps was not as consistent as that obtained during the touchdown impact phase. The electronic controller was designed and tuned for the touchdown impact phase of a landing and not for the roll-out phase. In addition, an unexpected interaction between pressure-relief valves in the hydraulic power unit and the control servovalve resulted in adverse performance of the control system during traverse of the step bumps for some of the tests. Because of these factors, only a limited number of tests indicated effective operation of the active gear during traverse of the step bumps. For those tests during which the control system was operating properly, the active gear was very effective in reducing the mass-center decelerating forces; maximum reductions of 60 percent at a ground speed of 8 knots, 55 percent at a speed of 40 knots, and 28 percent at a speed of 80 knots.

The results from the tests during traverse of the natural bumps show that, for a ground speed of 40 knots, the rate of change of surface elevation did not result in developing mass-center forces greater than the roll-out limit forces programmed into the control system. Consequently, the control system was inactive and the mass-center forces produced by the active gear were about the same as those of the passive gear. Interaction between the servovalve and the relief valves also occurred during traverse of the natural bumps at a ground speed of 80 knots, but the occurrence was not encountered as frequently as it was during traverse of the step bumps. During traverse of the natural bumps at a ground speed of 80 knots, the active gear was effective in reducing the mass-center forces; maximum reductions in decelerating force of 62 percent and accelerating force of 72 percent were obtained.

The overall results of this investigation show that a series-hydraulically controlled landing gear is feasible and that such a gear is very effective in reducing the loads, relative to those generated by the passive gear, transmitted by the gear to the airframe during ground operations.

Langley Research Center
National Aeronautics and Space Administration
Hampton, VA 23665
June 29, 1982

TABLE I.- SPECIFICATIONS OF HYDRAULIC-POWER-UNIT COMPONENTS

Component	Specifications
Low-pressure reservoir	0.19 m^3 (50 gal)
Hydraulic filters	10 μm with 20.7-MPa (3000-psig) rating
Hydraulic pump	0.04 m^3/min (9.3 gal/min) at 20.7 MPa (3000 psig) and 1800 rpm
Electric motor	Three phase, 80 A, 220 V
High-pressure accumulator	0.004 m^3 (1 gal), 20.7 MPa (3000 psig)
Servovalve	Three stage, 0.76 m^3/min (200 gal/min) for pressure drop of 6.9 MPa (1000 psig), 60 Hz
Pressure-relief valves	1.38 to 34.5 MPa (200 to 5000 psig), 0.454 m^3/min (120 gal/min)
Isolation valve	Gate, 20.7 MPa (3000 psig), 3.8-cm (1.5-in.) diam
Flexible hose	5.1-cm (2.0-in.) o.d., wire-wrapped, reinforced, burst pressure of 82.7 MPa (12 000 psig), working pressure of 20.7 MPa (3000 psig)
Bias-pressure pickup	Strain-gage pressure transducer, 34.5 MPa (5000 psig)
Surge suppressor	0.00095 m^3 (1 qt), working pressure of 20.7 MPa (3000 psig)

TABLE II.- MEASURED VARIABLES AND MEASURING EQUIPMENT

Measured variables	Equipment	
	Transducer type	Range
Model		
Pitching-beam normal acceleration	Servo accelerometer	±3g
Drop-fixture vertical acceleration	Servo accelerometer	±3g
Carriage longitudinal acceleration	Strain-gage accelerometer	±10g
Carriage lateral acceleration	Strain-gage accelerometer	±10g
Carriage vertical acceleration	Strain-gage accelerometer	±5g
Hub vertical acceleration	Servo accelerometer	±25g
Hub longitudinal acceleration	Servo accelerometer	±50g
Pitching-beam longitudinal acceleration	Servo accelerometer	±50g
Shock-strut pneumatic pressure	Strain-gage pressure	0 to 2000 psig
Shock-strut hydraulic pressure	Strain-gage pressure	0 to 2000 psig
Lift-simulator pneumatic pressure	Strain-gage pressure	0 to 500 psig
Hydraulic-power-unit pressure	Strain-gage pressure	0 to 5000 psig
Drop-fixture displacement	Rotary potentiometer	0 to 24 in.
Carriage displacement	Light-emitting diode	
NASA-modified IRIG-B time code	Frequency generator	100 Hz
Controller		
Controller enable	Microswitch	Logic level 0 to 5 V
Integrator enable	Electronic switch	Logic level 0 to 5 V
Servo-loop enable	Electronic switch	Logic level 0 to 5 V
Control (drop-fixture) acceleration	Servo accelerometer	±3g
Drop-fixture velocity decrement	Integrator circuit	0 to 100 in/sec
Limit force command		0 to 3360 lbf/V
Force error	Comparator circuit	0 to 3360 lbf/V
Strut position	Linear potentiometer	0 to 10 V
Strut-position error	Comparator circuit	0 to 10 V
Servovalve command		0 to 10 V
Feedback hydraulic pressure	Strain-gage pressure	0 to 5000 psig
Servovalve power-spool displacement	Linear-variable differential transformer	0 to ±0.13 in.

TABLE III.- SUMMARY OF TEST CONDITIONS AND TEST DATA

(a) Touchdown

Test number	Gear type	Attitude, deg	V_v		V_h		Strut pressure	
			m/sec	ft/sec	m/sec	knots	MPa	psig
1	Passive	0	1.5	5.0	0	0	1.35	196
2	Active	0	1.5	5.0	0	0	1.35	196
3	Passive	0	.91	3.0	0	0	1.30	188
4	Active	0	.91	3.0	0	0	1.30	188
5	Passive	0	1.2	4.0	0	0	1.35	196
6	Active	0	1.2	4.0	0	0	1.35	196
14	Passive	8	1.5	5.0	21	40	1.41	204
16	Active	8	1.5	5.0	21	40	1.32	192
23	Active	8	.91	3.0	21	40	.67	96
24	Passive	8	.91	3.0	21	40	1.43	208
27	Active	8	.91	3.0	4.1	8	1.63	236
28	Active	8	.91	3.0	4.1	8	1.54	224
30	Active	8	.91	3.0	21	40	.99	144
31	Active	8	.91	3.0	21	40	1.38	200
32	Active	8	.91	3.0	41	80	1.71	248
34	Passive	8	.91	3.0	41	80	2.32	336
35	Active	8	.91	3.0	41	80	1.65	240
36	Active	8	1.7	5.5	41	80	1.13	164
‡37	Passive	8	1.7	5.5	41	80	1.74	252
‡38	Active	8	1.7	5.5	41	80	1.16	168
40	Passive	2	1.7	5.5	41	80	1.71	248
42	Active	2	1.7	5.5	41	80	1.35	196
43	Active	2	1.7	5.5	21	40	1.74	252
44	Passive	2	1.7	5.5	21	40	2.12	308
45	Active	2	1.7	5.5	21	40	1.65	240
47	Passive	2	1.7	5.5	4.1	8	1.65	240
48	Active	2	1.7	5.5	4.1	8	1.65	240
49	Passive	0	1.7	5.5	0	0	1.82	264
51	Active	0	1.7	5.5	0	0	1.85	268
52	Active	13	1.7	5.5	21	40	.83	120
53	Active	13	1.7	5.5	41	80	1.16	168

‡Roll-out limit-force input at ±1.11 kN (±250 lbf).

TABLE III.- Continued

(b) Touchdown impact phase

Test number	Gear type	Initial impact						Rebound				Secondary impact					
		Mass-center force (*)		Maximum lift		Limit force		Mass-center force (†)		Limit force		Mass-center force (*)		Limit force		Maximum stroke	
		kN	lbf	kN	lbf	kN	lbf	kN	lbf	kN	lbf	kN	lbf	kN	lbf	cm	in.
1	Passive	-26.96	-6060	-14.28	-3210	----	----	12.90	2900	----	----	-3.25	-730	----	---	10.9	4.3
2	Active	-21.57	-4850	-14.01	-3150	8.63	1940	7.92	1780	----	----	-2.58	-580	2.67	600	12.7	5.0
3	Passive	-14.23	-3200	-12.99	-2920	----	----	7.38	1660	----	----	-4.00	-900	----	---	12.2	4.8
4	Active	-13.08	-2940	-13.52	-3040	3.87	870	5.60	1260	----	----	-2.85	-640	2.67	600	14.0	5.5
5	Passive	-22.69	-5100	-14.06	-3160	----	----	9.70	2180	----	----	-3.60	-810	----	---	11.7	4.6
6	Active	-18.46	-4150	-14.72	-3310	8.90	2000	5.69	1280	----	----	-2.67	-600	2.67	600	13.2	5.2
14	Passive	-23.66	-5320	-15.21	-3420	----	----	6.67	1500	----	----	-2.76	-620	----	---	10.7	4.2
16	Active	-21.71	-4880	-14.77	-3320	8.63	1940	9.16	2060	----	----	-2.49	-560	1.78	400	15.2	6.0
23	Active	-12.28	-2760	-13.08	-2940	3.74	840	6.32	1420	----	----	-2.40	-540	2.85	640	17.0	6.7
24	Passive	-14.06	-3160	-12.90	-2900	----	----	7.12	1600	----	----	-1.42	-320	----	---	8.1	3.2
27	Active	-12.72	-2860	-13.17	-2960	3.56	800	5.25	1180	----	----	-2.67	-600	2.67	600	15.2	6.0
28	Active	-12.28	-2760	-13.43	-3020	3.02	680	4.45	1000	----	----	-2.49	-560	2.40	540	15.2	6.0
30	Active	-11.21	-2520	-13.43	-3020	3.29	740	3.91	880	----	----	-2.49	-560	2.67	600	17.8	7.0
31	Active	-12.01	-2700	-14.06	-3160	2.85	640	4.45	1000	----	----	-2.67	-600	2.85	640	17.8	7.0
32	Active	-20.46	-4600	-14.50	-3260	3.56	800	2.94	660	----	----	-3.56	-800	2.67	600	15.7	6.2
34	Passive	-22.33	-5020	-13.52	-3040	----	----	6.14	1380	----	----	-4.18	-940	----	---	2.5	1.0
35	Active	-20.82	-4680	-16.01	-3600	3.47	780	4.36	980	----	----	-3.83	-860	2.67	600	18.8	7.4
36	Active	-27.40	-6160	-15.57	-3500	8.72	1960	6.85	1540	----	----	-3.29	-740	2.67	600	18.0	7.1
‡37	Passive	-31.32	-7040	-15.66	-3520	----	----	7.74	1740	----	----	-2.67	-600	----	---	5.3	2.1
‡38	Active	-29.36	-6600	-15.66	-3520	8.90	2000	10.85	2440	----	----	-9.43	-2120	1.33	300	22.4	8.8
40	Passive	-30.96	-6960	-15.84	-3560	----	----	12.01	2700	----	----	-4.18	-940	----	---	10.9	4.3
42	Active	-28.02	-6300	-15.66	-3520	8.36	1880	4.89	1100	----	----	-2.67	-600	2.67	600	13.0	5.1
43	Active	-26.78	-6020	-16.37	-3680	8.72	1960	8.90	2000	----	----	-3.47	-780	2.67	600	18.3	7.2
44	Passive	-30.69	-6900	-16.90	-3800	----	----	15.12	3400	----	----	-7.30	-1640	----	---	5.8	2.3
45	Active	-23.66	-5320	-16.81	-3780	8.72	1960	9.88	2200	----	----	-4.00	-900	2.67	600	18.0	7.1
47	Passive	-29.18	-6560	-16.37	-3680	----	----	12.46	2800	----	----	-4.72	-1060	----	---	12.2	4.8
48	Active	-20.02	-4500	-16.81	-3780	8.90	2000	5.69	1280	----	----	-3.20	-720	2.67	600	19.6	7.7
49	Passive	-29.98	-6740	-15.48	-3480	----	----	14.50	3260	----	----	-5.87	-1320	----	---	6.4	2.5
51	Active	-20.46	-4600	-16.19	-3640	9.43	2120	14.50	3260	----	----	-3.29	-740	2.67	600	18.5	7.3
52	Active	-23.13	-5200	-16.46	-3700	9.79	2200	6.94	1560	----	----	-3.47	-780	2.67	600	21.1	8.3
53	Active	-24.02	-5400	-16.01	-3600	8.99	2020	6.94	1560	----	----	-3.56	-800	2.67	600	18.8	7.4

* Decelerating force
† Accelerating force
‡ Roll-out limit-force input at ±1.11 kN (±250 lbf)
---- Control system inactive

TABLE III.- Continued

(c) Traverse of step bumps

[Blank space indicates no data obtained]

Test number	Gear type	First bump						Second bump					
		Mass-center force (*)		Limit force		Maximum stroke		Mass-center force (*)		Limit force		Maximum stroke	
		kN	lbf	kN	lbf	cm	in.	kN	lbf	kN	lbf	cm	in.
1	Passive												
2	Active												
3	Passive												
4	Active												
5	Passive												
6	Active												
14	Passive	-5.34	-1200	----	---	14.2	5.6	-7.70	-1730	----	---	15.5	6.1
16	Active	-3.69	-830	2.67	600	10.7	4.2	-3.43	-770	2.67	600	11.4	4.5
23	Active	-5.43	-1220	2.67	600	15.7	6.2	-6.94	-1560	2.67	600	17.5	6.9
24	Passive	-6.14	-1380	----	---	11.7	4.6	-3.69	-830	----	---	11.7	4.6
27	Active	-3.20	-720	2.67	600	13.2	5.2	-4.18	-940	2.67	600	13.2	5.2
§28	Active	-6.23	-1400	2.40	540	14.0	5.5	-3.56	-800	2.40	540	17.5	6.9
§30	Active	-7.47	-1680	2.67	600	18.3	7.2	-5.34	-1200	2.67	600	15.5	6.1
§31	Active	-6.85	-1540	2.67	600	17.3	6.8	-6.49	-1460	2.67	600	16.8	6.6
§32	Active	-6.94	-1560	2.67	600	13.5	5.3	-5.07	-1140	2.67	600	11.4	4.5
34	Passive	-6.09	-1370	----	---	5.1	2.0	-7.70	-1730	----	---	5.6	2.2
§35	Active	-7.65	-1720	2.67	600	14.7	5.8	-7.34	-1650	2.67	600	18.8	7.4
§36	Active	-7.38	-1660	2.67	600	17.0	6.7	-5.96	-1340	2.67	600	17.0	6.7
37	Passive	-6.63	-1490	----	---	8.1	3.2	-9.21	-2070	----	---	9.1	3.6
‡38	Active	-6.41	-1440	1.33	300	13.7	5.4	-23.6	-5300	1.33	300	22.4	8.8
40	Passive	-4.54	-1020	----	---	14.2	5.6	-6.41	-1440	----	---	15.7	6.2
§42	Active	-4.80	-1080	2.67	600	16.8	6.6	-7.70	-1730	2.67	600	18.0	7.1
43	Active	-5.60	-1260	2.67	600	15.2	6.0	-5.78	-1300	2.67	600	15.7	6.2
44	Passive	-6.23	-1400	----	---	8.4	3.3	-7.74	-1740	----	---	9.4	3.7
45	Active	-5.78	-1300	2.67	600	14.7	5.8	-5.07	-1140	2.67	600	13.2	5.2
47	Passive	-2.54	-570	----	---	13.7	5.4	-3.87	-870	----	---	14.0	5.5
48	Active	-1.87	-420	2.67	600	14.2	5.6	-1.65	-370	2.67	600	14.7	5.8
49	Passive												
51	Active												
52	Active	-5.78	-1300	2.67	600	18.8	7.4	-5.65	-1270	2.67	600	18.0	7.1
§53	Active	-4.89	-1100	2.67	600	16.3	6.4	-11.1	-2500	2.67	600	16.8	6.6

* Decelerating force
‡ Roll-out limit-force input at ±1.11 kN (±250 lbf)
§ Relief-valve/servovalve interaction
---- Control system inactive

TABLE III.- Concluded

(d) Traverse of natural bumps

[Blank space indicates no data]

Test number	Gear type	First bump				Second bump				Third bump				All bumps	
		Mass-center force (*)		Maximum stroke		Mass-center force (*)		Maximum stroke		Mass-center force (*)		Maximum stroke		Limit force	
		kN	lbf	cm	in.	kN	lbf	cm	in.	kN	lbf	cm	in.	kN	lbf
1	Passive														
2	Active														
3	Passive														
4	Active														
5	Passive														
6	Active														
14	Passive	-0.98	-220	14.0	5.5	-1.25	-280	13.7	5.4	-1.33	-300	14.2	5.6	----	---
16	Active	-1.07	-240	9.1	3.6	-1.51	-340	9.4	3.7	-1.33	-300	9.4	3.7	0	0
23	Active	-1.47	-330	11.0	4.3	-1.29	-290	10.9	4.3	-1.29	-290	11.2	4.4	0	0
24	Passive	-1.56	-350	11.0	4.3	-1.78	-400	10.7	4.2	-2.18	-490	11.2	4.4	----	---
§27	Active														
§28	Active														
§30	Active	-1.07	-240	12.2	4.8	-1.69	-380	12.2	4.8	-3.02	-680	14.0	5.5	0	0
§31	Active	-1.16	-260	11.9	4.7	-1.51	-340	12.2	4.8	-2.31	-520	12.2	4.8	0	0
§32	Active	-2.71	-610	11.9	4.7	-2.89	-650	11.9	4.7	-7.38	-1660	----	---	2.67	600
§34	Passive	-2.98	-670	3.8	1.5	-5.83	-1310	4.6	1.8	-4.80	-1080	2.9	1.7	----	---
§35	Active	-2.67	-600	14.2	5.6	-2.14	-480	11.2	4.4	-8.32	-1870	----	---	2.67	600
§36	Active	-2.22	-500	13.7	5.4	-1.60	-360	11.4	4.5	(§)	(§)	(§)	(§)	2.67	600
‡37	Passive	-3.07	-690	7.0	2.8	-5.92	-1330	7.9	3.1	-3.74	-840	7.4	2.9	----	---
‡38	Active	(‖)	(‖)	(‖)	(‖)	(‖)	(‖)	(‖)	(‖)	(‖)	(‖)	(‖)	(‖)	1.33	300
§40	Passive	-1.96	-440	14.5	5.7	-.98	-220	14.0	5.5	-1.16	-260	14.7	5.8	----	---
§42	Active	-2.67	-600	13.3	5.2	-2.27	-510	10.9	4.3	-2.80	-630	13.5	5.3	2.67	600
43	Active	-2.58	-580	11.4	4.5	-2.76	-620	12.2	4.8	-1.16	-260	11.7	4.6	2.67	600
44	Passive	-1.33	-300	7.1	2.8	-.98	-220	7.9	3.1	-.98	-220	7.9	3.1	----	---
45	Active	-1.51	-340	10.7	4.2	-1.42	-320	11.2	4.4	-1.60	-360	10.7	4.2	0	0
47	Passive														
48	Active														
49	Passive														
51	Active														
§52	Active	-.98	-220	13.0	5.1	-1.33	-300	13.2	5.2	-2.58	-580	13.2	5.2	2.67	600
§53	Active	-2.67	-600	12.4	4.9	-2.94	-660	14.2	5.6	-1.96	-440	13.0	5.1	2.67	600

* Decelerating force
‡ Roll-out limit-force input at ±1.11 kN (±250 lbf)
§ Relief-valve/servovalve interaction
‖ Controller malfunctioned
---- Control system inactive

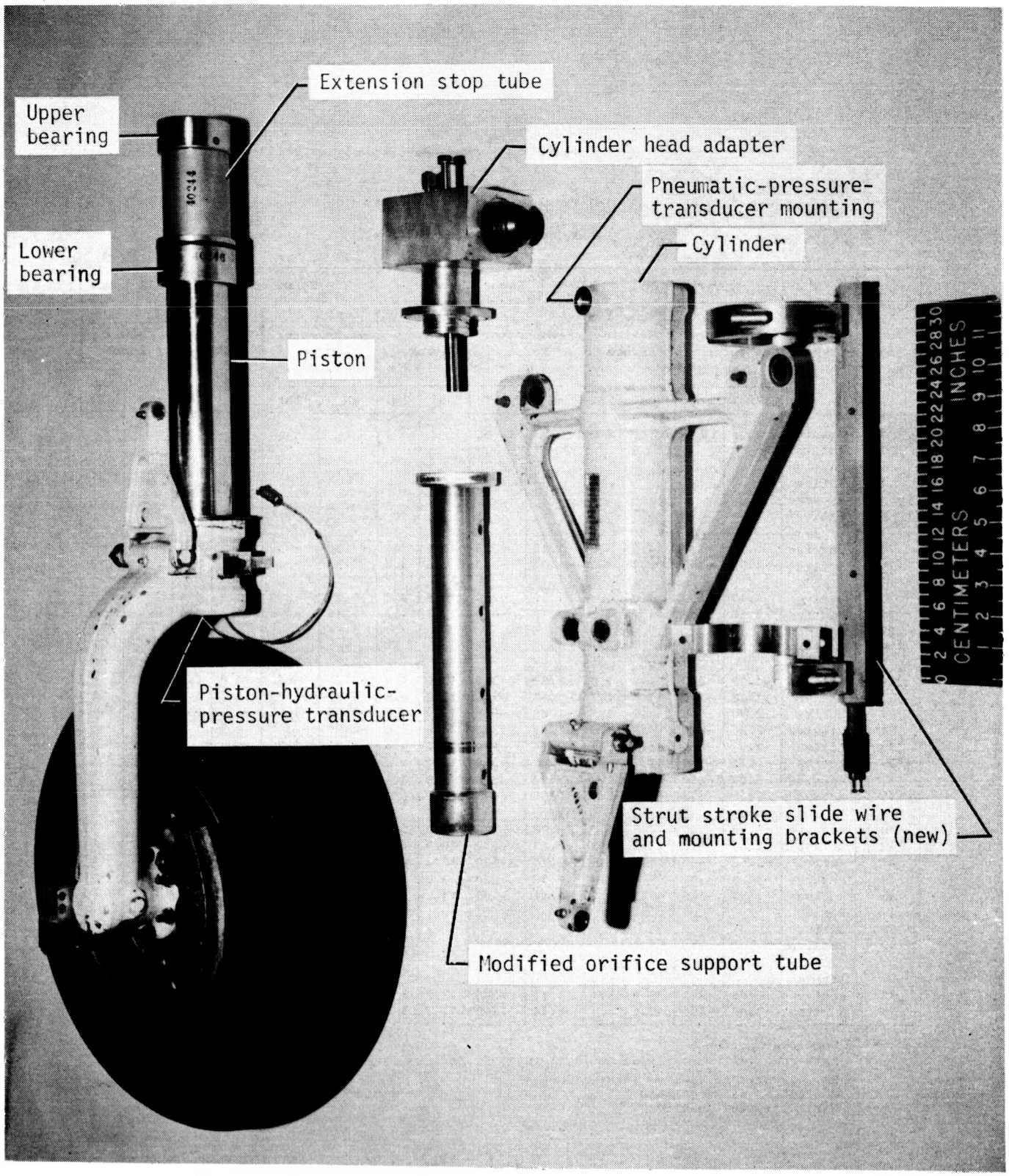

(a) Components.

Figure 1.- Modified main landing gear.

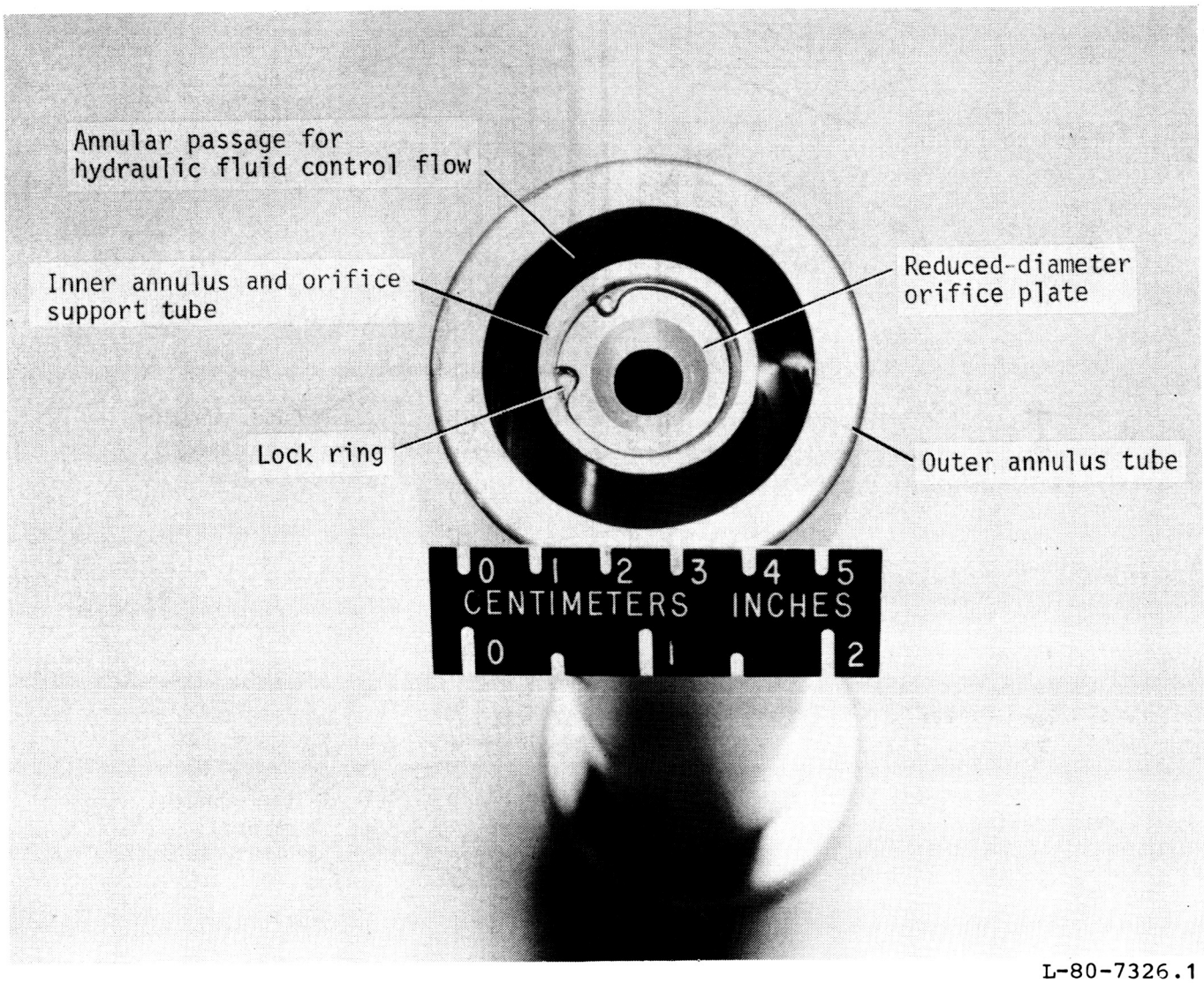

L-80-7326.1

(b) End view of modified orifice support tube.

Figure 1.- Continued.

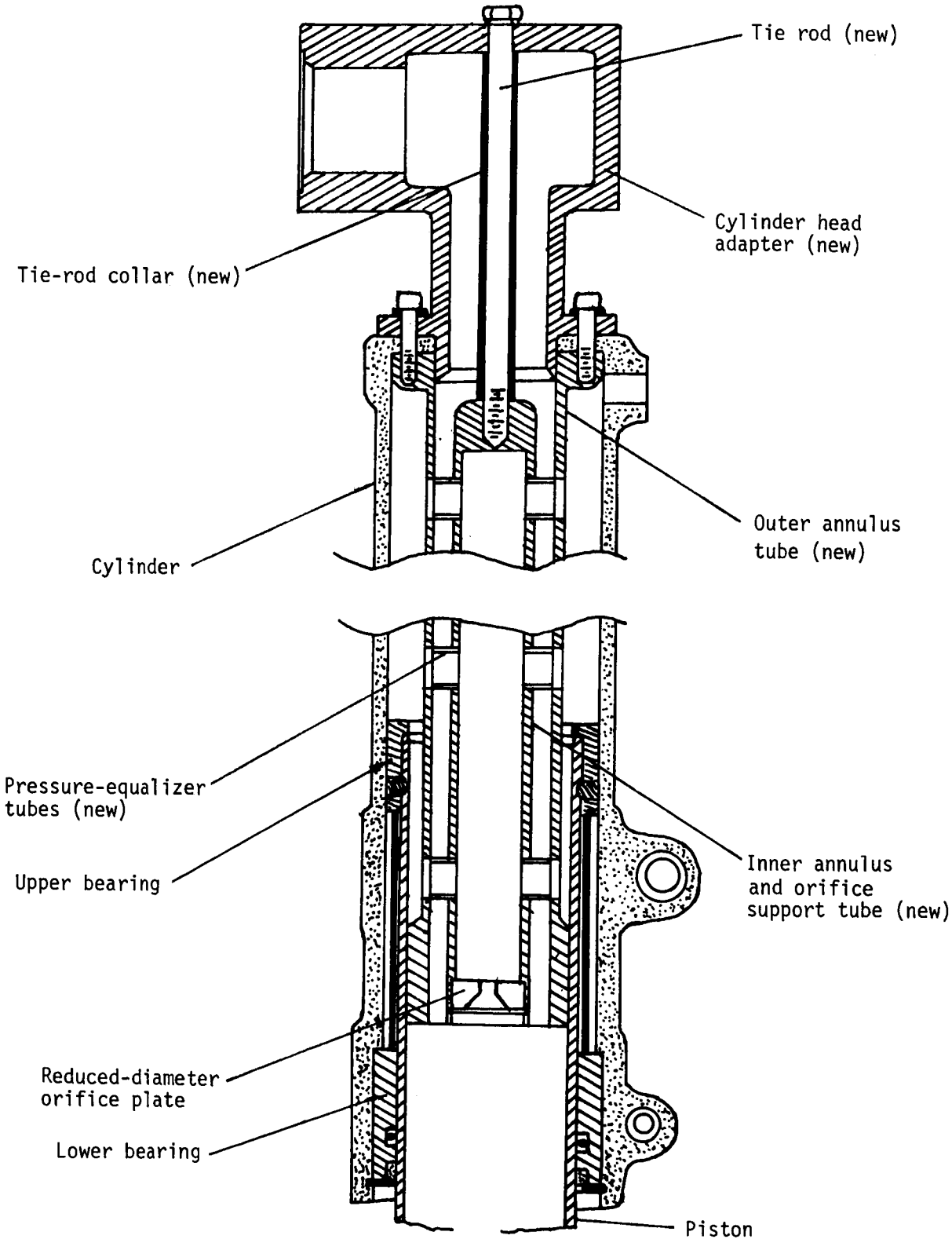

(c) Details of modified strut assembly.

Figure 1.- Concluded.

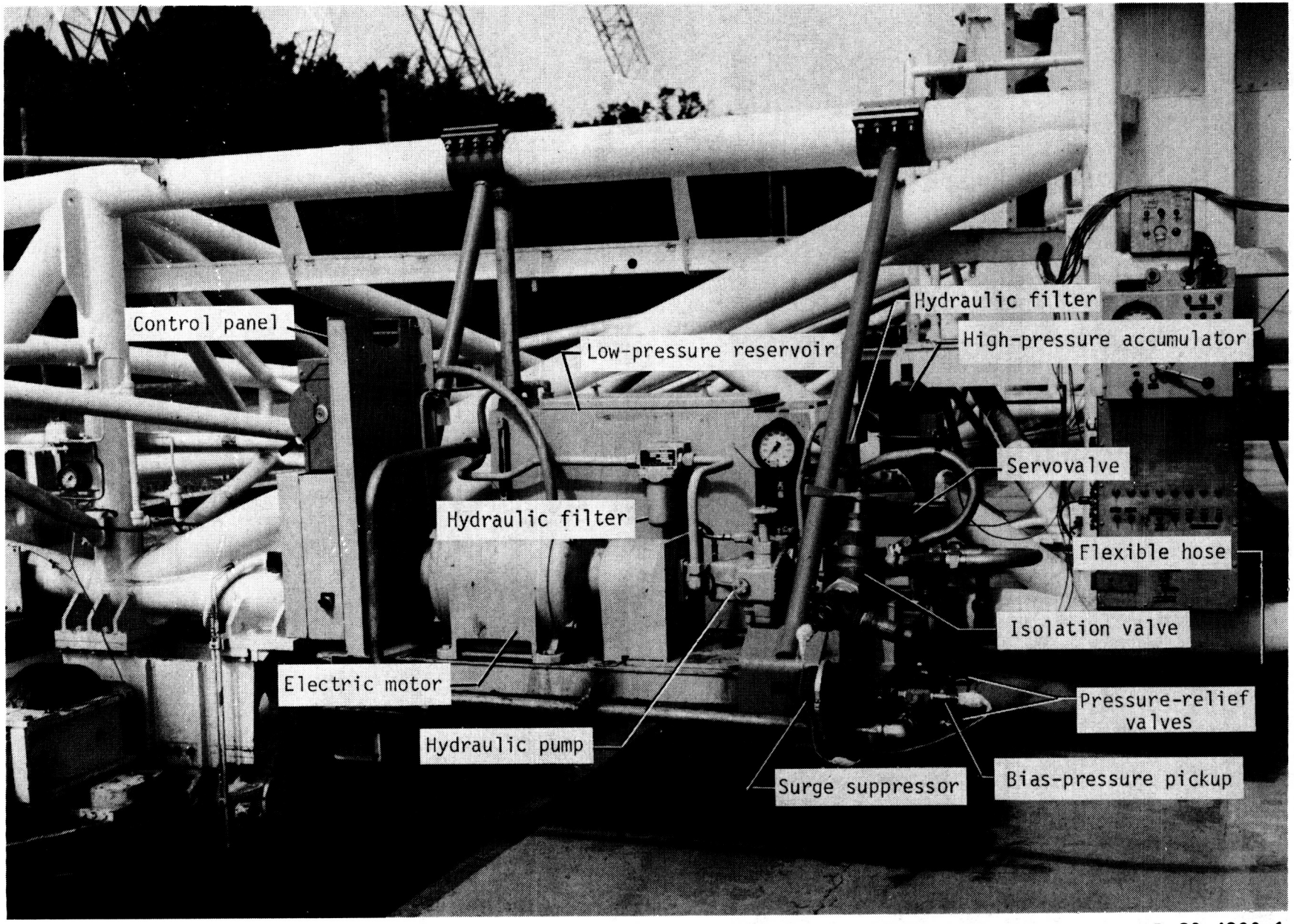

L-80-4900.1

Figure 2.- Hydraulic power unit.

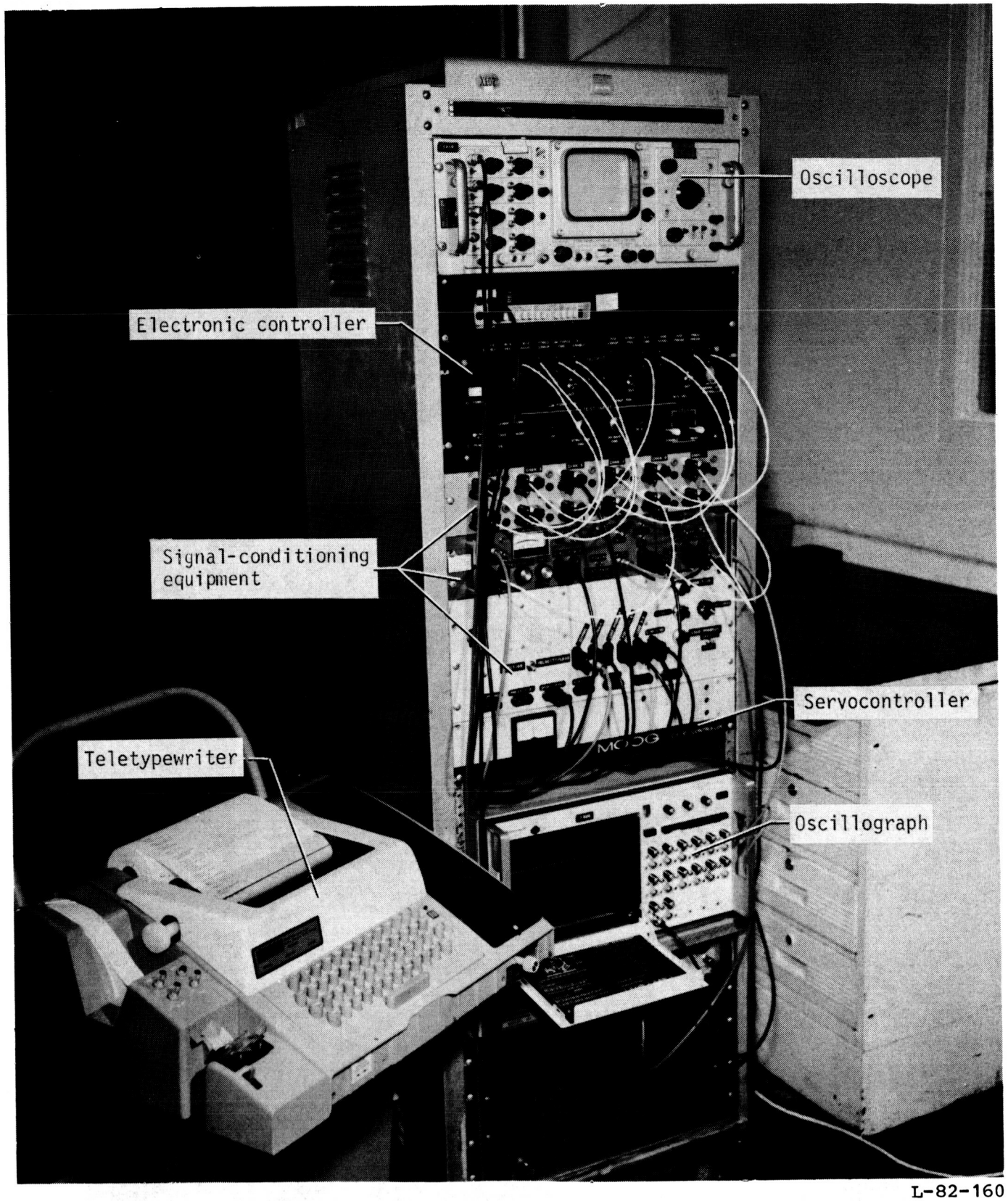

L-82-160

Figure 3.- Bench setup of control, signal-conditioning, and diagnostic electronic equipment.

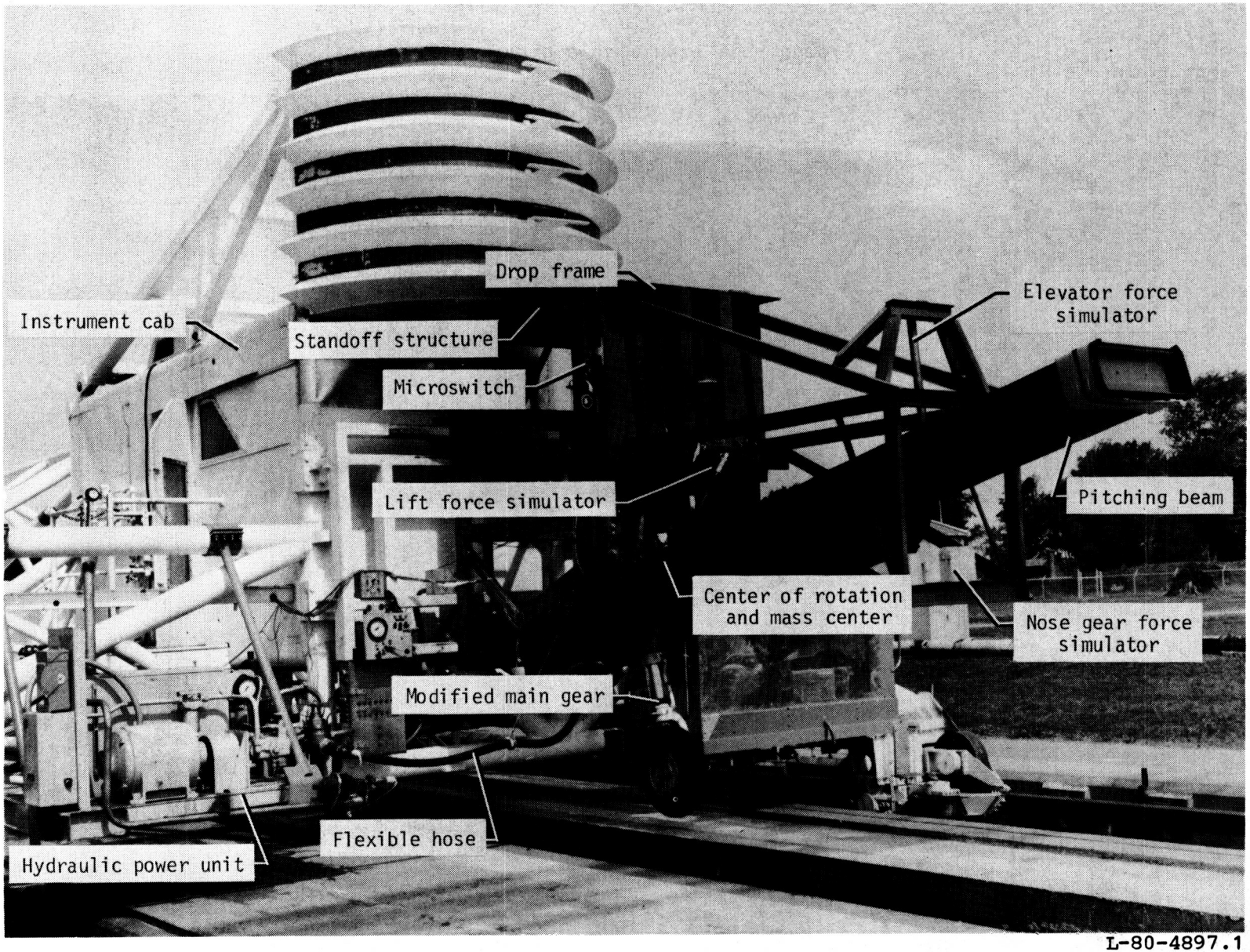

Figure 4.- Test fixture and equipment mounted on test carriage at Langley Landing Loads Track.

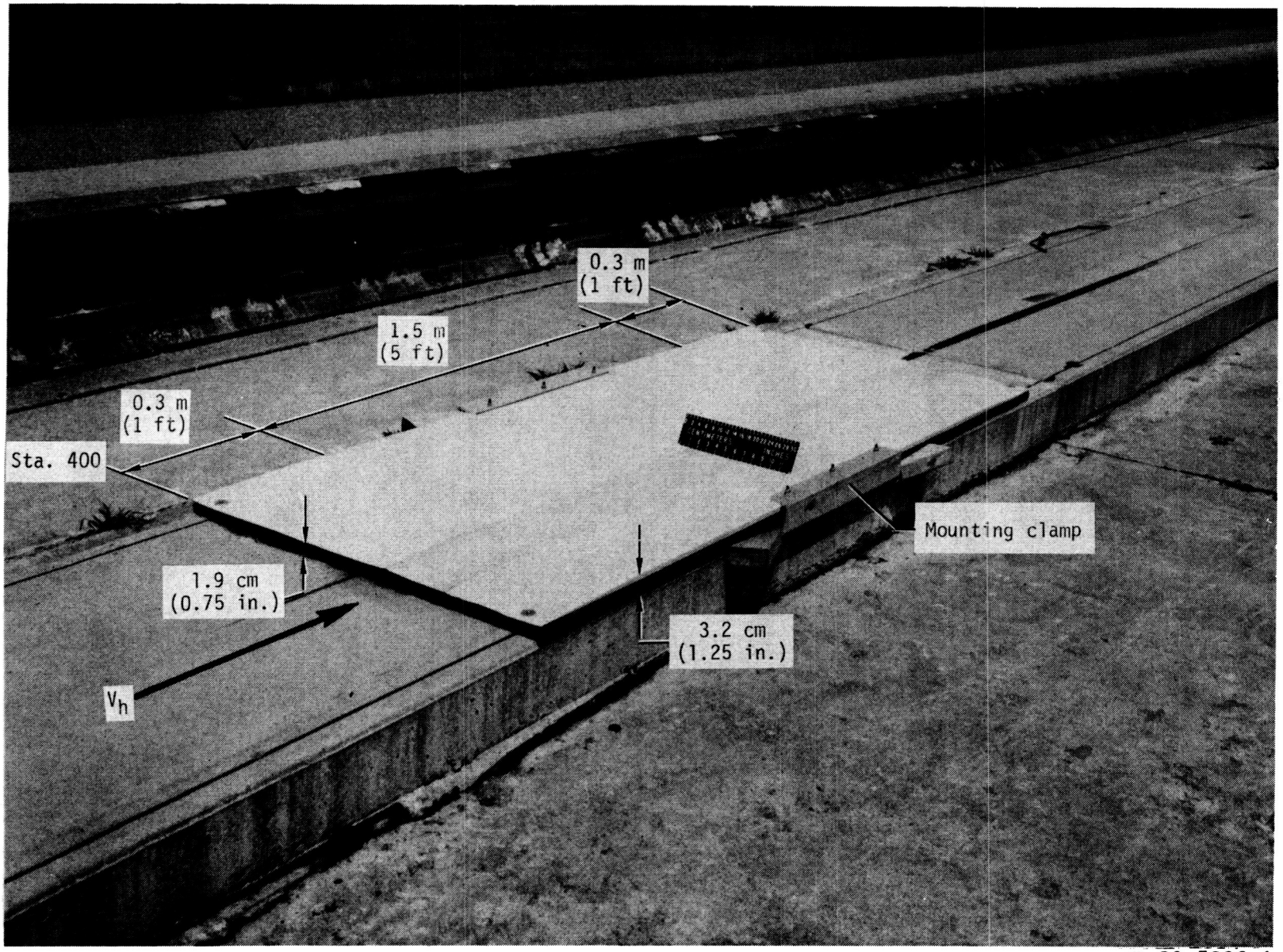

L-80-5826.1

(a) Dimensions of single step bump.

Figure 5.- Step bumps installed on track surface.

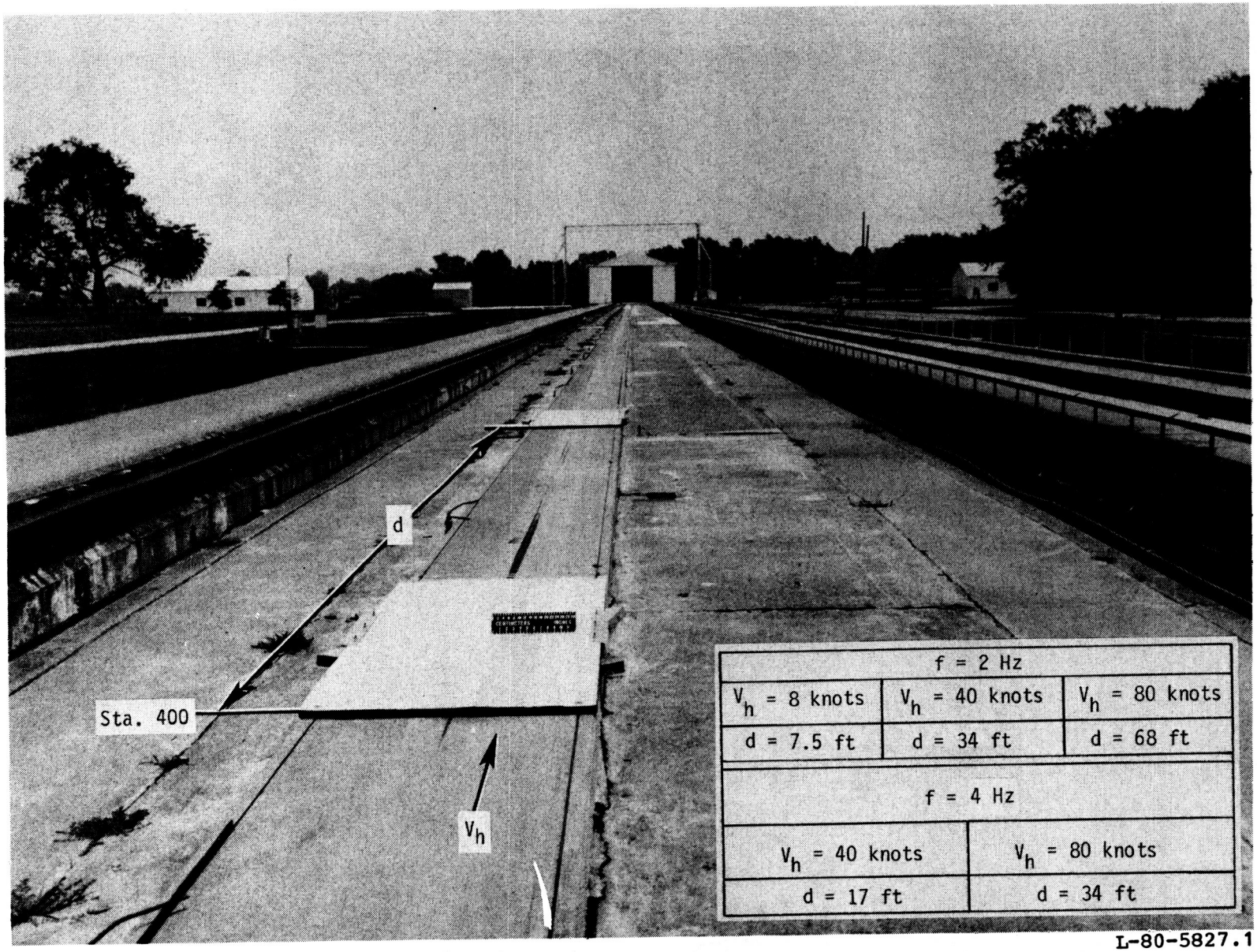

(b) Frequency of bump encounter as function of carriage speed and bump spacing.

Figure 5.- Concluded.

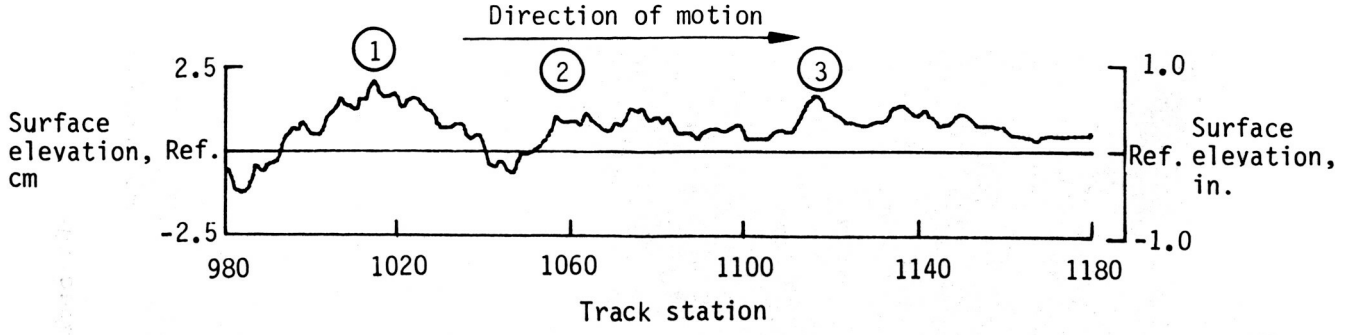

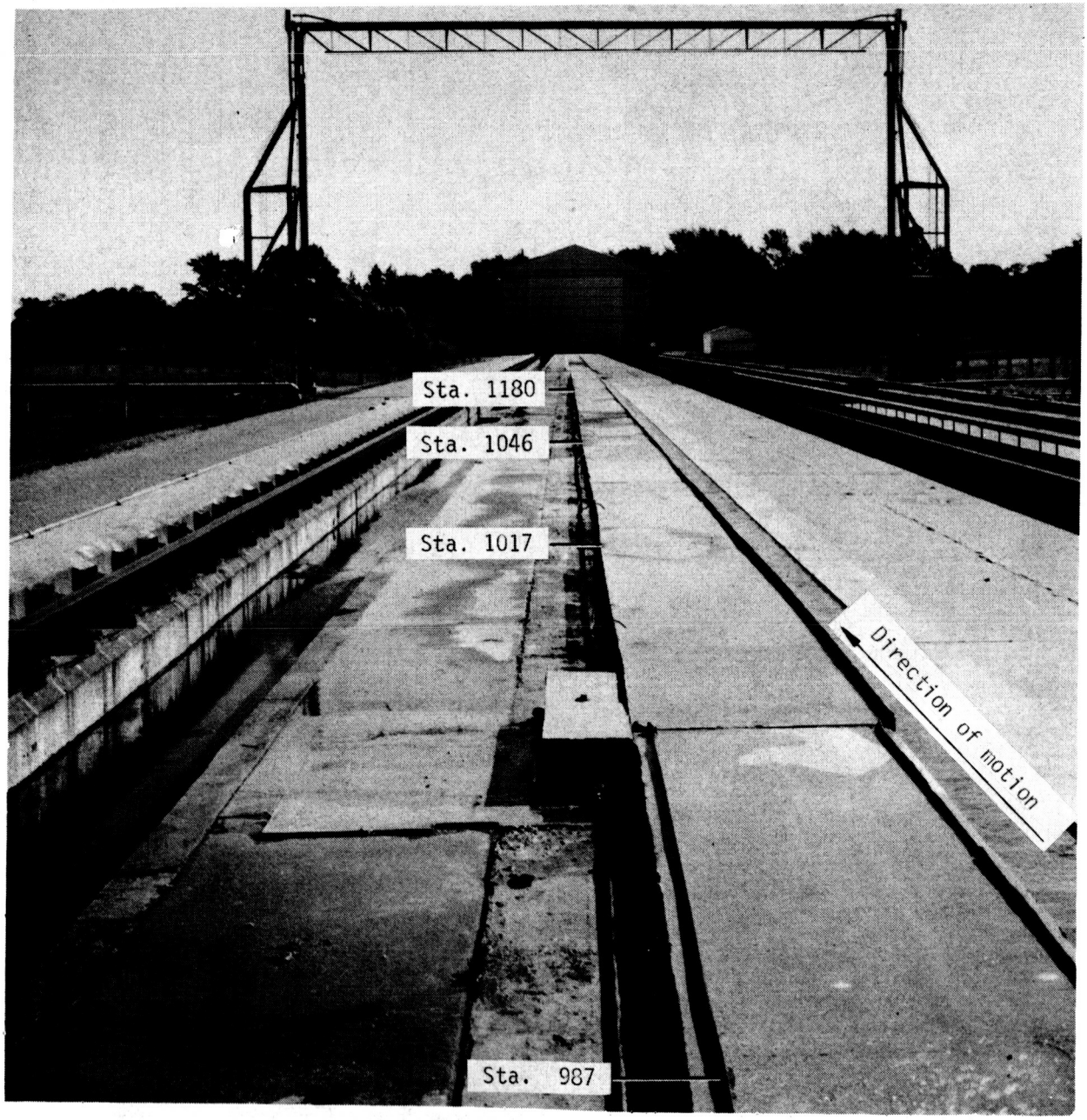

L-81-10,134.1

Figure 6.- Photograph and track surface profile of natural bumps.

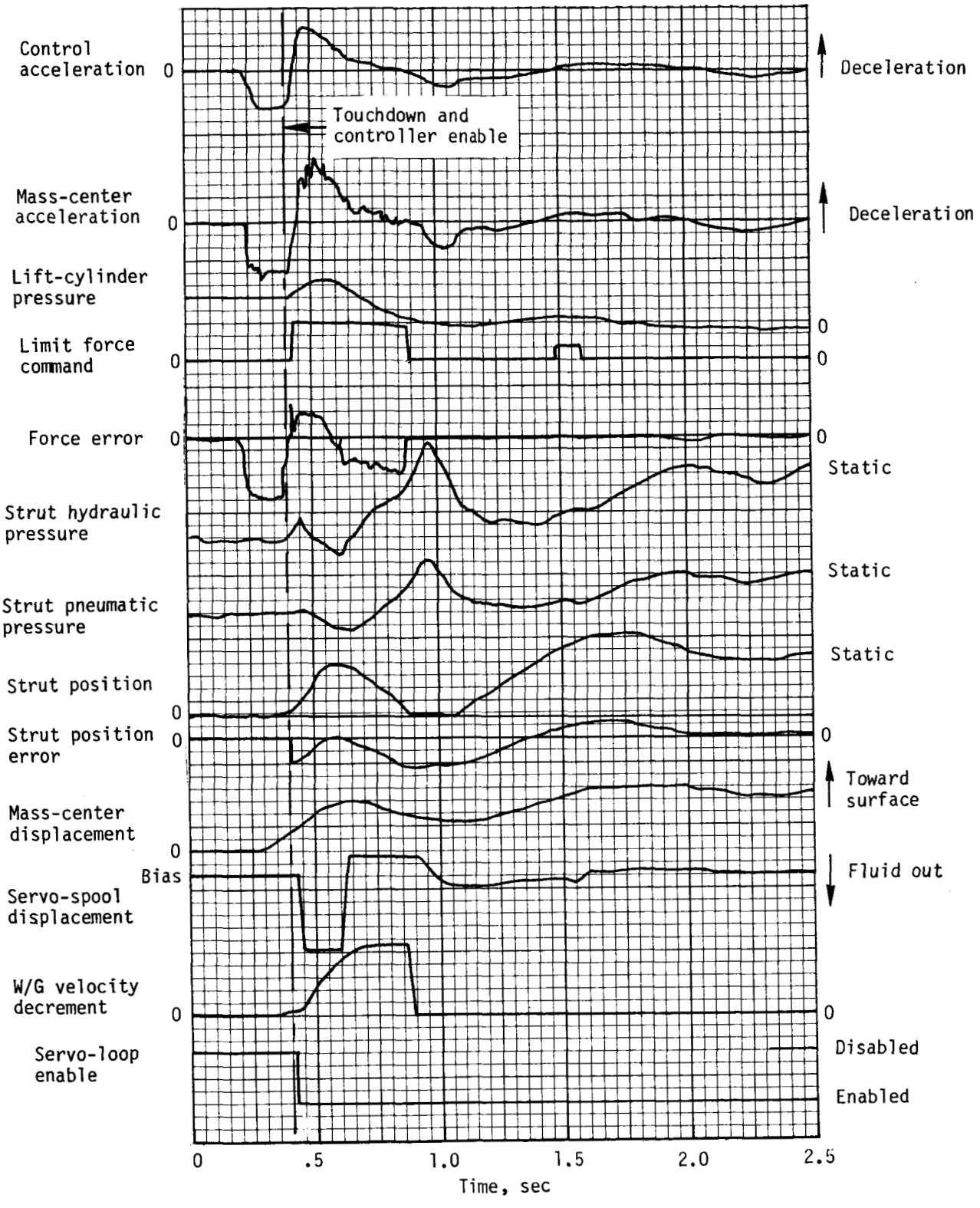

(a) Landing impact.

Figure 7.- Typical oscillograph traces of active-gear data. V_h = 8 knots; V_v = 1.7 m/sec (5.5 ft/sec); test 48.

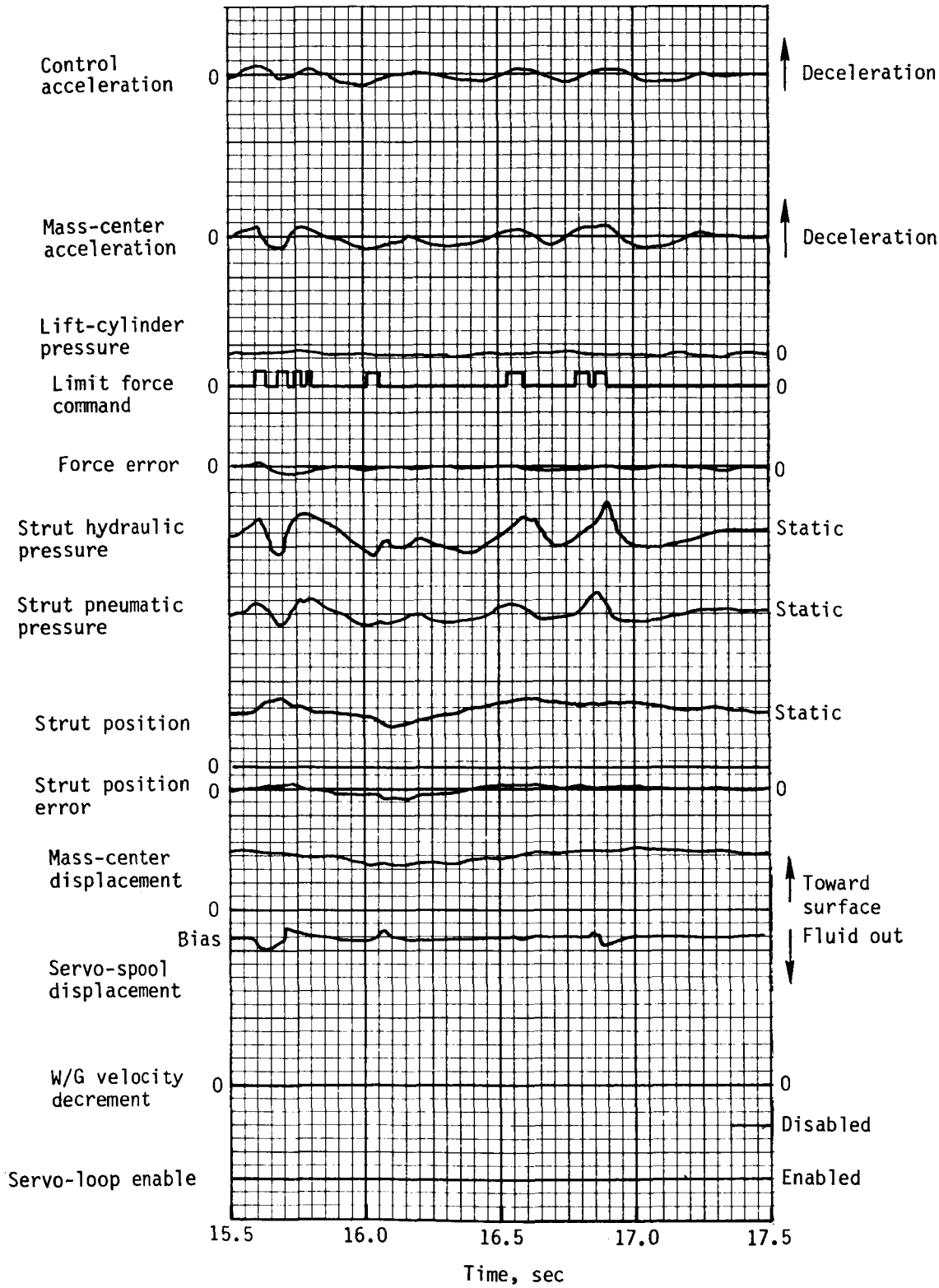

(b) Traverse of step bumps.

Figure 7.- Concluded.

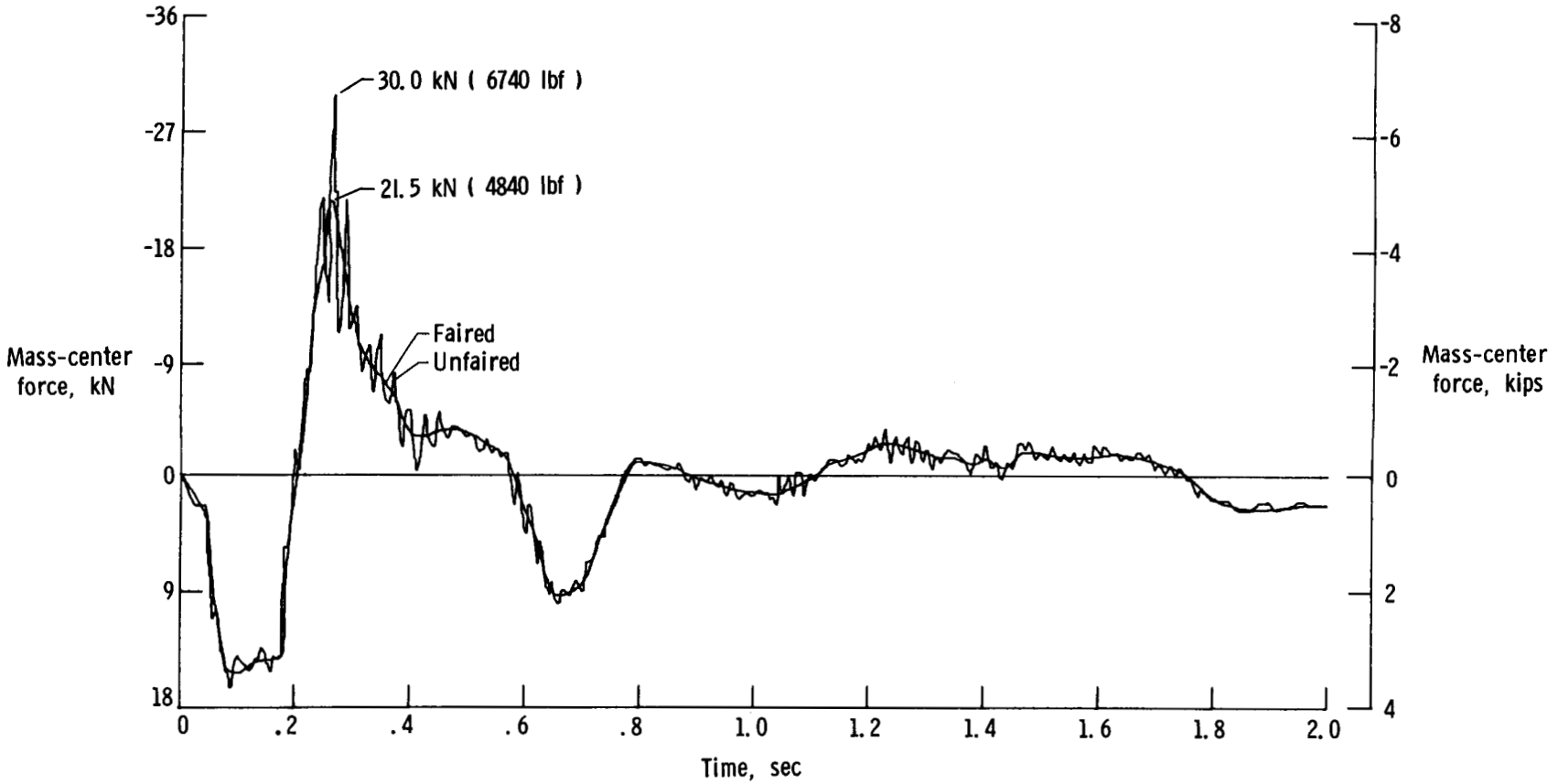

(a) Active-gear force data during touchdown impact.

Figure 8.- Fairing of computer-generated time histories of mass-center force data for obtaining basic forcing function. V_h = 40 knots; V_v = 1.5 m/sec (5.0 ft/sec); test 16.

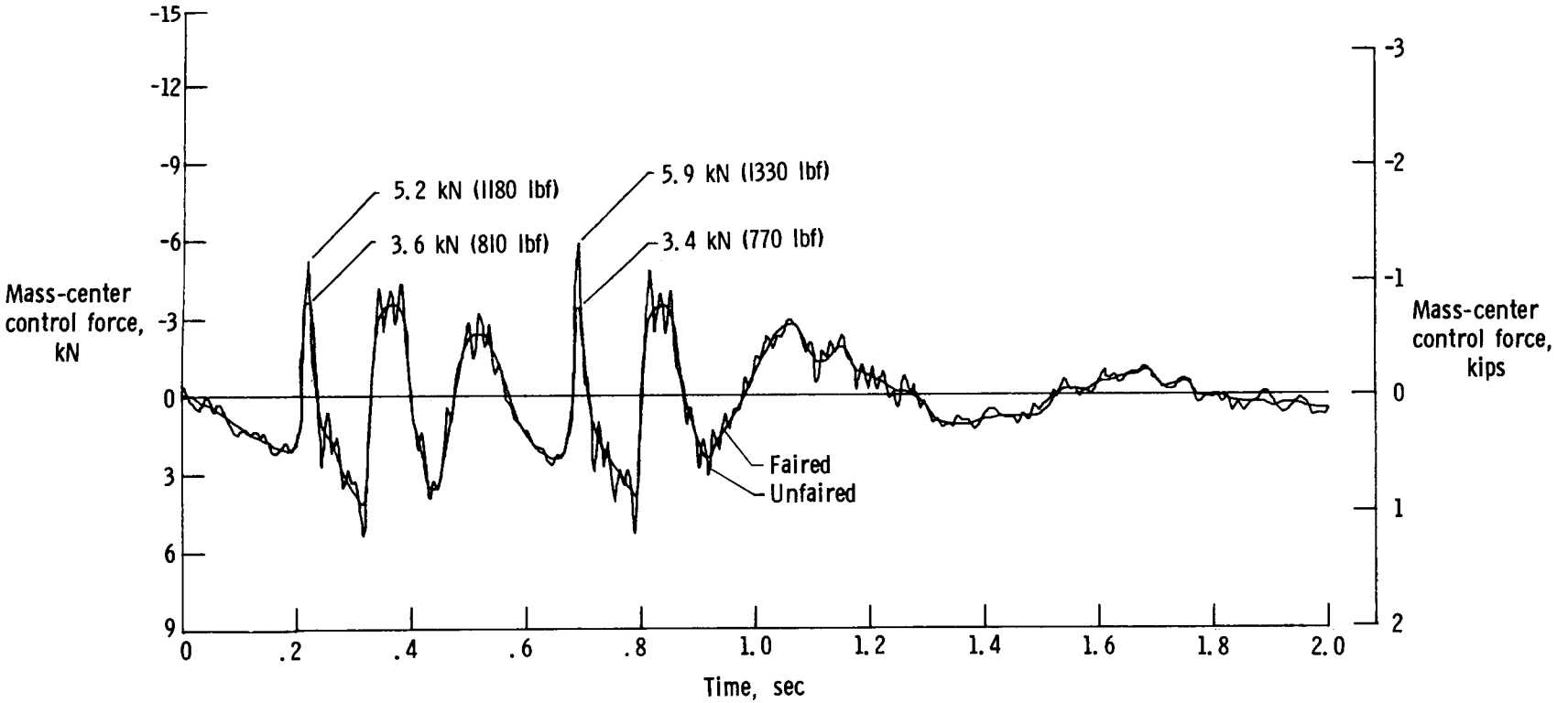

(b) Active-gear force data during traverse of step bumps.

Figure 8.- Concluded.

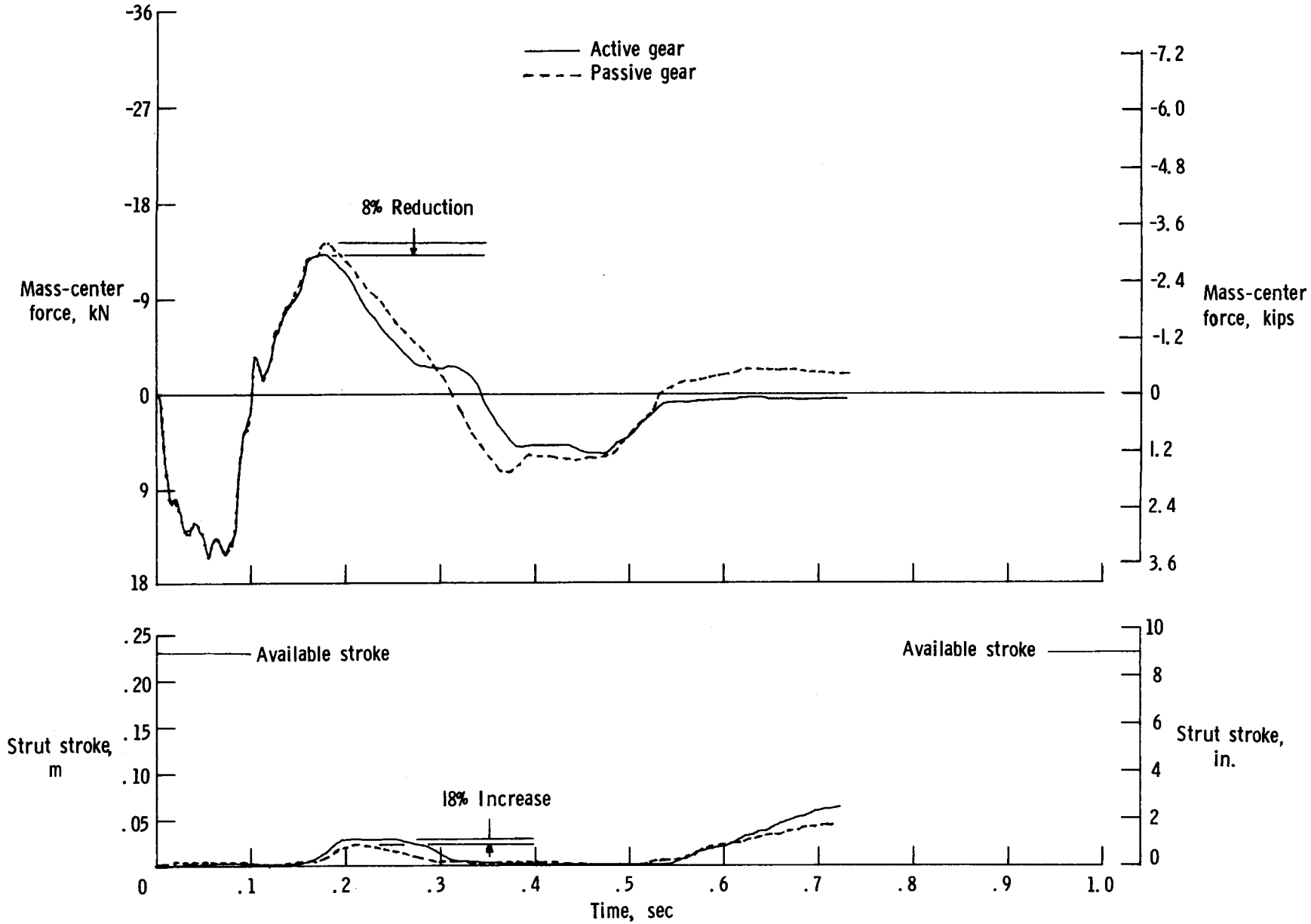

(a) V_v = 0.9 m/sec (3.0 ft/sec); $p_a = p_p$ = 1248 kPa (181 psig); tests 4 and 3.

Figure 9.- Vertical-drop tests of passive and active gears.
V_h = 0 m/sec (0 ft/sec); θ = 0°.

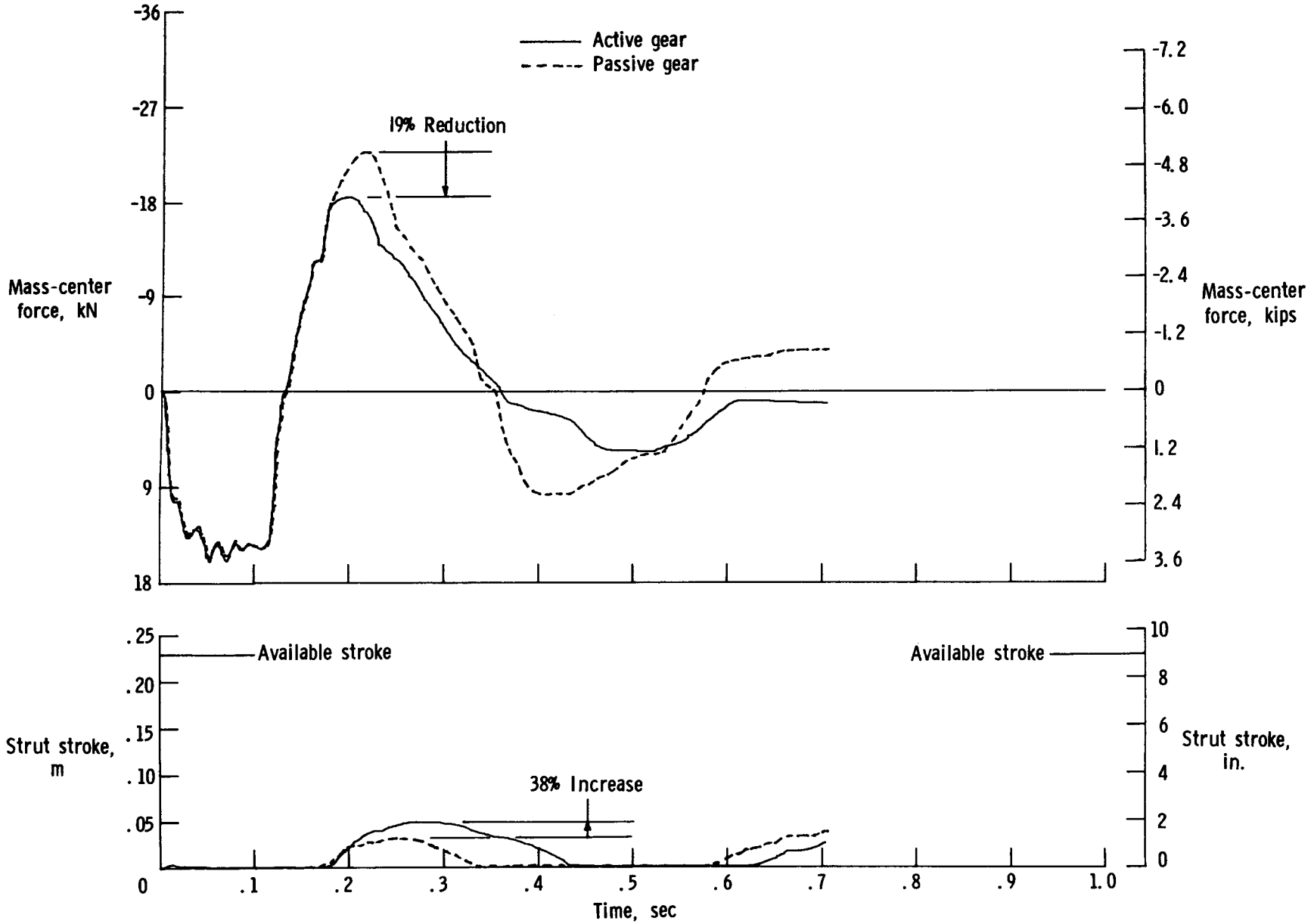

(b) V_v = 1.2 m/sec (4.0 ft/sec); $p_a = p_p$ = 1351 kPa (196 psig); tests 6 and 5.

Figure 9.- Continued.

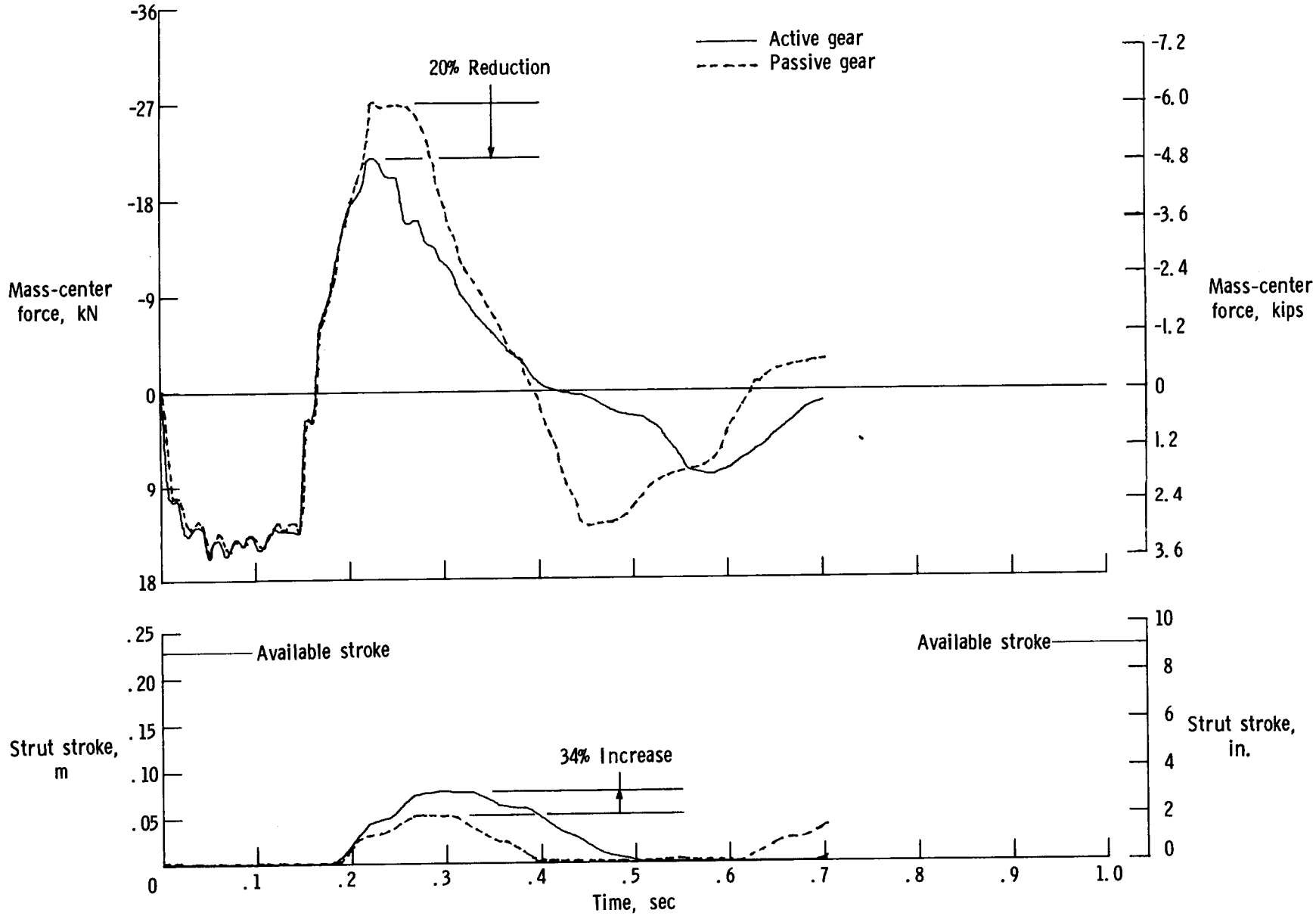

(c) V_v = 1.5 m/sec (5.0 ft/sec); $p_a = p_p$ = 1351 kPa (196 psig); tests 2 and 1.

Figure 9.- Continued.

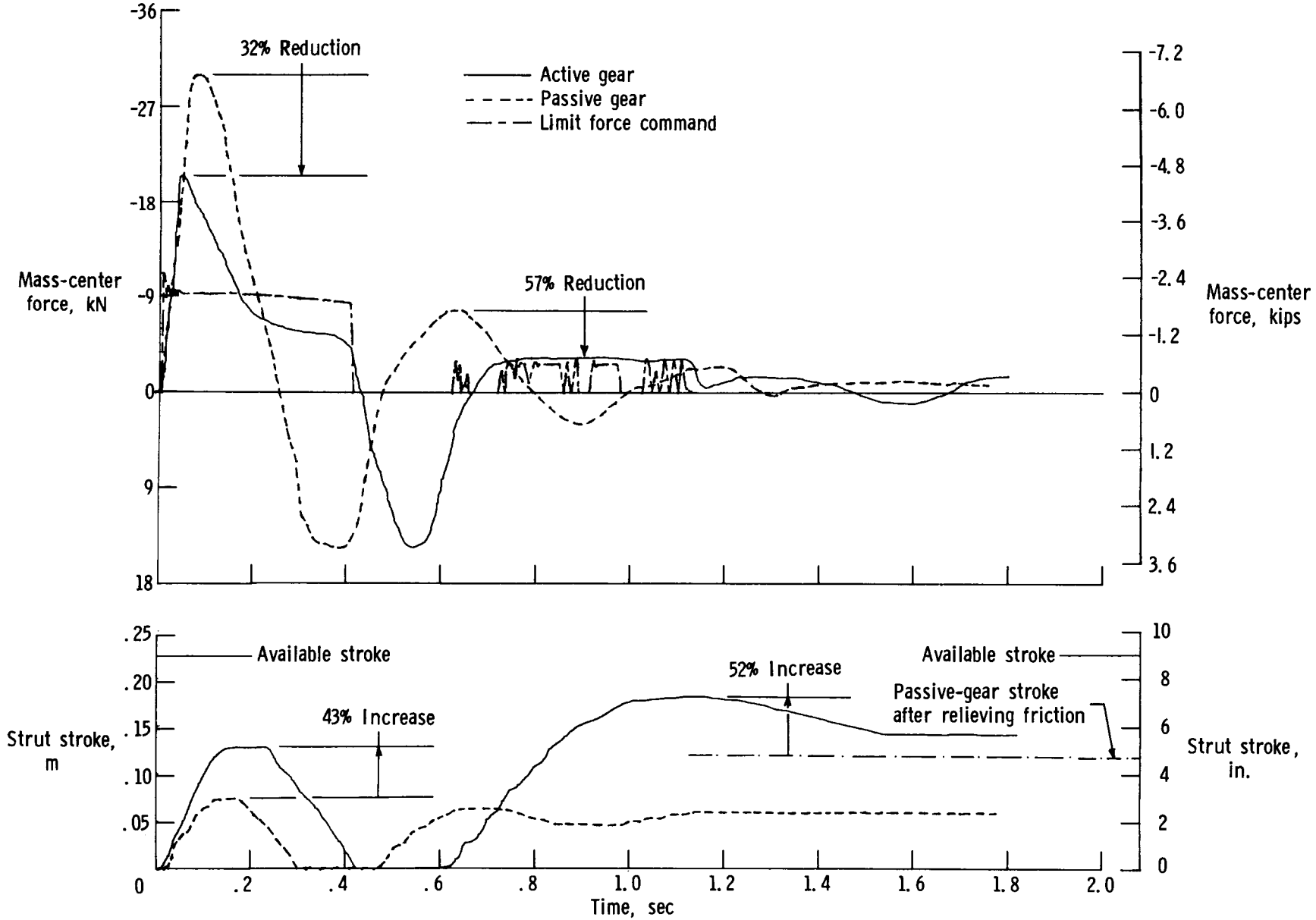

(d) V_v = 1.7 m/sec (5.5 ft/sec); $p_a = p_p$ = 1834 kPa (266 psig); tests 51 and 49.

Figure 9.- Concluded.

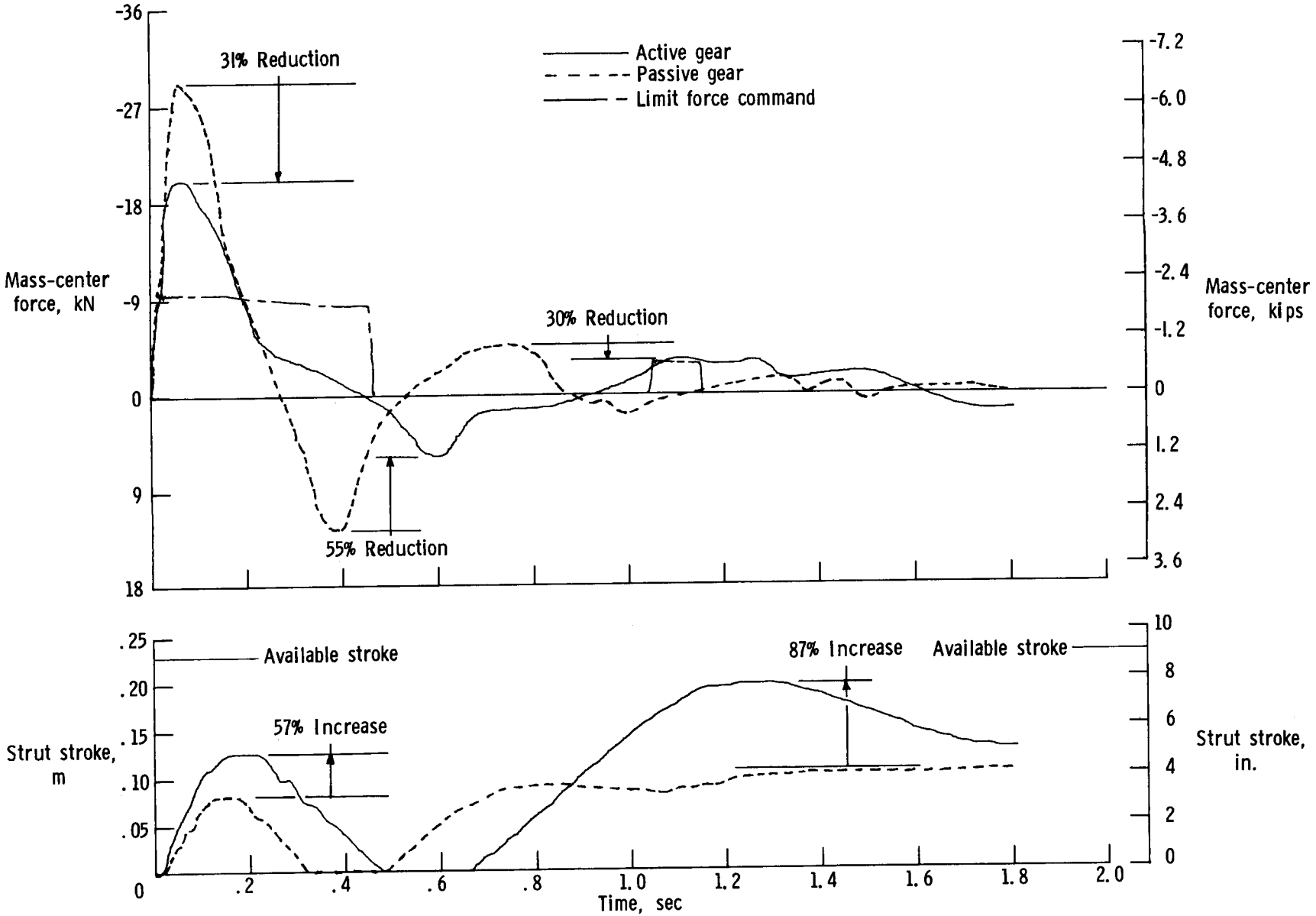

(a) V_h = 8 knots; V_v = 1.7 m/sec (5.5 ft/sec); $p_a = p_p$ = 1739 kPa (260 psig); θ = 2°; tests 48 and 47.

Figure 10.- Touchdown impact data obtained from landing-simulation tests of active and passive gears.

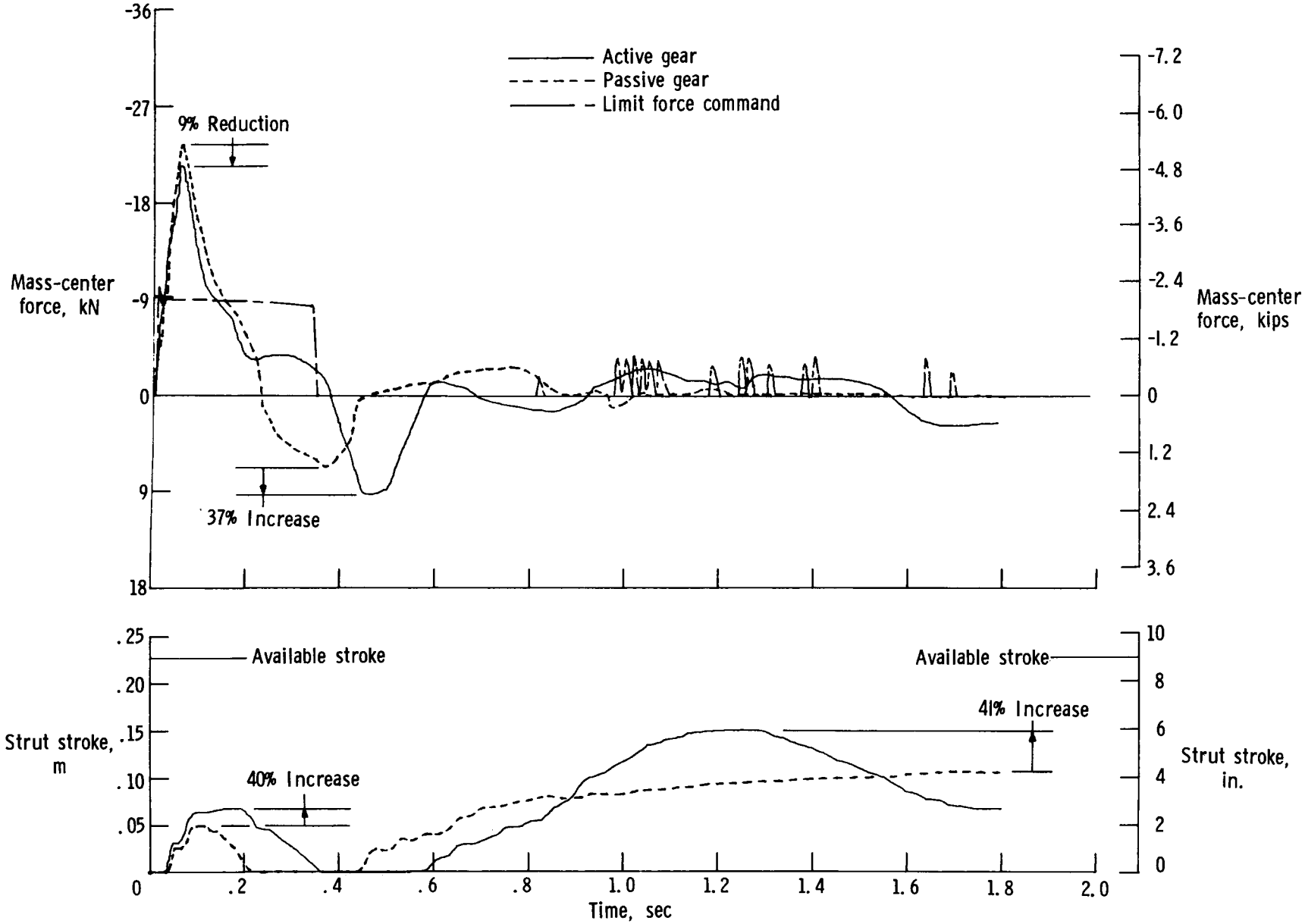

(b) V_h = 40 knots; V_v = 1.5 m/sec (5.0 ft/sec); p_a = 1328 kPa (192 psig); p_p = 1407 kPa (204 psig); θ = 8°; tests 16 and 14.

Figure 10.- Continued.

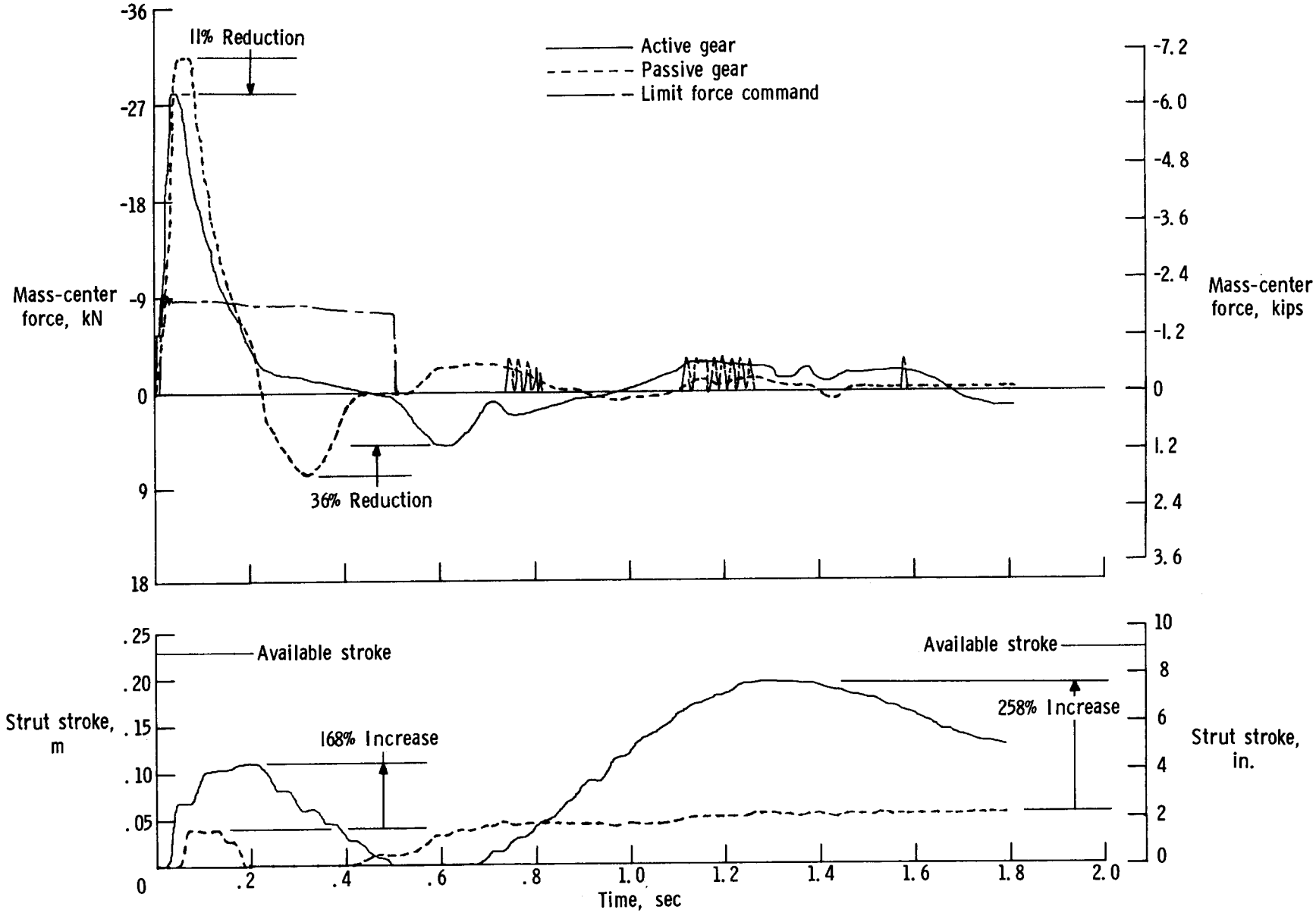

(c) V_h = 80 knots; V_v = 1.7 m/sec (5.5 ft/sec); p_a = 1351 kPa (196 psig); p_p = 1737 kPa (252 psig); θ_a = 2°; θ_p = 8°; tests 42 and 37.

Figure 10.- Continued.

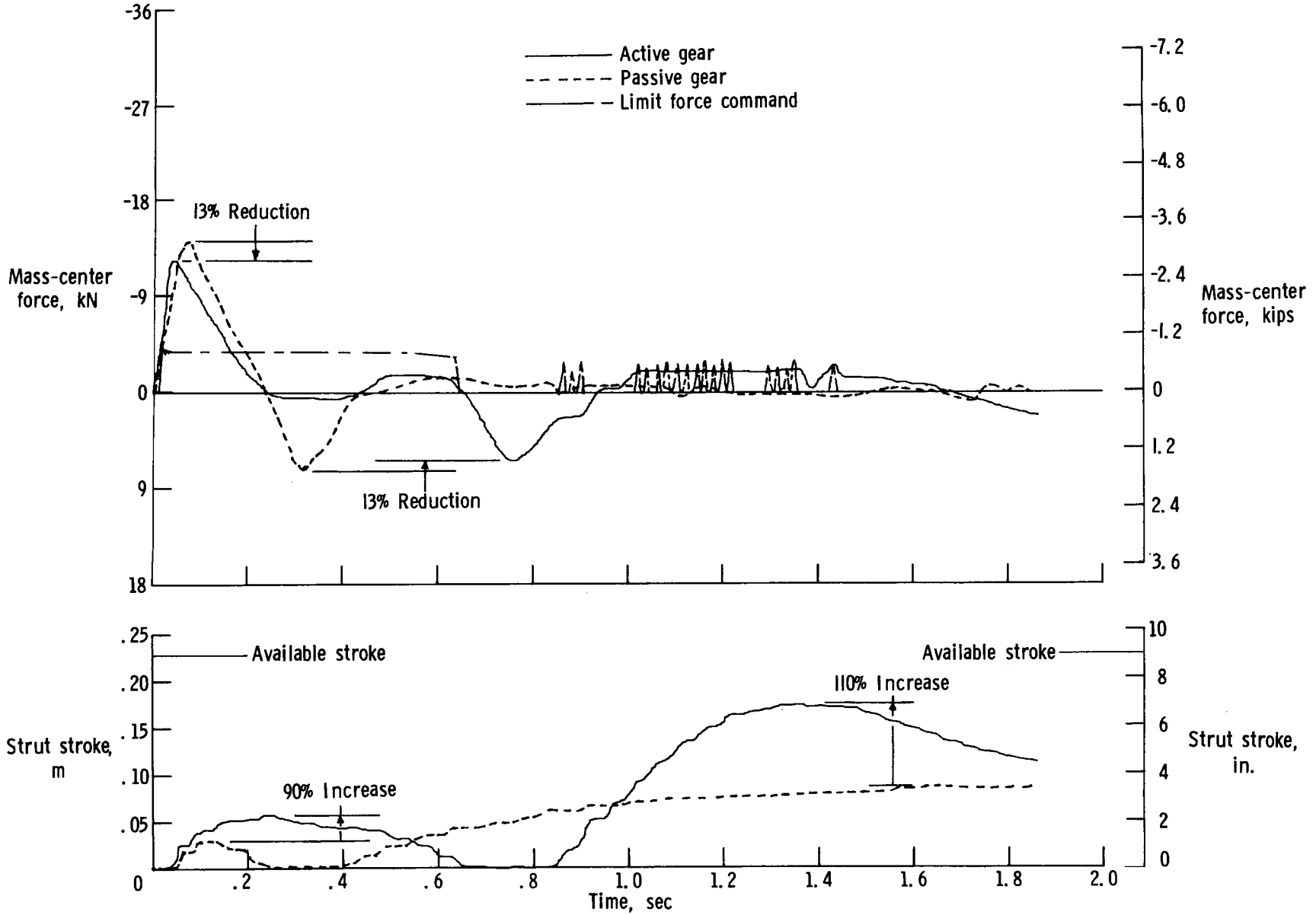

(d) V_h = 40 knots; V_v = 0.9 m/sec (3.0 ft/sec); p_a = 662 kPa (96 psig); p_p = 1434 kPa (208 psig); θ = 8°; tests 23 and 24.

Figure 10.- Continued.

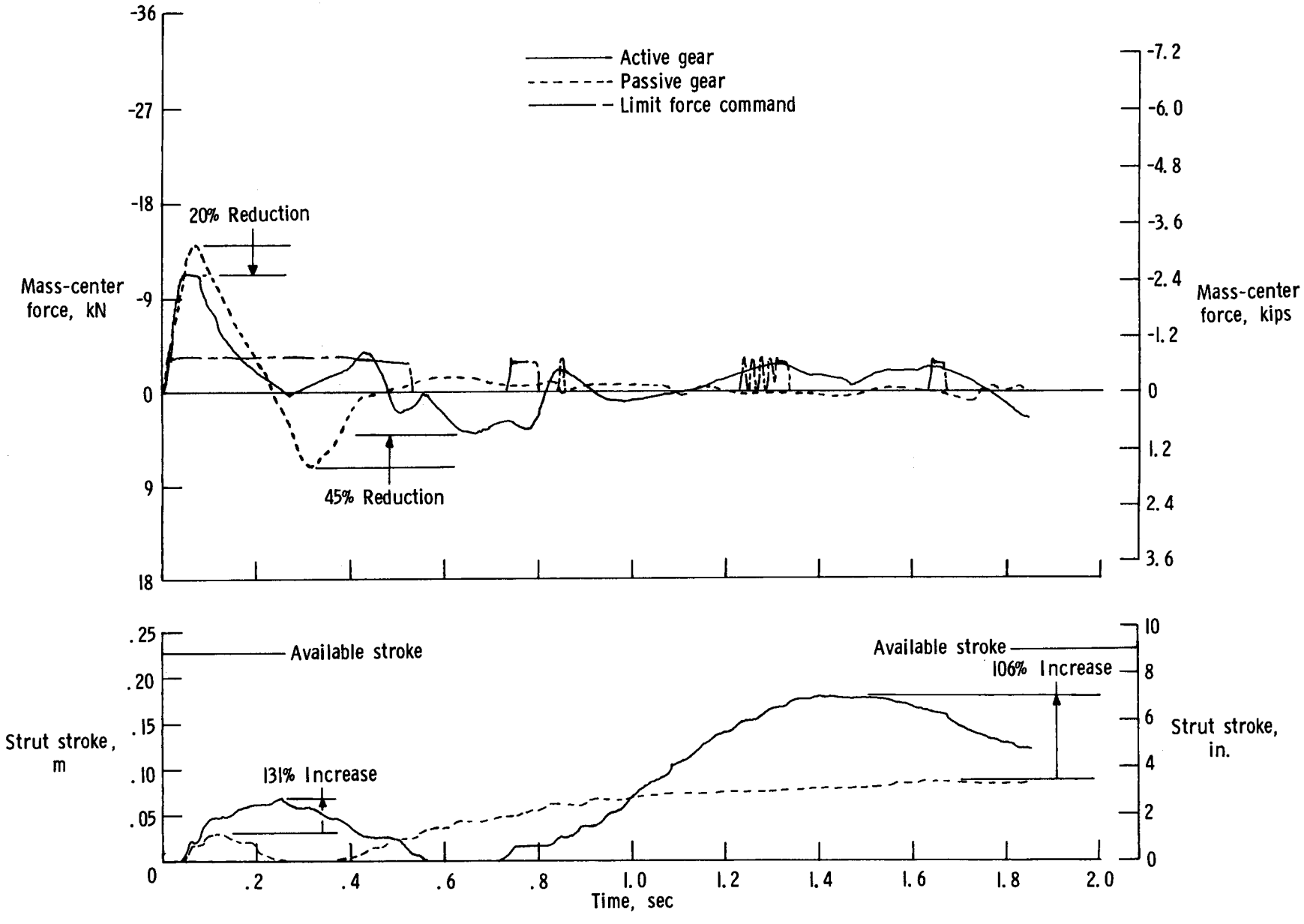

(e) V_h = 40 knots; V_v = 0.9 m/sec (3.0 ft/sec); p_a = 993 kPa (144 psig); p_p = 1434 kPa (208 psig); θ = 8°; tests 30 and 24.

Figure 10.- Continued.

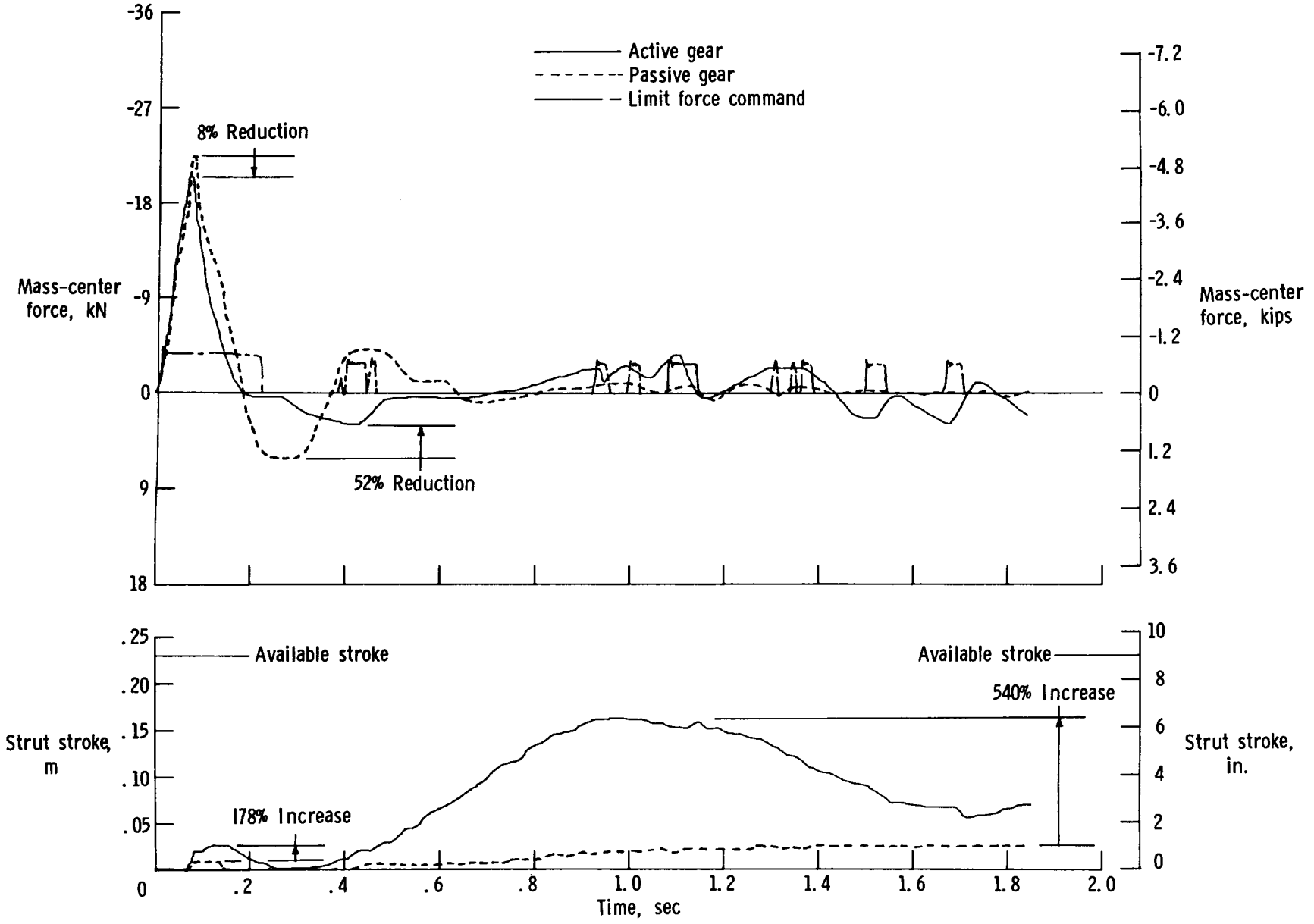

(f) V_h = 80 knots; V_v = 0.9 m/sec (3.0 ft/sec); p_a = 1710 kPa (248 psig); p_p = 2317 kPa (336 psig); θ = 8°; tests 32 and 34.

Figure 10.- Continued.

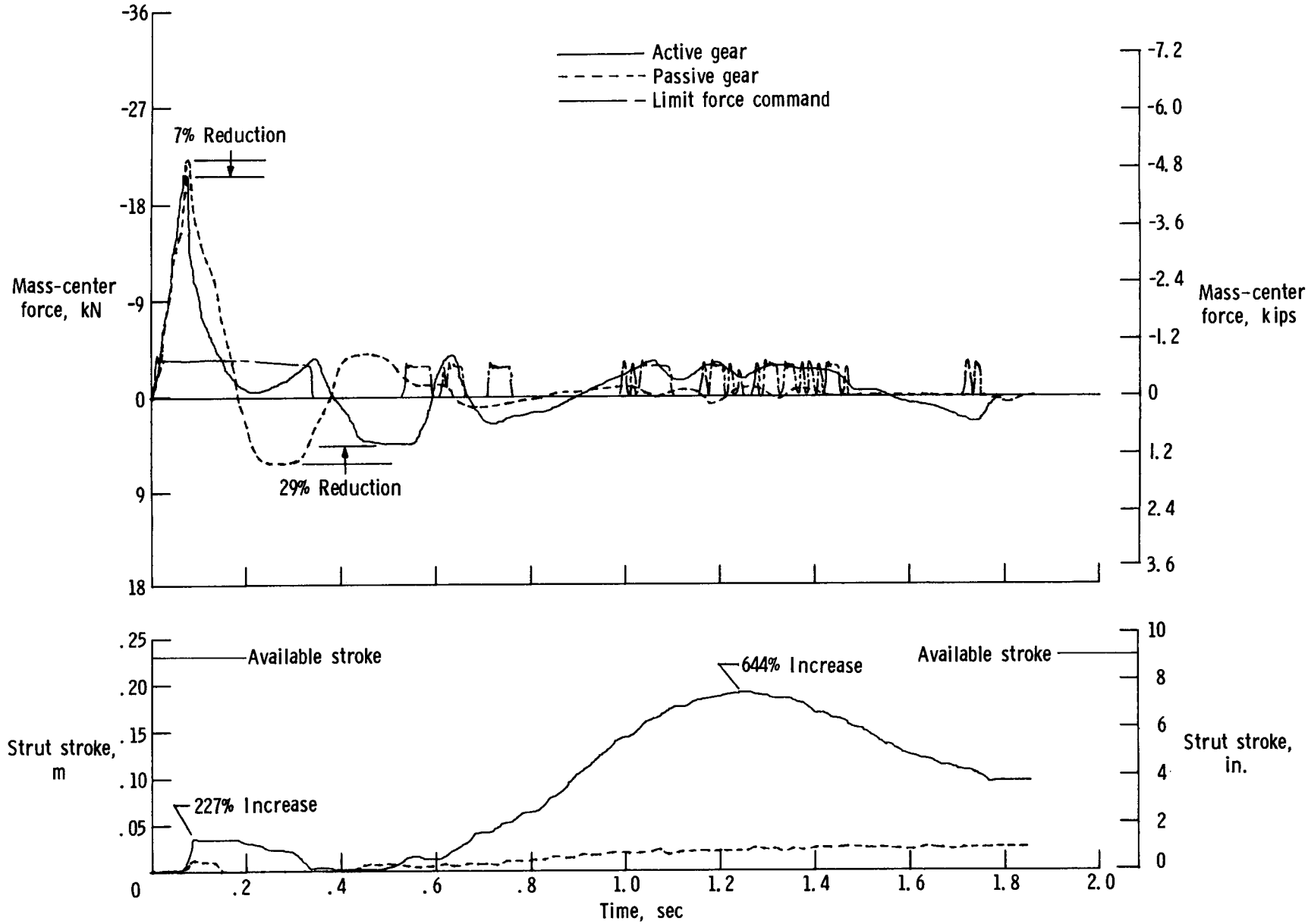

(g) V_h = 80 knots; V_v = 0.9 m/sec (3.0 ft/sec); p_a = 1655 kPa (240 psig); p_p = 2317 kPa (336 psig); θ = 8°; tests 35 and 34.

Figure 10.- Concluded.

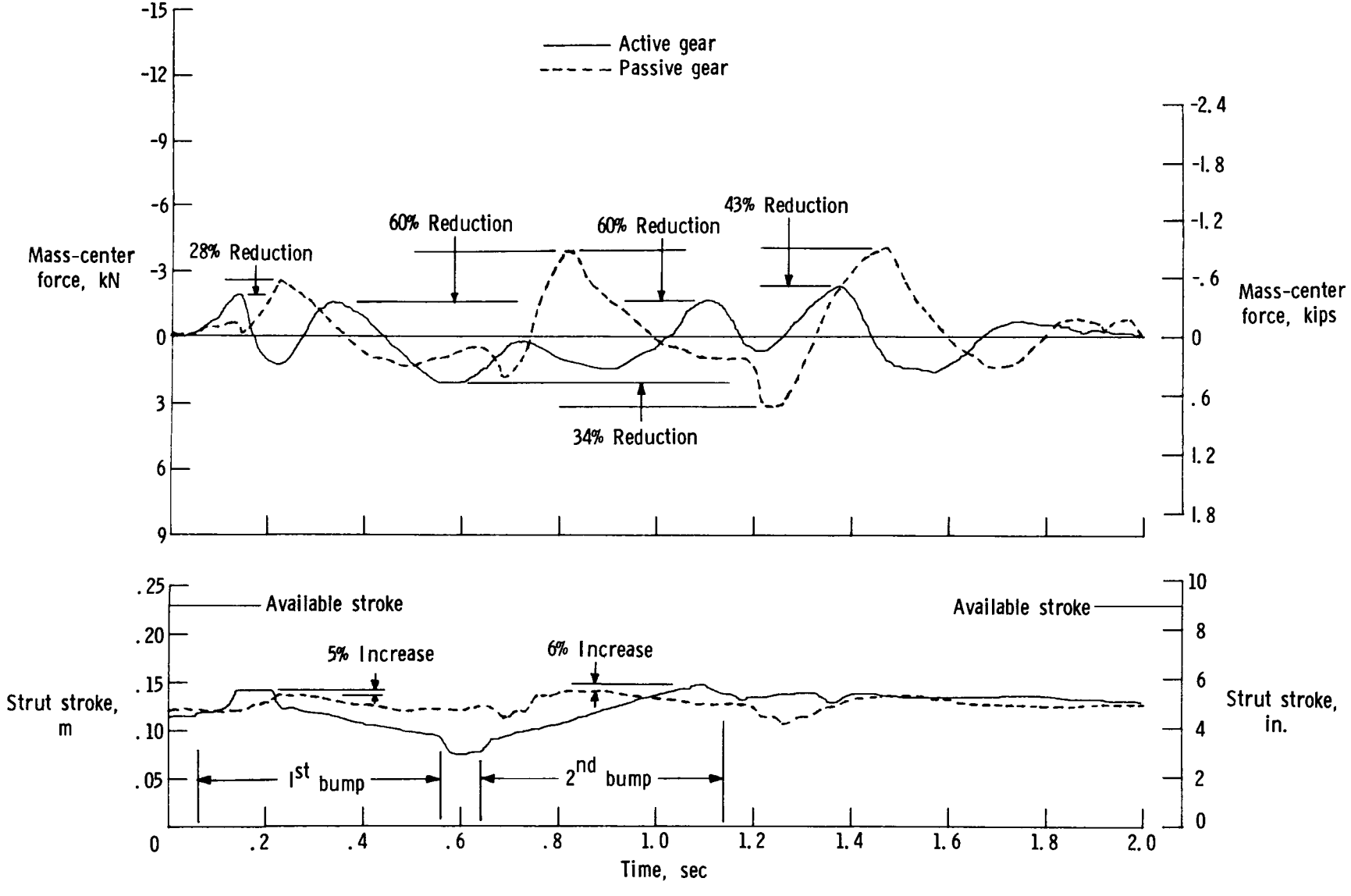

(a) V_h = 8 knots; f = 2 Hz; tests 48 and 47.

Figure 11.- Data obtained during traverse of step bumps.

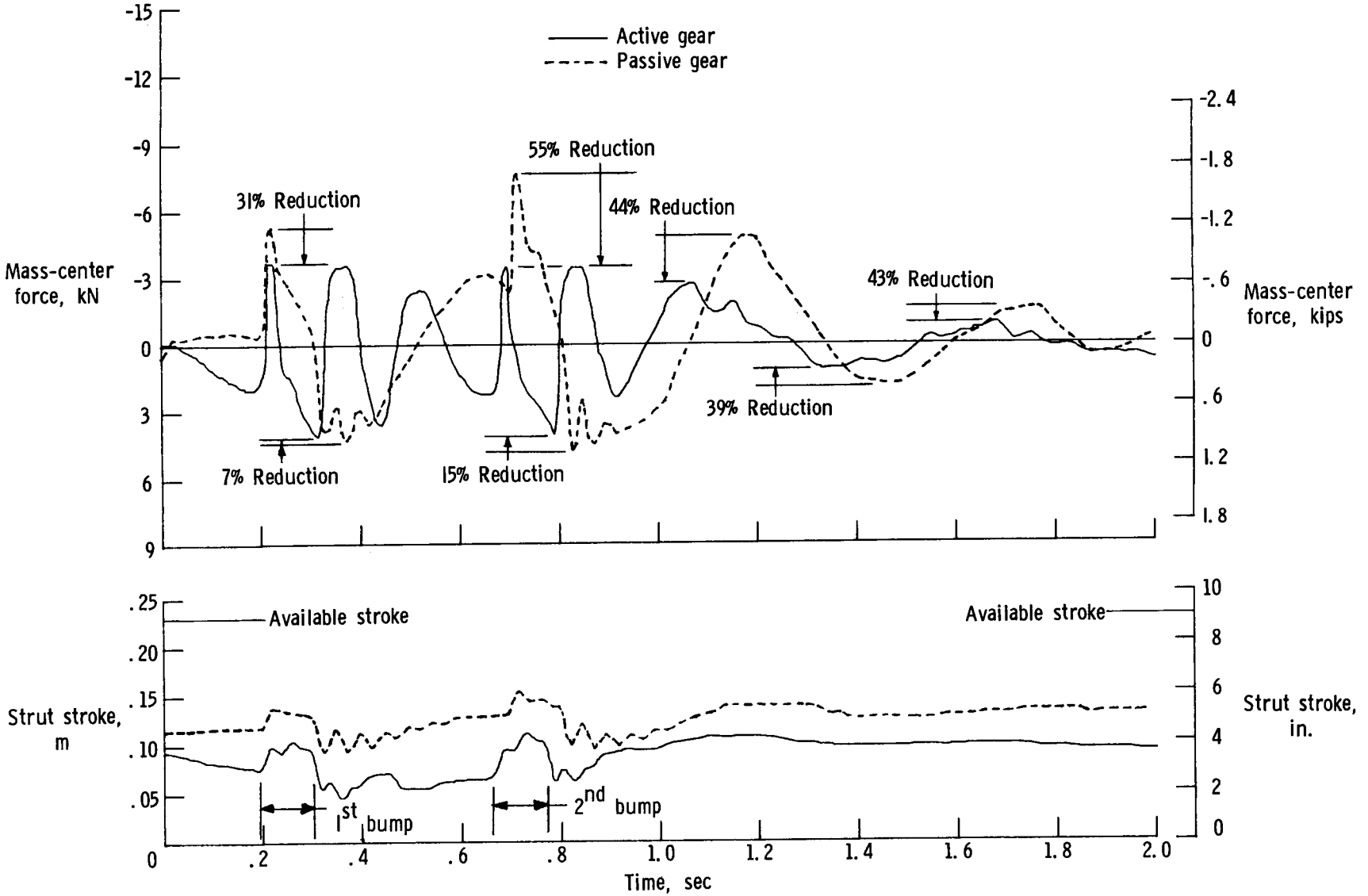

(b) V_h = 40 knots; f = 2 Hz; tests 16 and 14.

Figure 11.- Continued.

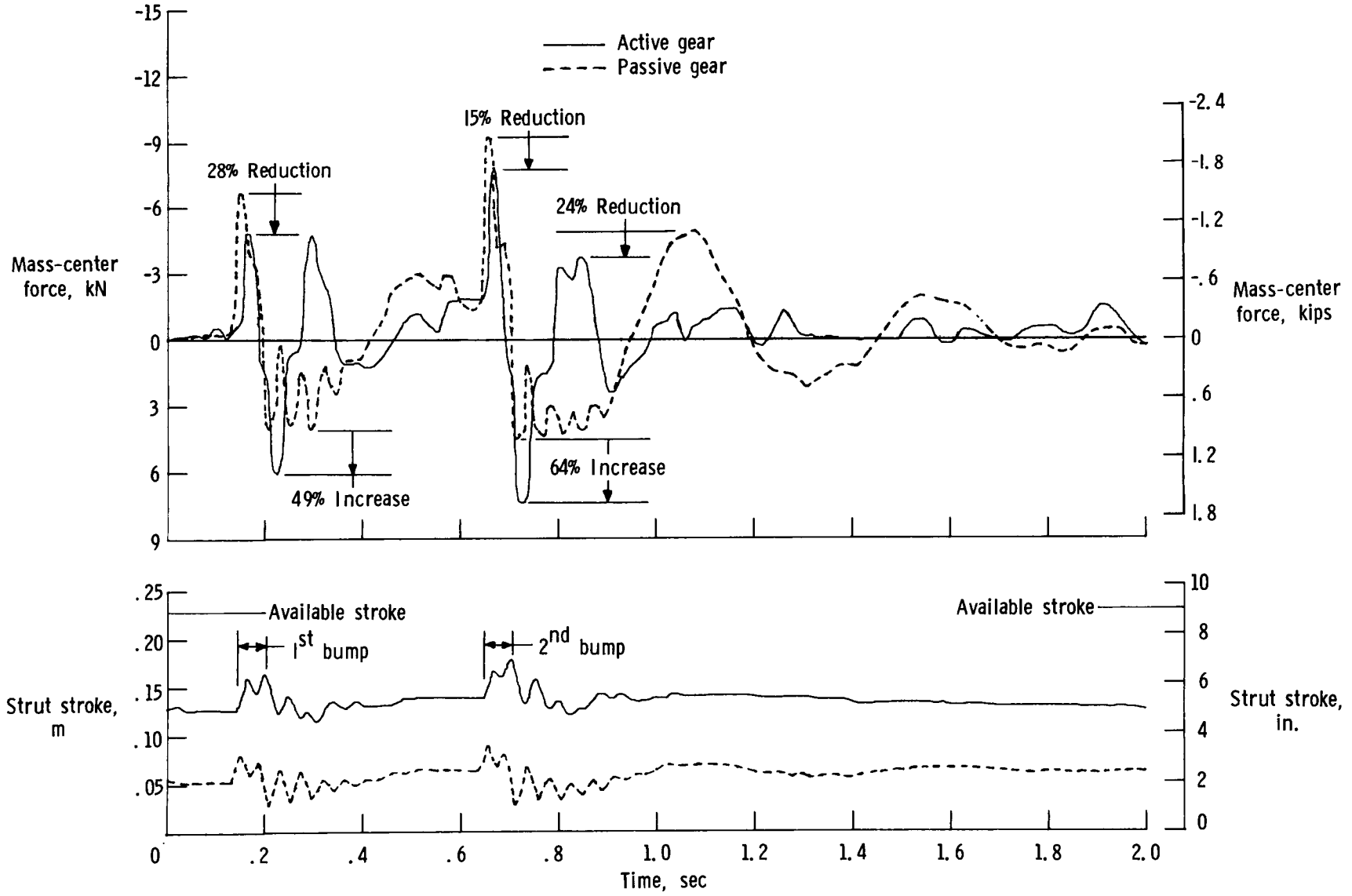

(c) V_h = 80 knots; f = 2 Hz; tests 42 and 37.

Figure 11.- Continued.

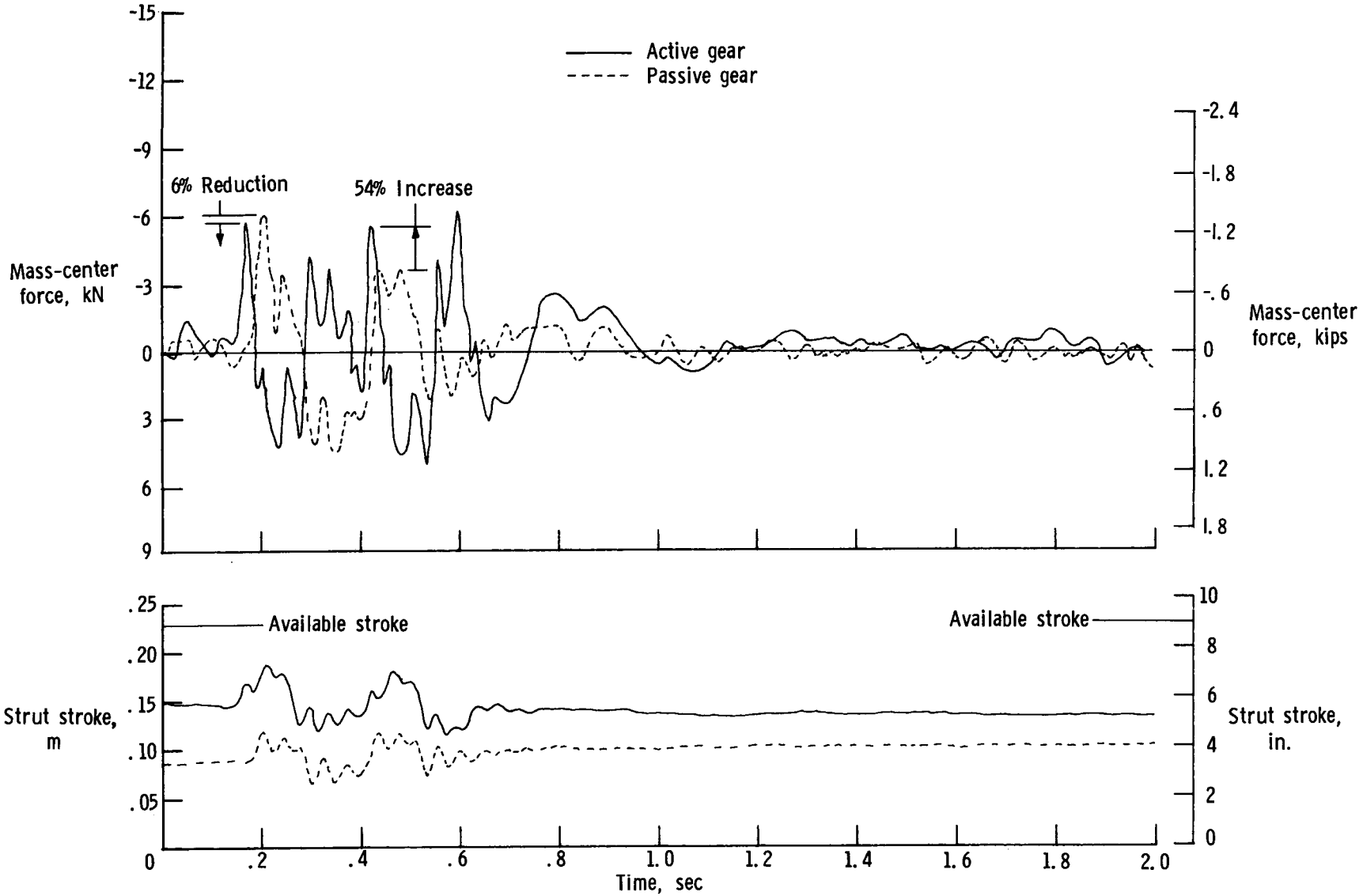

(d) V_h = 40 knots; f = 4 Hz; tests 52 and 24.

Figure 11.- Concluded.

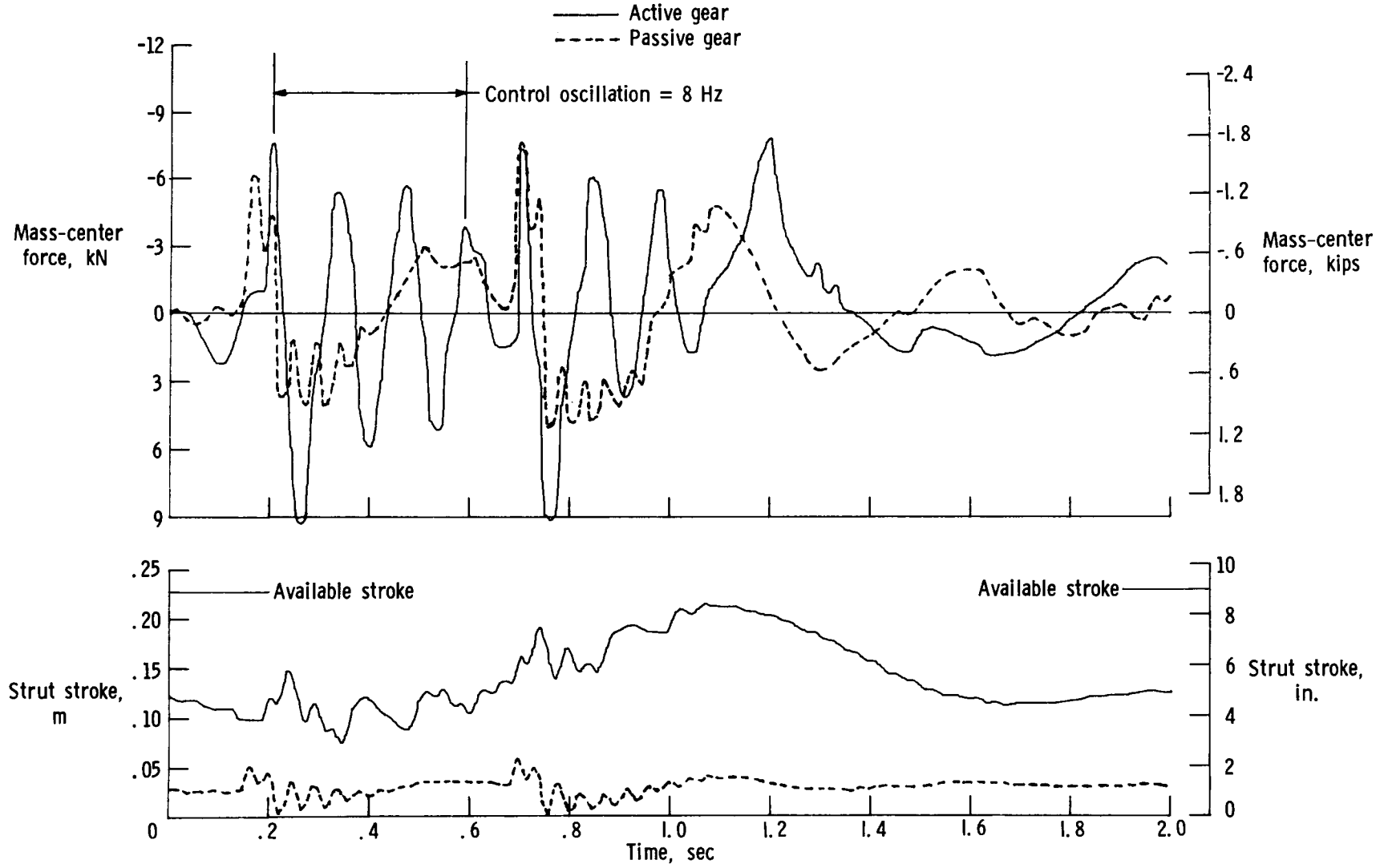

(a) Mass-center force and strut stroke.

Figure 12.- Illustration of effects of interaction between servovalve and relief valves during traverse of step bumps. V_h = 80 knots; f = 2 Hz; tests 35 and 34.

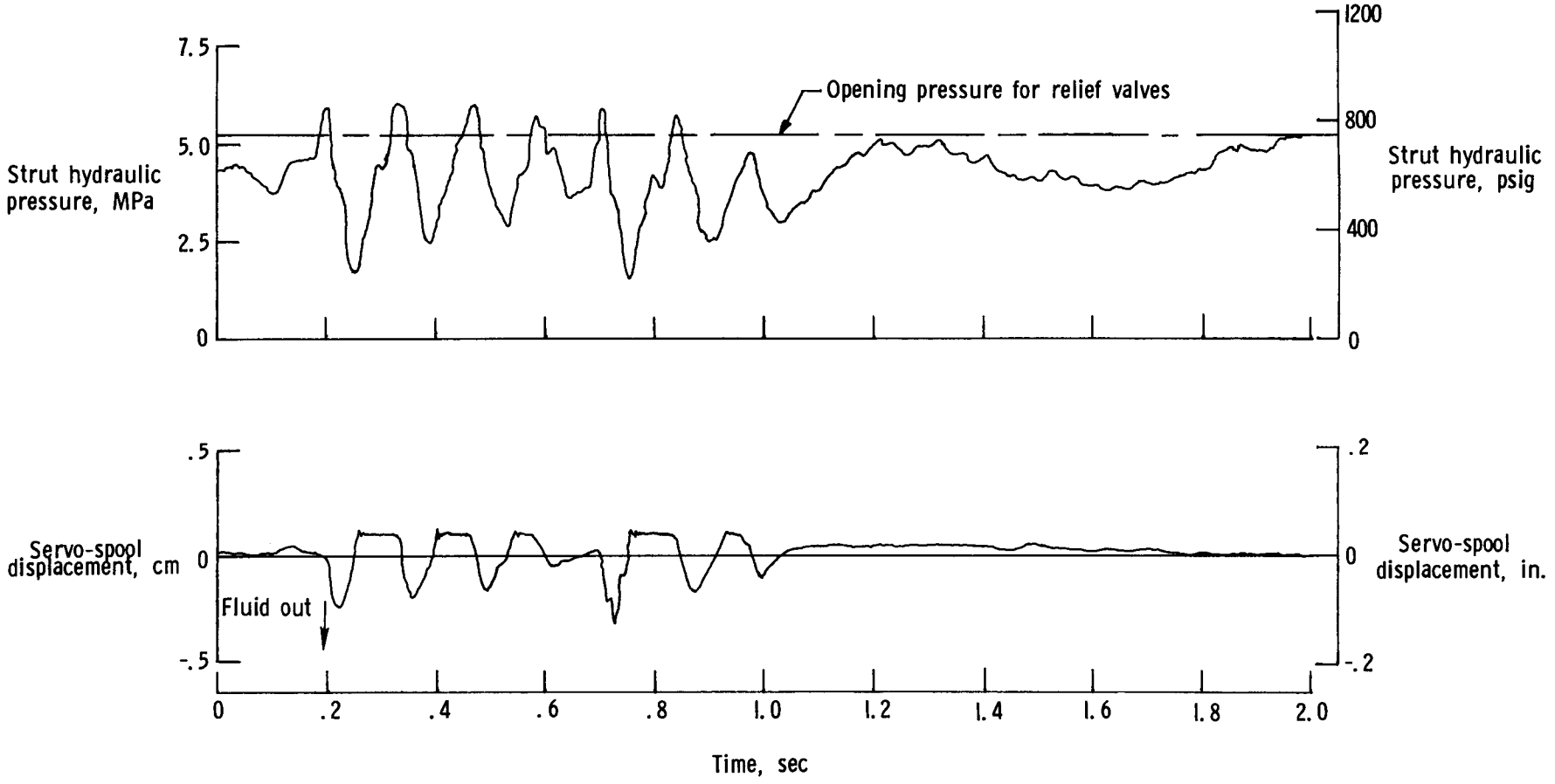

(b) Strut hydraulic pressure and servo-spool displacement.

Figure 12.- Concluded.

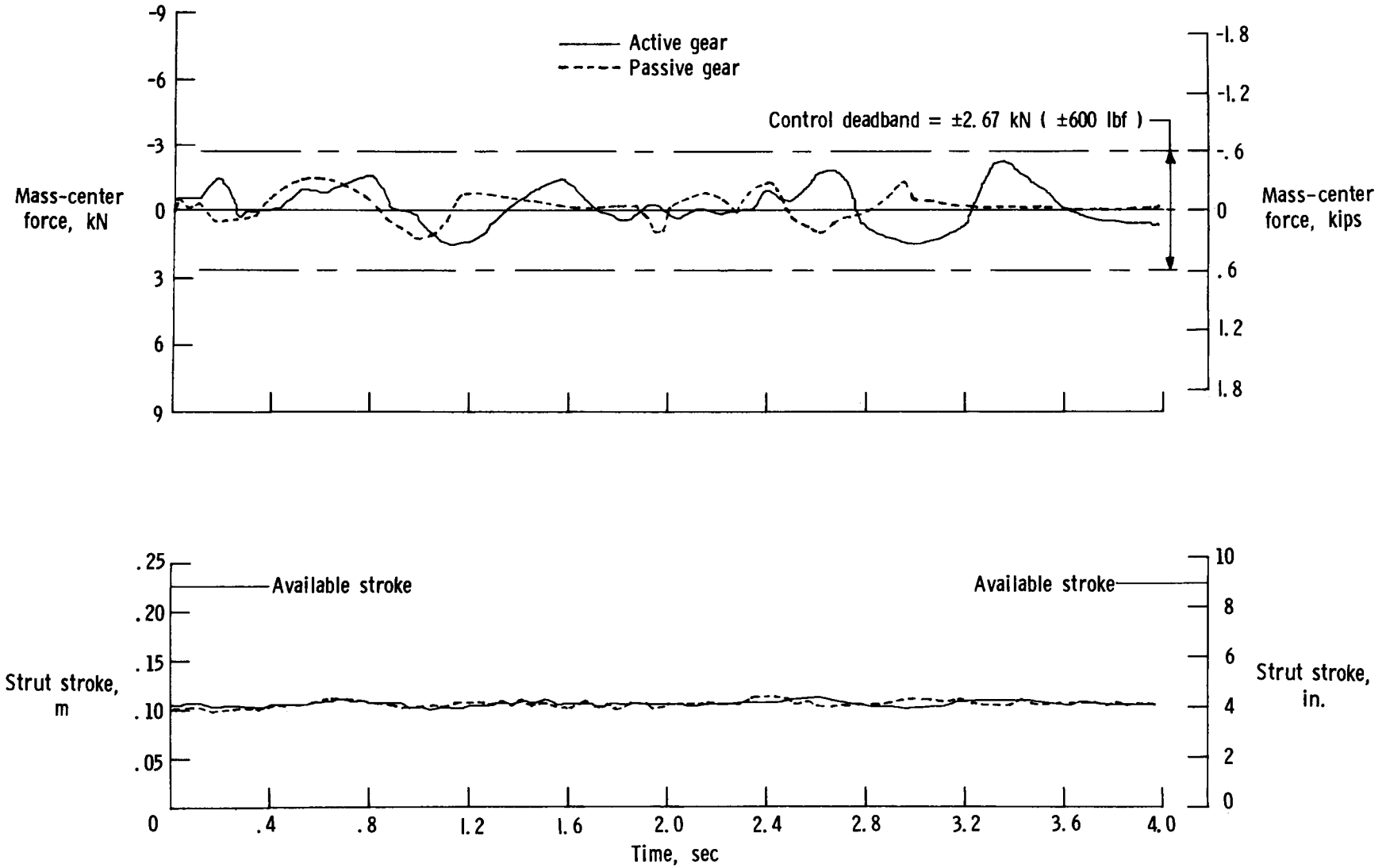

(a) V_h = 40 knots; tests 23 and 24.

Figure 13.- Typical data obtained during traverse of natural bumps.

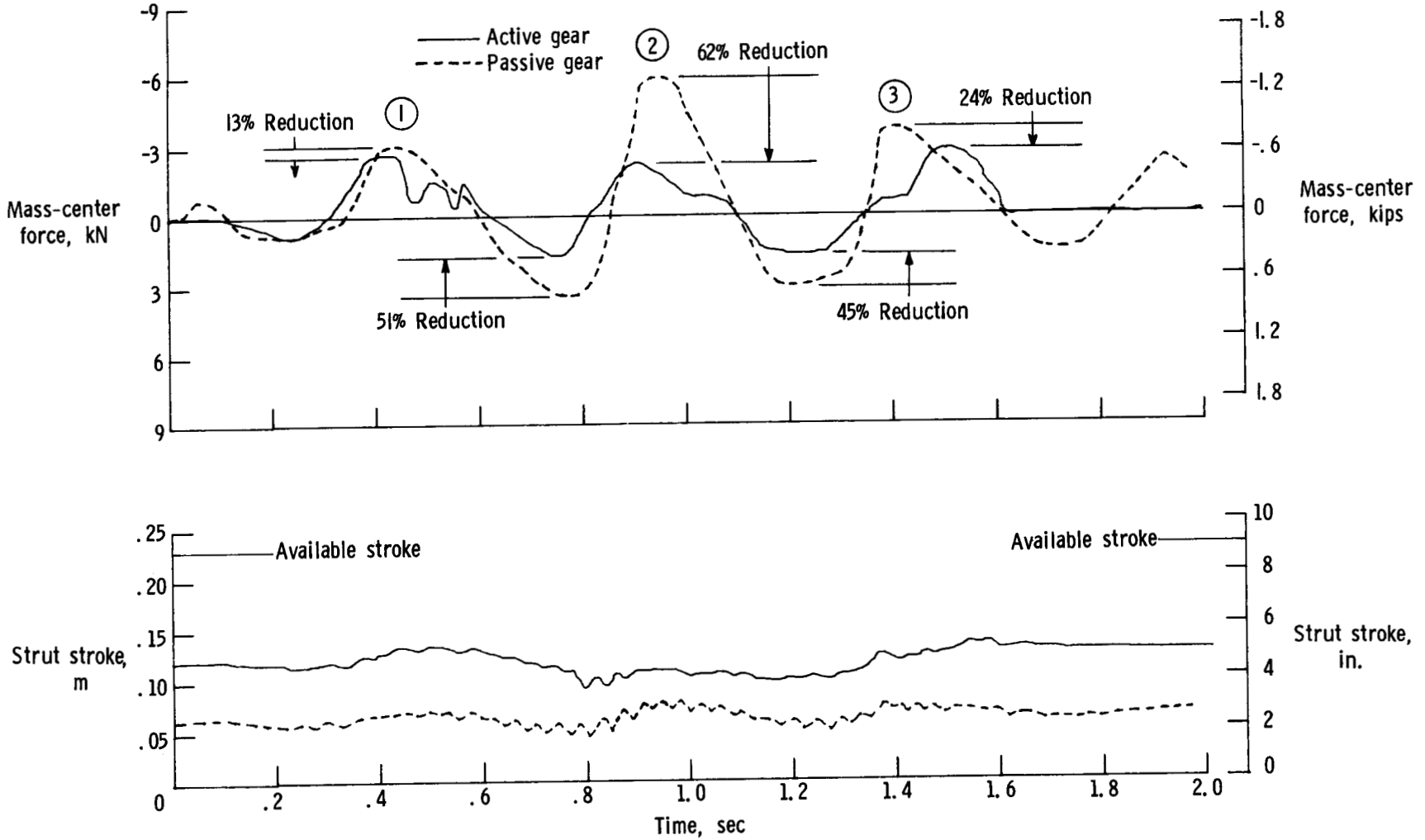

(b) V_h = 80 knots; tests 42 and 37.

Figure 13.- Continued.

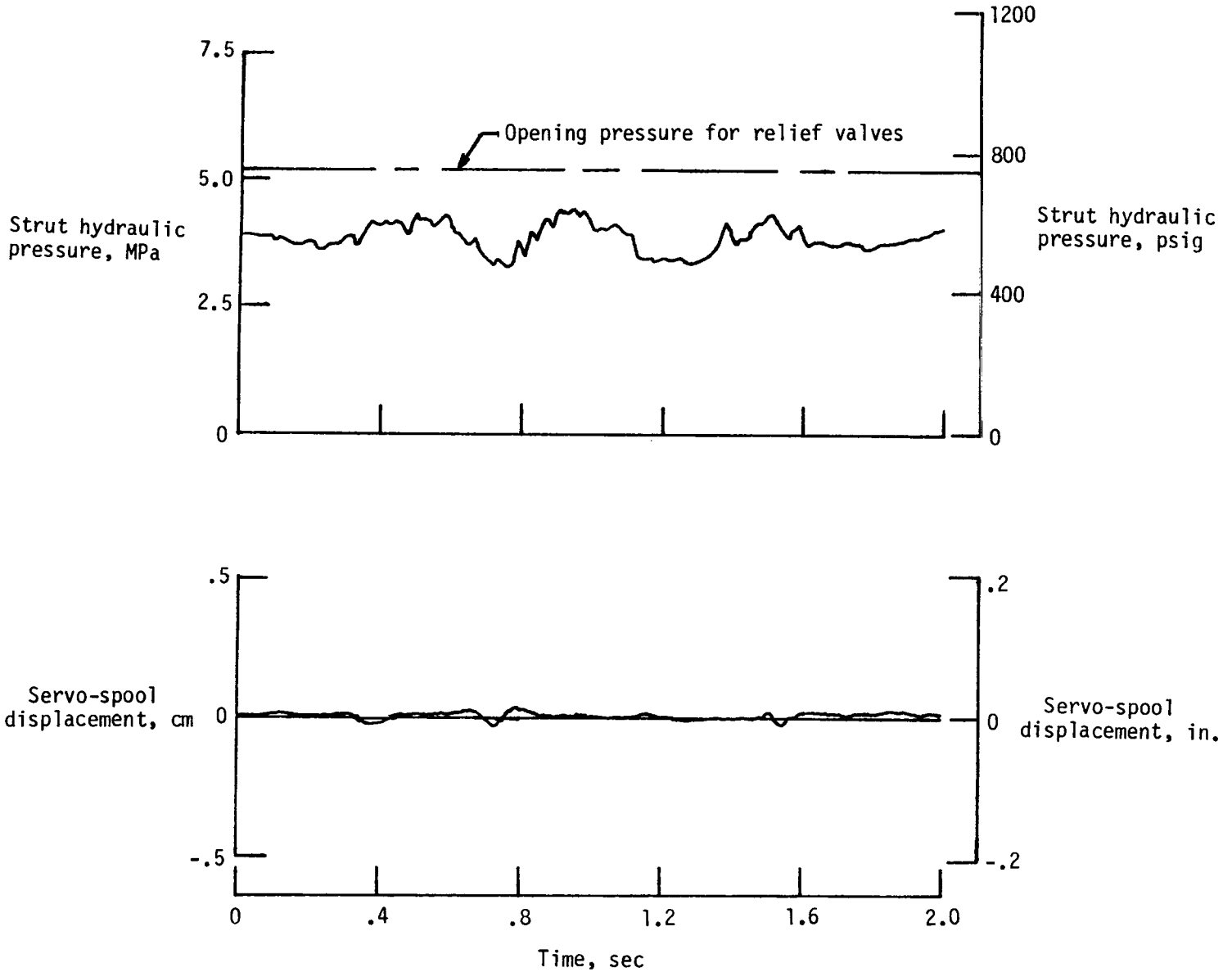

(c) Strut hydraulic pressure and servo-spool displacement for active gear at V_h = 80 knots; test 42.

Figure 13.- Continued.

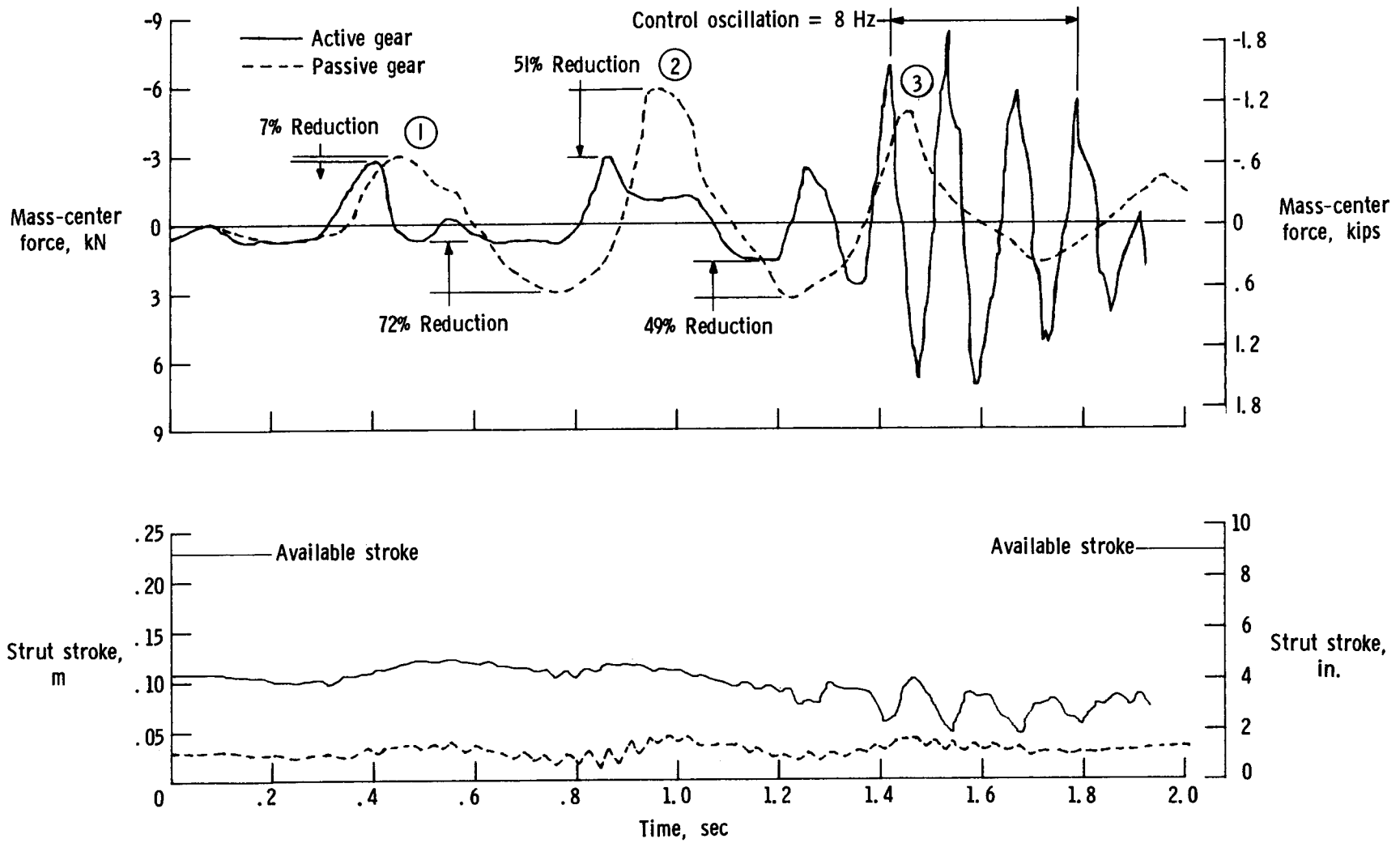

(d) V_h = 80 knots; tests 32 and 34.

Figure 13.- Continued.

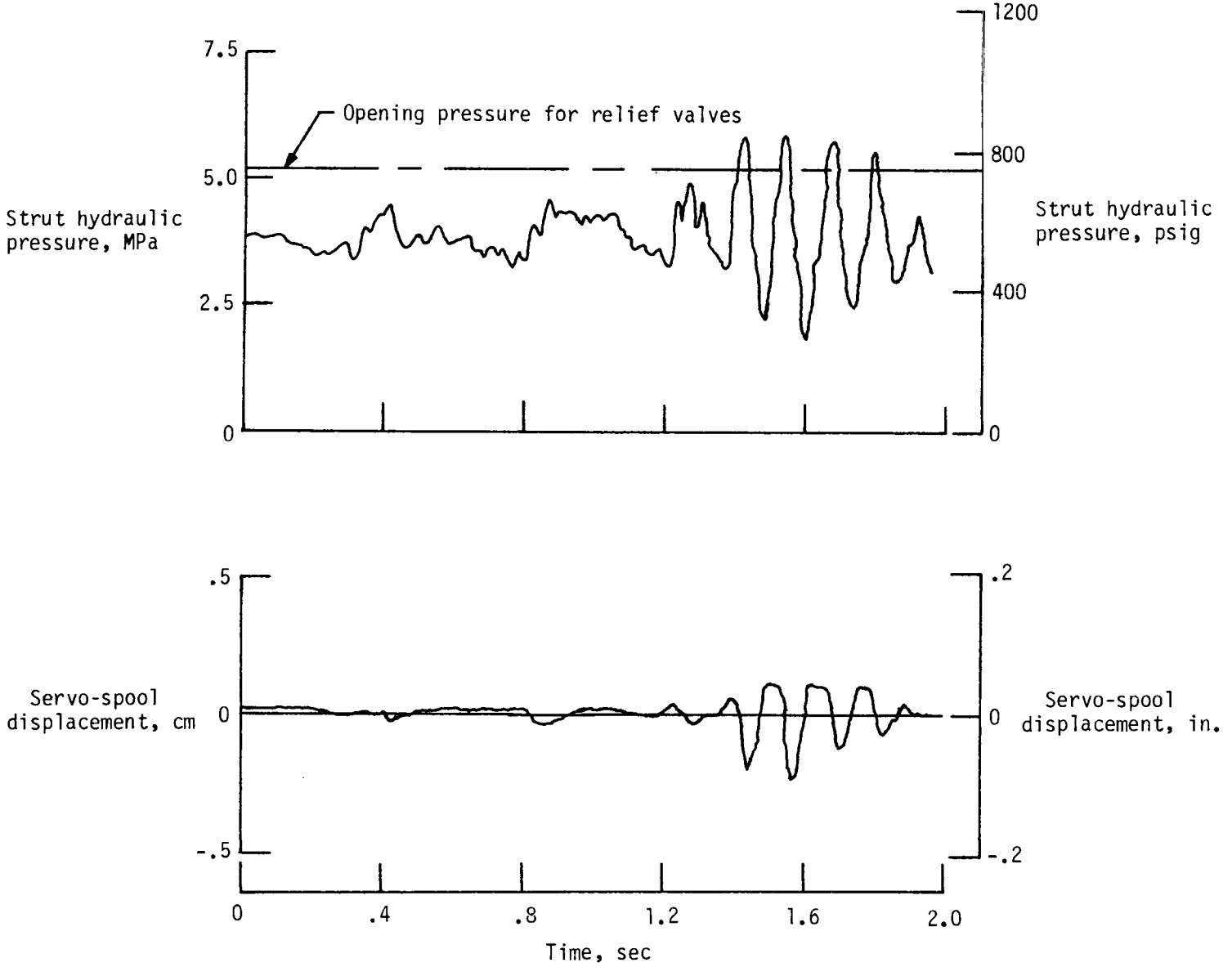

(e) Strut hydraulic pressure and servo-spool displacement during active-gear traverse of natural bumps at V_h = 80 knots; test 32.

Figure 13.- Concluded.

APPENDIX

CONTROL PHILOSOPHY

The control philosophy of the original version of the electronic controller is shown in the software flow chart of reference 4. In this investigation it became apparent that the original control philosophy was not adequate to control the gear during more realistic landing simulations. The control laws, therefore, were changed through hardware and software modifications of the electronic controller.

START

The software flow chart for the electronic controller used in this investigation is presented in figure A1. The following discussion illustrates the operation of the electronic controller as the control laws were applied to operate the control servovalve and, hence, the gear. Prior to a test, the controller was "on" in the disabled (reset) mode (START on the flow chart). With application of power to the controller, the central processing unit (CPU) disabled the interrupts, initialized the arithmetic board, set the electronic switches, and set the front-panel lights to indicate these conditions. The CPU initiated a query loop for determining the disabled (reset) or enabled status of the controller. For the experiments of this study, activation of a microswitch enabled the controller when the tire contacted the track surface. At time of activation, the CPU enabled the controller and set a light on the front panel of the controller to indicate this condition.

MODE DETERMINATION

The landing mode of operation of the controller requires different control laws for the touchdown impact phase and the landing roll-out phase. For the take-off mode of operation, the control laws are essentially the same as those employed during the landing roll-out phase. Because of this difference, the controller must determine the mode of operation. As the aircraft approaches the runway in the landing mode, the gear shock struts are fully extended; whereas, the aircraft is supported by the gear shock struts at essentially the designed static gear deflection in the take-off mode. Therefore, after the controller is enabled, the CPU acquires the strut position and compares the value to an input take-off or landing threshold (TLTHRESH) value of the strut stroke. The TLTHRESH value for this investigation was input as 2.54 cm (1.0 in.) since the static stroke for the gear was 11.4 cm (4.5 in.). For a strut position greater than TLTHRESH, the CPU transfers to the take-off logic section of the program.

LANDING MODE

This investigation was conducted for the landing mode only; hence, the gear was above the track surface (gear fully extended and strut position equal to zero) prior to a test. Therefore, the CPU selects the landing mode, enables the integrator circuit, and sets lights on the front panel to indicate these conditions. The integrator circuit integrates the wing/gear interface acceleration (W/G ACCEL) to obtain the change in wing/gear interface velocity (wing/gear interface velocity decrement, W/G VEL DEC). The touchdown value of the wing/gear interface velocity is equivalent to the sink rate. The CPU acquires the sink rate, the instantaneous value of the W/G

VEL DEC, and calculates the instantaneous value of the wing/gear interface velocity (W/G VEL) through an algebraic summing of the sink rate and the W/G VEL DEC. The CPU then acquires the instantaneous values of the wing/gear interface inertia force (FWG), the W/G VEL, and the strut position (strut stroke). With these values the CPU calculates the kinetic energy at the wing/gear interface (KE) and the remaining work capability of the shock strut (PE). The CPU compares these energies and, if the PE is less than the KE, loops back in the program to obtain the sink rate, updates the values of FWG and W/G VEL DEC, and recalculates the energies. The CPU remains in this loop until the PE equals or exceeds the KE. When PE > KE, the CPU stores the instantaneous value of the FWG as the limit force command (LFC). To insure that the initial control effect on the gear is the removal of fluid, the CPU acquires the FWG and compares it with the LFC. If the FWG is less than the LFC, the CPU continues to sample updated values of the FWG and compare the values with the LFC.

ACTIVE CONTROL

When the FWG becomes greater than the LFC, the CPU initiates active control of the gear by disabling the bias-pressure loop (which maintains charging pressure in the gear) and enabling the servo loop. The servo loop then initiates the computation of the force error (FWG-LFC) and transmits a signal proportional to the force error to the servovalve. The CPU continues to control the servovalve and, additionally, calculates the transition velocity (TRANS VEL), calculates an updated value of the W/G VEL, and compares the two values. If the W/G VEL is greater than the TRANS VEL, the CPU loops back in the program, calculates an updated value of the W/G VEL, and continues in this loop until the W/G VEL becomes less than the TRANS VEL. When the W/G VEL becomes less than TRANS VEL, the CPU initiates the transition phase by acquiring the value of the LFC and decreases LFC at the input design value of the transition rate.

TRANSITION

During the transition phase, the CPU continues the comparison of the updated values of the LFC and the FWG and controls the gear. The transition phase continues until the LFC becomes less than zero or the shock strut becomes fully extended. Control of the gear is established on the basis that the gear is in contact with the landing surface and the shock strut is compressed. Therefore, the CPU acquires the strut position and compares it with a strut threshold value of 1.0 cm (0.4 in.) for this investigation. If the strut position is greater than the threshold value, the CPU acquires the LFC and compares it with zero. If the LFC is greater than zero, the CPU loops back and continues control of the gear and transition of the LFC.

ROLL-OUT PHASE

If the aircraft rebounds and the shock strut becomes fully extended or the LFC becomes less than zero, the CPU initiates the roll-out phase; that is, the LFC is set identically equal to zero and the force feedback switch is opened (control deactivated). To insure that the gear is not active as long as it is fully extended and to accommodate control during secondary impact, the CPU gets the strut position and compares it with the threshold value. If the strut position is not greater than the threshold value, the CPU loops back, obtains an updated value of the strut position and compares it with the threshold value. When the strut position becomes greater than the threshold value, the CPU sets the trip point (a storage address) to the

designed value of the roll-out LFC and compares it with the FWG. If the FWG is not less than the trip point, the CPU sets the LFC to the roll-out value, closes the force feedback switch (activates control of the gear), sets the trip point to the cutoff value of the LFC, computes the force error, and controls the gear. The CPU continues to control the gear in this mode until the FWG becomes less than the LFC cutoff value of the trip point. The CPU then resets the trip point to the LFC roll-out value, checks to ascertain if the FWG is negative, and if so, compares the absolute value of the FWG with the trip point. If the absolute value of the FWG is not less than the trip point, the CPU sets the LFC to the roll-out value, closes the force feedback switch, reverses the sign of the LFC analog signal, sets the trip point to the cutoff value of the LFC, computes the force error, and controls the gear. If the absolute value of the FWG is less than the trip point, the CPU loops back to the start of the roll-out phase. The CPU continues to operate in this mode until the controller is reset.

TAKE-OFF MODE

If the strut position had been greater than the TLTHRESH value following controller enable, the CPU would have transferred to the take-off mode in the computer program. The CPU sets the lights and switches for the take-off mode and controls the gear in the same manner as the previously discussed landing roll-out phase. However, an additional strut position test is included following the negative FWG test, and if the strut position is greater than the threshold value, the CPU continues to operate as it does in the landing roll-out phase. When the gear has become fully extended as it would at lift-off, the strut position becomes less than the threshold value and causes the CPU to disable the servo loop, enable the bias-pressure loop, and return to the start of the program.

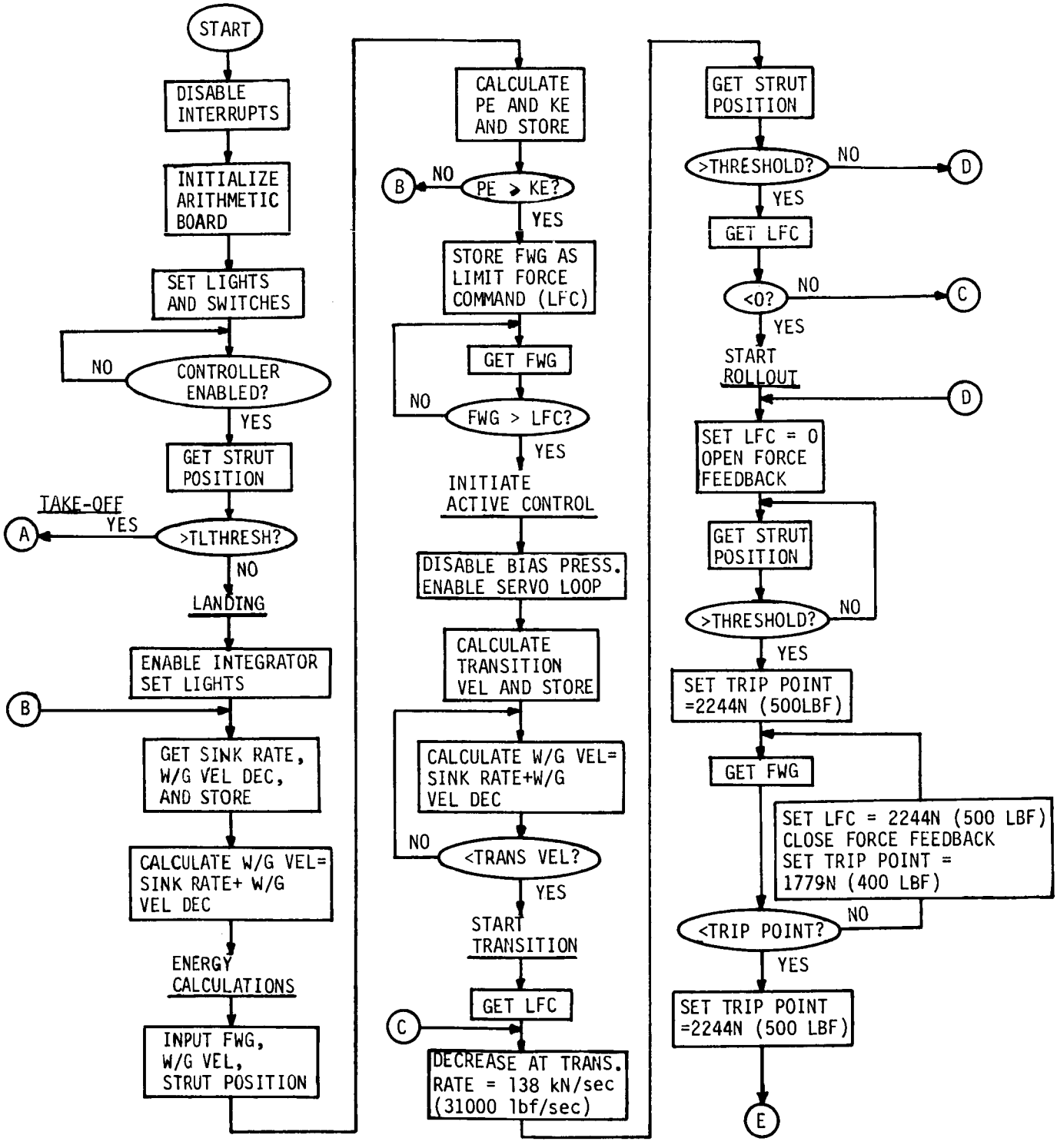

Figure A1.- Software flow chart for electronic controller. Discrete values shown are for gear employed in this investigation.

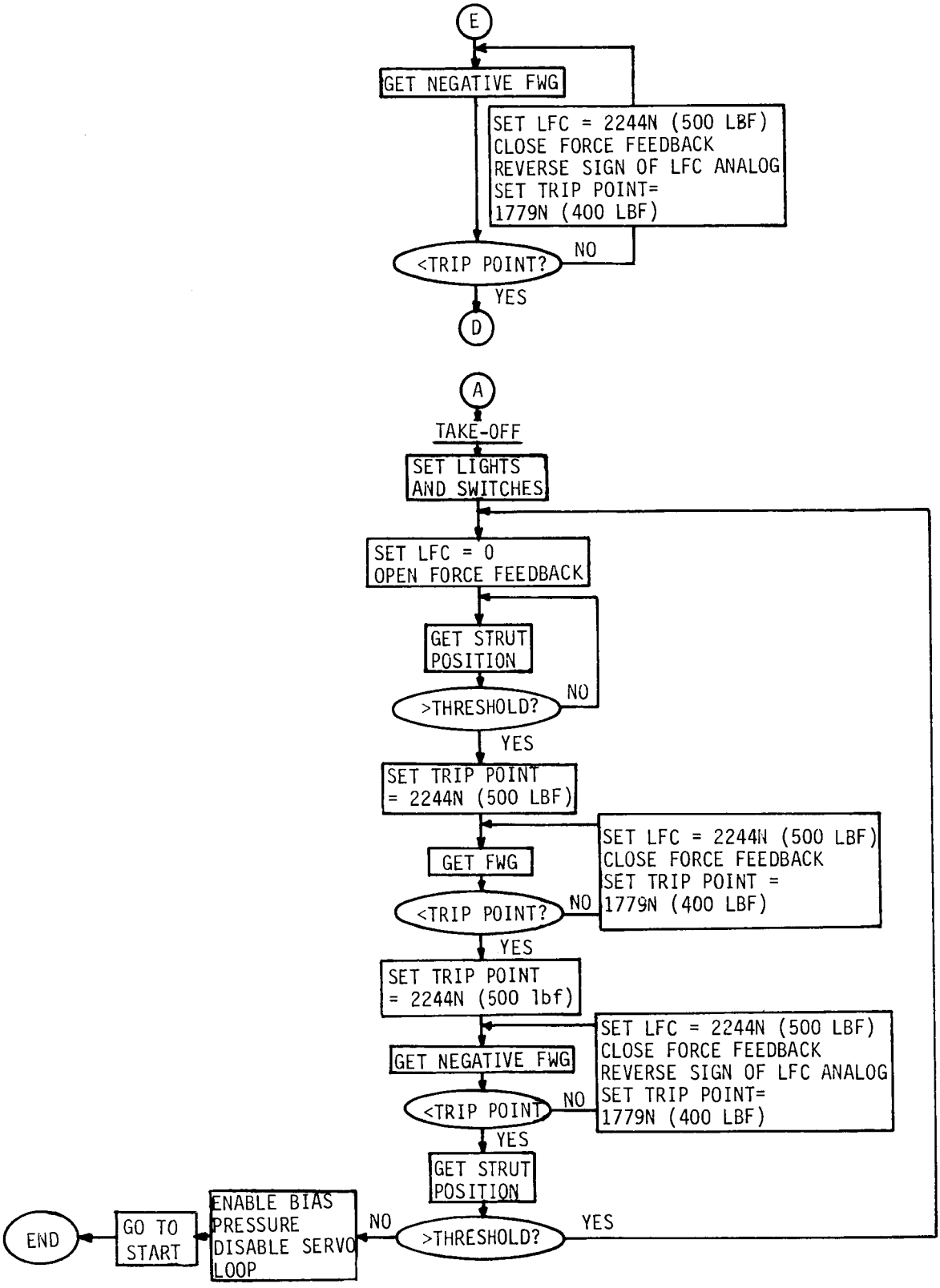

Figure A1.- Concluded.

REFERENCES

1. DC-10 Landing Gear Modified. Aviat. Week & Space Technol., vol. 98, no. 12, Mar. 19, 1973, p. 181.

2. Ropelewski, Robert R.: Airbus Test Tempo Quickening. Aviat. Week & Space Technol., vol. 98, no. 10, Mar. 5, 1973, pp. 32-35.

3. McGehee, John R.; and Carden, Huey D.: A Mathematical Model of an Active Control Landing Gear for Load Control During Impact and Roll-Out. NASA TN D-8080, 1976.

4. Ross, Irving; and Edson, Ralph: An Electronic Control for an Electrohydraulic Active Control Aircraft Landing Gear. NASA CR-3113, 1979.

5. Dreher, Robert C.; and Yager, Thomas J.: Friction Characteristics of 20 × 4.4, Type VII, Aircraft Tires Constructed With Different Tread Rubber Compounds. NASA TN D-8252, 1976.

6. Fasanella, Edwin L.; McGehee, John R.; and Pappas, M. Susan: Experimental and Analytical Determination of Characteristics Affecting Light Aircraft Landing-Gear Dynamics. NASA TM X-3561, 1977.

7. Standard for Metric Practice. E 380-79, American Soc. Testing & Mater., c.1980.

SYMBOLS

The units used for the physical quantities defined in this paper are given first in the International System of Units (SI) and parenthetically in the U.S. Customary Units. Measurements and calculations were made in U.S. Customary Units. Factors relating the two systems are given in reference 7.

d	distance between step bumps, m (ft)
f	frequency, Hz
p	strut hydraulic pressure, kPa (psig)
V	velocity, m/sec (knots)
W/G	wing/gear interface
θ	pitch angle, deg

Subscripts:

a	active gear
h	horizontal
p	passive gear
v	vertical

1. Report No.	2. Government Accession No.	3. Recipient's Catalog No.
NASA TP-2042		

4. Title and Subtitle	5. Report Date
EXPERIMENTAL INVESTIGATION OF ACTIVE LOADS CONTROL FOR AIRCRAFT LANDING GEAR	August 1982
	6. Performing Organization Code: 505-44-33-01
7. Author(s): John R. McGehee and Robert C. Dreher	8. Performing Organization Report No.: L-15224
	10. Work Unit No.
9. Performing Organization Name and Address: NASA Langley Research Center, Hampton, VA 23665	11. Contract or Grant No.
	13. Type of Report and Period Covered: Technical Paper
12. Sponsoring Agency Name and Address: National Aeronautics and Space Administration, Washington, DC 20546	14. Sponsoring Agency Code

15. Supplementary Notes

16. Abstract

Aircraft dynamic loads and vibrations resulting from landing impact and from runway and taxiway unevenness are recognized as significant factors in causing fatigue damage, dynamic stress on the airframe, crew and passenger discomfort, and reduction of the pilot's ability to control the aircraft during ground operations. One potential method for improving operational characteristics of aircraft on the ground is the application of active-control technology to the landing gears to reduce ground loads applied to the airframe. An experimental investigation was conducted which simulated the landing dynamics of a light airplane to determine the feasibility and potential of a series-hydraulic active-control main landing gear. The experiments involved a passive gear and an active-control gear. Results of this investigation show that a series-hydraulically controlled gear is feasible and that such a gear is very effective in reducing the loads transmitted by the gear to the airframe during ground operations.

17. Key Words (Suggested by Author(s))	18. Distribution Statement
Aircraft landing gear Active controls Landing loads	Unclassified - Unlimited Subject Category 05

19. Security Classif. (of this report)	20. Security Classif. (of this page)	21. No. of Pages	22. Price
Unclassified	Unclassified	70	A04

For sale by the National Technical Information Service, Springfield, Virginia 22161 NASA-Langley, 1982